13381-1-F = RL-2261

THE UNIVERSITY OF MICHIGAN

COLLEGE OF ENGINEERING

DEPARTMENT OF ELECTRICAL AND COMPUTER ENGINEERING

Radiation Laboratory

INVESTIGATIONS OF ELECTROMAGNETIC SCATTERING BY COLUMNAR ICE CRYSTALS

Herschel Weil and Thomas B. A. Senior

5 March 1976

Final Report
Grant NSG 5044

Prepared for

NASA Goddard Space Flight Center
Greenbelt, Maryland 20771

Ann Arbor, Michigan

Abstract

An integral equation approach is developed to determine the scattering and absorption of electromagnetic radiation by thin walled cylinders of arbitrary cross-section and refractive index. Based on this method extensive numerical data are presented at wavelengths in the infrared for hollow hexagonal cross section cylinders which simulate columnar sheath ice crystals.

TABLE OF CONTENTS

1. Introduction

This is the Final Report on NASA Grant NSG 5044 and describes the work carried out in computing the scattering and absorption of electromagnetic radiation by columnar sheath ice crystals. In this first section we begin by citing some of the important geophysical problems which require such data, and note some of the consequences of the lack of sufficiently accurate values for the scattering and absorption properties of single ice crystals. After surveying the work done in recent years to remedy this deficiency, we then summarise our own contributions to the subject. The detailed results are given in the remaining sections of the report.

The reflection, transmission and absorption of visible and infrared radiation by clouds and by polluted atmospheres is of considerable importance in many practical areas. Cirrus clouds are composed of ice crystals. They are found over the entire globe and their infrared and optical scattering properties have a profound effect on the atmospheric heat balance. The clouds scatter and absorb the primarily infrared radiation resulting from the earth and the lower regions of the atmosphere as well as the mainly shorter wavelength solar radiation incident from above. The difference then plays a major part in the atmospheric heat balance which governs the global location of energy sources and sinks and, hence, the atmospheric circulation patterns (Cox, 1971; AFWG, 1972). Similarly, but on a much smaller scale, the cirrus clouds created artificially by jet contrails have been observed to markedly affect local weather (Appleman, 1966; Reinking, 1968); and a knowledge of the scattering by clouds is also needed in using satellite measurements of the IR emission of water vapor to estimate the relative humidity of regions above the clouds. Finally, we remark that the use of LIDAR as an atmospheric probling tool depends on the difference in the reradiation of the aerosols and the much smaller background molecules (Grams, 1975).

Techniques for calculating the transfer of electromagnetic radiation through clouds of particles have been summarized by Plass et al. (1973), and one of their most basic ingredients is a knowledge of the scattering and absorption properties of the individual particles. This may involve either single scattering or multiple scattering in the case of optically thick clouds. Since each scattering event can affect the polarisation by producing an electric field having a component orthogonal to the incident vector as well as parallel to it, and this field is in turn incident on another particle, an accurate treatment of the transfer problem will involve the complete scattering and absorption matrices for a single particle.

In an atmospheric cloud, the particles are either water droplets or ice crystals. The water drops are close to spherical and it is not unreasonable to model them as spheres. This enables Mie theory to be applied and the results obtained are reasonably accurate. Ice crystals, however, are another story. The shapes, sizes, concentrations and fall patterns which have been observed in clouds have been discussed by Mossop and Ono, 1969; Ono, 1969; Aufm Kampe and Weickman, 1957; and Heymsfield and Knollenberg, 1972. Both plate crystals, i.e. cylinders of length much less than their diameter, and columnar crystals, i.e. long thin cylinders, hollow as well as solid, are commonly found, and for shapes as varied as this, a sphere cannot provide an accurate simulation of the scattering behavior. Nevertheless, for lack of a more accurate method for calculating the scattering properties, the Mie theory has been widely used even for ice crystals, thereby introducing unknown and possibly large errors in the values for the radiation transfer, which are the end products of extensive and expensive computations (Kattewar and Plass, 1972).

The importance of using the proper scattering matrix when the particles are irregular is clear from the data presented by Holland and Gagné (1970). They measured the elements of the scattering matrix for clouds of irregularly shaped, randomly oriented silicon flakes. The results were quite different from the matrix elements predicted by Mie theory, particularly for back and forward scatter, and the depolarization was also poorly predicted by the theory.

The last few years have seen several attempts to calculate the scattering of more realistically-shaped crystals, and it is appropriate to mention here the work of Jacobowitz (1971) and Liou (1972 a and b; 1973) which has been directed at the scattering properties of columnar ice crystals. Jacobowitz's data were obtained for infinitely long crystals hexagonal in cross section using ray tracing. All end effects were necessarily omitted, including the 45^{o} deviation of the rays passing through the end faces which contributes to the large halo observed about ice clouds (see Minnaert, 1954, section 104). The method also excludes all diffraction effects produced, for example, by the six longitudinal edges of the cylinder, as well as polarization effects, and the calculations were limited to cylinders not less than 40μ in diameter (for a wavelength of $0.55\ \mu$) with the apparent objective of assuring the reasonable validity of geometrical optics. Finally, no account was taken of internal absorption by the ice in spite of the fact that the appreciable imaginary part of the refractive index at some infrared wavelengths suggests that absorption may not be negligible.

Liou's analyses are based on the assumption that the ice crystal can be modelled by an infinitely long, homogeneous dielectric cylinder of circular cross section. For this simplified geometry there is a mathematically exact expression for the scattered field in the form of a series of Bessel and Hankel functions analogous to the Mie series for a sphere. It is therefore possible to compute the scattering matrix precisely, with all polarization information present, and with internal absorption taken into account. Nevertheless, end effects are omitted by virtue of the model chosen, and the assumption of a circular cylinder necessarily suppresses those features of the scattering which are peculiar to the hexagonal cross section of an actual ice crystal.

The retention of the hexagonal geometry is one of the key features of the work carried out under the present Grant. Based on an integral equation approach, a numerical technique has been developed to compute the scattering patterns, and the scattering and absorption spectra for cylindrical dielectric shells of arbitrary cross sectional shape when illuminated by a plane wave of either principal polarization. The dielectric can be lossy, and by applying the method to infinitely long cylinders

hexagonal in cross section, scattering and absorption data have been generated applicable to hollow columnar (sheath) ice crystals in the infrared.

The method originated from a study of the scattering properties of resistive sheets and membranes (Knott and Senior, 1974) in which the non-zero thickness sheets were simulated by infinitesimally thin sheets of appropriate electromagnetic properties. Accordingly, a hexagonal shell cylinder whose actual walls are composed of a material of (complex) dielectric constant n, having thickness τ (small compared to the free space wavelength λ), is replaced by a hexagonal membrane having a complex relative resistivity

$$\frac{R}{Z} = \frac{i\lambda}{(n^2-1)2\pi\tau}$$

ohms per square. It is then possible to derive an integral equation for the current which an incident plane wave of either principal polarization induces in the membrane, and the integral equation is quite amenable to solution by digital techniques. The formulation of the equation and its subsequent solution constitute a significant contribution to the theory and application of integral equation methods to electromagnetic scattering and absorption problems. The mathematical details are given in the Appendix along with a listing of the computer programs employed in generating the data in this Report. For the most part the formulas are applicable for arbitrary angles of incidence, but the numerical results presented here are for broadside incidence only. The problem is then two-dimensional, and we now turn to a presentation and discussion of the data obtained.

2. Numerical Results

Our numerical results are given in the form of cross sections which are defined as follows. For a power density S incident on the cylinder, the bistatic scattering cross section is

$$\sigma(\theta) = 2\pi I/S$$

where I is the power scattered per unit length of the cylinder per unit angle about the direction θ and measured in the far field of the cylinder. The angle θ is defined so that $\theta = 0$ is in the backscattering direction and $\theta = \pi$ is in the forward. The total (or integrated) scattering cross section is then

$$\sigma_T = \frac{1}{2\pi} \int_0^{2\pi} \sigma(\theta) d\theta \ .$$

The absorbed power is measured by the absorption cross section

$$\sigma_A = \frac{1}{S} \text{(power absorbed)}$$

and the extinction cross section is the sum

$$\sigma_{ext} = \sigma_T + \sigma_A \ .$$

Formulas relating these two dimensional cross sections to the currents which are computed are given in the Appendix, eqs. (37) through (41).

The computations were carried out using the refractive indices $n = n_r + in_i$ for ice in the infrared wavelength range given by Irvine and Pollack (1968; hereafter referred to as IP) and Schaaf and Williams (1973; referred to as SW). Their data are plotted in Figs. 1 and 2 and show significant discrepancies in certain wavelength ranges. To obtain some idea of how sensitive the scattering is to the particular refractive index chosen, computations have been made at two wavelengths using the values from each reference.

For a given wavelength and perimeter of the hexagonal sheath, the scattering has been computed for the incident plane wave polarized with its electric

vector parallel to the axis of the cylinder (E polarization) and also with its magnetic vector parallel to the axis (H polarization). The directions of incidence and observation are always in a plane perpendicular to the axis, but for each polarization we have considered two directions of incidence corresponding to 'edge-on' and 'face-on' as regards the hexagon, viz.

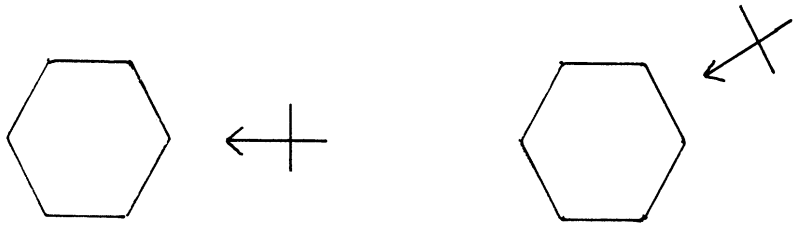

edge-on face-on

Most of the calculations have been for a hexagonal cylinder 3 μm on a side with a wall thickness $\tau = 0.1\ \mu$m. Only these data are presented here though we have carried out some exploratory calculations for other parameter values. Table 1 lists the wavelength, the corresponding refractive index and its source, the appropriate resistivity value and the Figure numbers where the computer-generated plot of the bistatic scattering versus θ can be found. Each of these Figures shows the data for edge-on and face-on incidence on the left and right respectively, with the intensity on top and the phase below. The phase is that of a scattered field component at a large (constant) distance from the axis of the cylinder and is shown relative to that of a line source on the axis. The intensity plotted is actually the dimensionless quantity $\sigma(\theta)/\lambda$ in dB. This particular normalization is convenient for computation and presentation purposes, but since $\sigma(\theta)$ is a very complicated function of λ (through, for example, the refractive index), it must be borne in mind that $\sigma(\theta)/\lambda$ is <u>not</u> a wavelength-independent quantity.

Spectral information is presented in Figs. 31 through 35 where $\sigma(0)$, $\sigma(\pi)$, σ_T, σ_A and σ_{ext} are plotted (in dB μm) versus λ. Note that the explicit factor λ has been removed, so that here the 'normalization' is relative to a micron (μm).

2.1 Angular Data

The curves in Figs. 3 through 30 are self explanatory. They clearly show

Table 1: Computed Data for Hexagonal (Shell) Cylinder
3 μm on side, 0.1 μm thick

$\lambda(\mu m)$	Pol.	n	Ref.	R/Z	Fig. No.
0.76	E	1.307	IP	i1.70784	3
	H				4
1.61	E	1.293 + i0.000365	IP	0.00536 + i3.81395	5
	H				6
2.0	E	1.291 + i0.00161	IP	0.02977 + i4.77438	
	H				
2.25	E	1.254 + i0.001	SW	0.02740 + i6.25466	7
	H				8
	E	1.278 + i0.000213	IP	0.00486 + i5.65462	
	H				
2.6	E	1.206 + i0.00080	IP	0.03876 + i9.10650	9
	H				10
2.8	E	1.152 + i0.0123	IP	13.5260 + i1.17250	11
	H				12
3.0	E	1.130 + i0.2273	IP	7.79740 + i3.41910	13
	H				14
	E	1.045 + i0.429	SW	5.26973 - i0.54082	15
	H				16
3.1	E	1.280 + i0.3252	IP	4.20510 + i2.69040	17
	H				18
3.3	E	1.530 + i0.0625	IP	0.55090 + i3.84930	19
	H				20
3.5	E	1.422 + i0.0163	IP	0.24680 + i5.44060	21
	H				22
8.0	E	1.312 + i0.045	SW	2.82939 + i17.23610	23
	H				24
9.0	E	1.269 + i0.043	SW	4.09006 + i22.80586	25
	H				26
11.0	E	1.093 + i0.242	SW	31.03981 + i7.98514	27
	H				28
12.5	E	1.387 + i0.422	SW	12.08921 + i7.70071	29
	H				30

how the number of maxima and minima in $0 \leqslant \theta \leqslant \pi$ increases with decreasing λ, and at wavelengths which are much longer than the side length of the hexagon, i.e. $\lambda \gtrsim 8\,\mu$m, the cross section has almost no angular structure. Changing the incidence from edge-on to face-on has most effect in the directions closest to backscattering, and we also note the substantial differences between the results for E and H polarizations.

2.2 Spectral Data

The particular cross sections $\sigma(0)$, $\sigma(\pi)$, σ_T, σ_A and σ_{ext} are shown as functions of λ in the infrared range in Figs. 31 through 35. Each Figure has two parts, covering the ranges 0.76 to 3.5 μm and 8 to 12.5 μm. Separate curves have been included wherever the results for edge-on and face-on incidence are clearly distinguishable. For the most part this is only with the backscattering cross section or for $\lambda \lesssim 1.5\,\mu$m, and in other cases the differences are confined to the immediate vicinity of local maxima or minima in the data.

In the shorter wavelength range most of the data were computed using the IP values for the refractive index. This range covers the main absorption band centered on $\lambda = 3\,\mu$m and a secondary one at $\lambda = 2\,\mu$m as seen in the IP data plotted in Fig. 2. The wavelengths close to these show the main discrepancies between the IP and SW data, and at $\lambda = 2.25$ and $3\,\mu$m we therefore ran computations using both sets. The different refractive indices at $\lambda = 2.25\,\mu$m do indeed produce substantial differences in the cross sections, and because of this sensitivity, we have not extended our detailed computations through the third absorption band centered at $\lambda \simeq 1.25\,\mu$m in the IP data. For $\lambda < 1.61\,\mu$m the scattering has been computed only at the single wavelength $\lambda = 0.76\,\mu$m of interest for a particular application. Since the IP data are given only for $\lambda \geqslant 0.95\,\mu$m, the necessary refractive index was obtained by extrapolation.

The SW data for the refractive index were used in the longer wavelength range $8.0 \leqslant \lambda \leqslant 12.5\,\mu$m.

The geometrical effects are particularly pronounced for $0.76 \leqslant \lambda \leqslant 3.5\,\mu$m. This is not surprising since the dimensions of the cylinder are then comparable to

the wavelength, or are low multiples thereof, and this is the region where resonance effects and other interactions between the various contributors to the scattering are most important. As an example, while σ_A has a strong local maximum near the maximum in n_i at $\lambda = 3.075\ \mu m$, the shape and overall width of the maximum in σ_A is apparently affected by the side length of the hexagon being close to this wavelength. $\sigma(0)$ and $\sigma(\pi)$ both show a corresponding drop in this absorption region. The behavior is quite different near the secondary maximum in n_i at $\lambda = 2\ \mu m$. For H-polarization but not for E, σ_A is large as expected, while $\sigma(0)$ and $\sigma(\pi)$ have local maxima for λ just above 2 μm with both polarizations.

Further evidence for the way in which a geometrical effect can dominate a material absorption effect can be found by comparing the absorption cross sections at 2.25 μm computed from the IP and SW data. At this wavelength the SW value for n_i is roughly five times the IP value, with n_r almost equal in both listings, but the SW value produced an absorption cross section which is about eleven times less than that given by the IP value for the refractive index.

It is therefore obvious that any predictions of absorption and scattering based only on the properties of the material of which the scatterer is composed may be considerably in error.

3. Conclusions and Suggestions for Future Work

In this Report we have derived the theoretical basis for determining the scattering and absorption of electromagnetic radiation by thin-walled cylinders of infinite length and arbitrary cross sectional shape. Numerical procedures have been developed and have been used to obtain data for hexagonal cylinders which model sheath crystals of the type found in cirrus clouds. The procedures are economical for cylinders whose cross sections are not more than about 15 wavelengths in perimeter, with the cost decreasing rapidly with decreasing size.

For wavelengths comparable to or less than the face length of the hexagon, the results (particularly for the back scattering) are quite sensitive to the polarization and direction of the incident plane wave, i.e. on whether the field is incident edge-on or face-on as shown on p.6. At any given wavelength, the results can also be very sensitive to the refractive index employed. Geometric effects can so influence the absorption that it is not at all safe to assume that the absorption versus wavelength curve will follow that of the imaginary part of the refractive index.

The time available for the present study did not permit an adequate investigation of the effect of wall thickness, nor allow us to do a detailed comparison of the results with those of the Mie-type series for hollow cylinders circular in cross section. Although our data for the bistatic scattering cross section versus angle are somewhat similar to those previously published (Liou, 1972a) for solid circular cylinders at near broadside incidence, data showing the precise role played by the geometry should have a high priority in any future continuation of the study. With only minor modifications our computer programs can also handle irregular additions to the hexagonal surface, thereby simulating rimed crystals, and allowing us to compute the effects of riming. Since the theory for non-broadside incidence has been derived, we would also like to develop the computer programs necessary to obtain numerical data in this more general case, and once these types of data are in hand, it would be possible and desirable to examine the forms of averaging that could simplify the practical applicability of the data without losing its essential properties.

REFERENCES

ARWG, (1972), "Major problems in atmospheric radiation: An evaluation and recommendations for future efforts," Bull. Amer. Meteo. Soc., 53, 950-956.

Aufm Kampe, H.J. and Weickman, H.K., (1957), "Physics of clouds," in Meteorological Research Reviews, Summaries of Progress from 1951-1955, 3

Appleman, H.S., (1966), "Effect of supersonic aircraft on cirrus formation and climate," AMS/AIAA Conf. on Aerospace Meteorology, Paper No. 66-369.

Bateman, H., (1915), Electrical and Optical Wave Motion, Cambridge University Press, p. 19.

Cox, Stephen K., (1971), "Cirrus clouds and the climate," J. Atmos. Sci., 28, 1513-1515.

Fritz, S. and Krishna, P. Rao, (1971), "On the infrared transmission through cirrus clouds and the estimation of relative humidity from satellites," J. Appl. Meteo., 6, 1088-1096.

Grams, G.W., (1975), "Lidar: Some current uses and potential applications in the atmospheric sciences," Atmospheric Technology (NCAR), Winter 1974-1975.

Heymsfield, A.J. and Knollenberg, R.G., (1972), "Properties of cirrus generating cells," J. Atmos. Sciences, 29, 1358-1366.

Holland, A.C. and Gagné, G., (1970), "The scattering of polarized light by polydisperse systems of irregular particles," Applied Optics, 9, 1113-1173.

Irvine, Wm.M. and Pollack, J.B., (1968), "Infrared optical properties of water and ice spheres," Icarus, 8, 324-360.

Jacobowitz, H., (1971), "A method for computing the transfer of solar radiation through clouds of hexagonal ice crystals," J. Quant. Spectrosc. Radiat. Transfer, 11, 691-695.

Kattawar, George W. and Plass, Gilbert N., (1972), "Degree and direction of polarization of multiple scattered light. 1. Homogeneous cloud layers," Applied Optics, 11, 2851-2865.

Knott, E.F. and T.B.A. Senior (1974), "Non-specular radar cross section study," University of Michigan Radiation Laboratory Report 0110764-1-T (AFAL-TR-73-422).

Liepa, Valdis V. et al., (1974), "Scattering from two-dimensional bodies with absorber sheets," University of Michigan Radiation Laboratory Report 0110764-2-T (AFAL-TR-74-119).

Liou, Kuo-Nan, (1972a), "Electromagnetic scattering by arbitrarily oriented ice cylinders," Appl. Optics, 11, 667-674.

Liou, Kuo-Nan, (1972b), "Light scattering by ice clouds in the visible and infrared: A theoretical study," J. Atmos. Sci., 29, 524-536.

Mossop, S.C. and Ono, A., (1969), "Measurements of ice crystal concentration in clouds," J. Atmos. Sci., 26, 130-137.

Ono, A., (1969), "The shape and riming properties of ice crystals in natural clouds," J. Atmos. Sci., 26, 138-147.

Plass, Gilbert N., Kattawar, George W., and Catchings, Frances E., (1973), "Matrix operator theory of radiative transfer Rayleigh scattering," Applied Optics, 12, 314-328.

Poggio, A.J. and E.K. Miller (1973), "Integration equation solutions of three-dimensional scattering problems," in Computer Techniques for Electromagnetics (ed. R. Mittra), Pergamon Press, New York.

Reinking, R., (1968), "Insolation reduction by contrails," Weather, 23, 171-173.

Schaaf, Joel W. and Williams, Dudley, (1973), "Optical constants of ice in the infrared," J. Optical Soc. of America, 63, 726-732.

Senior, T.B.A., (1975), "The spherical cavity problem," the Air Force Weapons Laboratory Interaction Notes, Note 220.

Stratton, J.A., Electromagnetic Theory, Mc-Graw-Hill Book Co., New York, 1941.

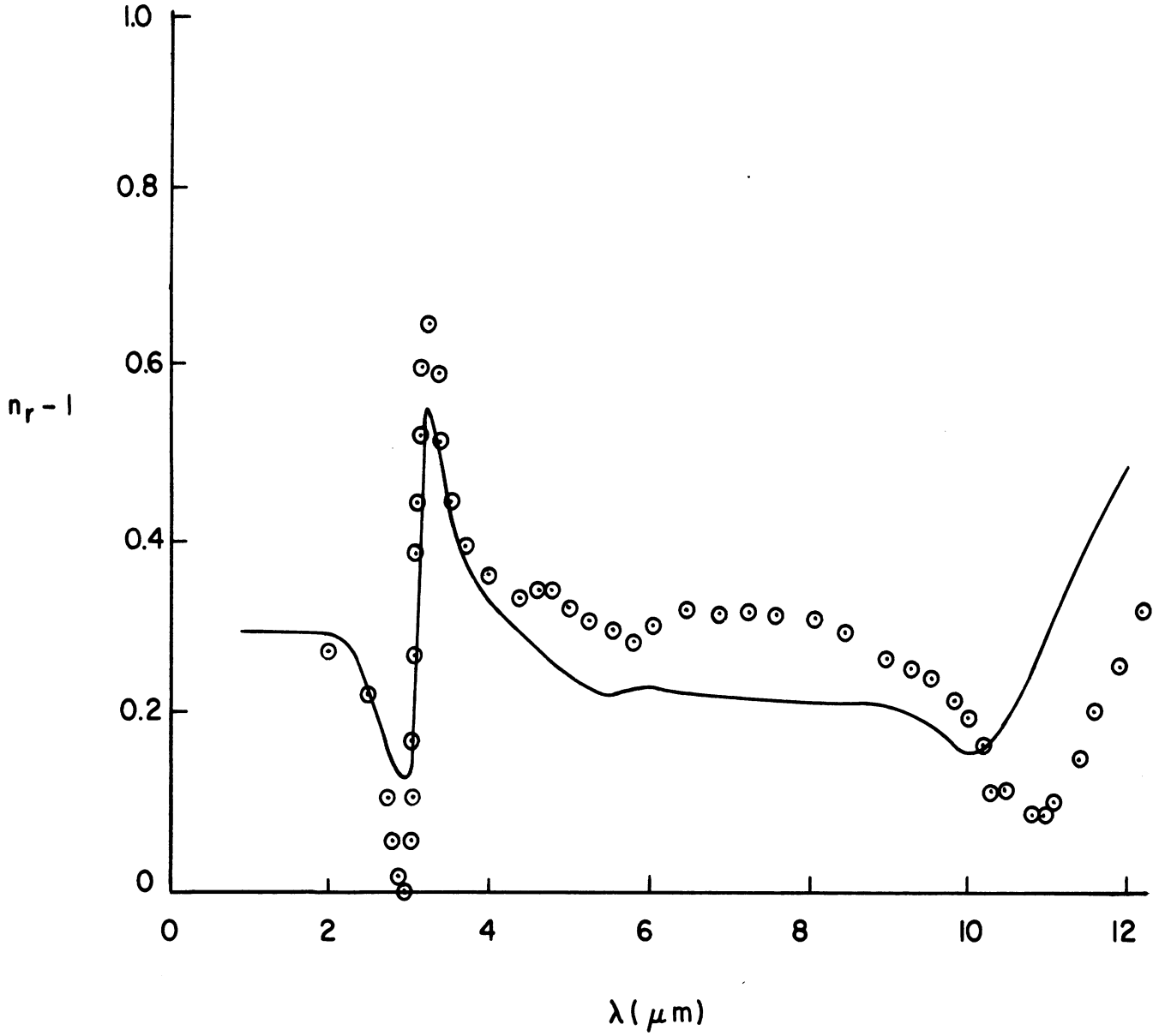

Fig. 1: Data for the (reduced) real part of the refractive index of ice:
___ (Irvine and Pollack, 1968), • • • (Schaaf and Williams, 1973).

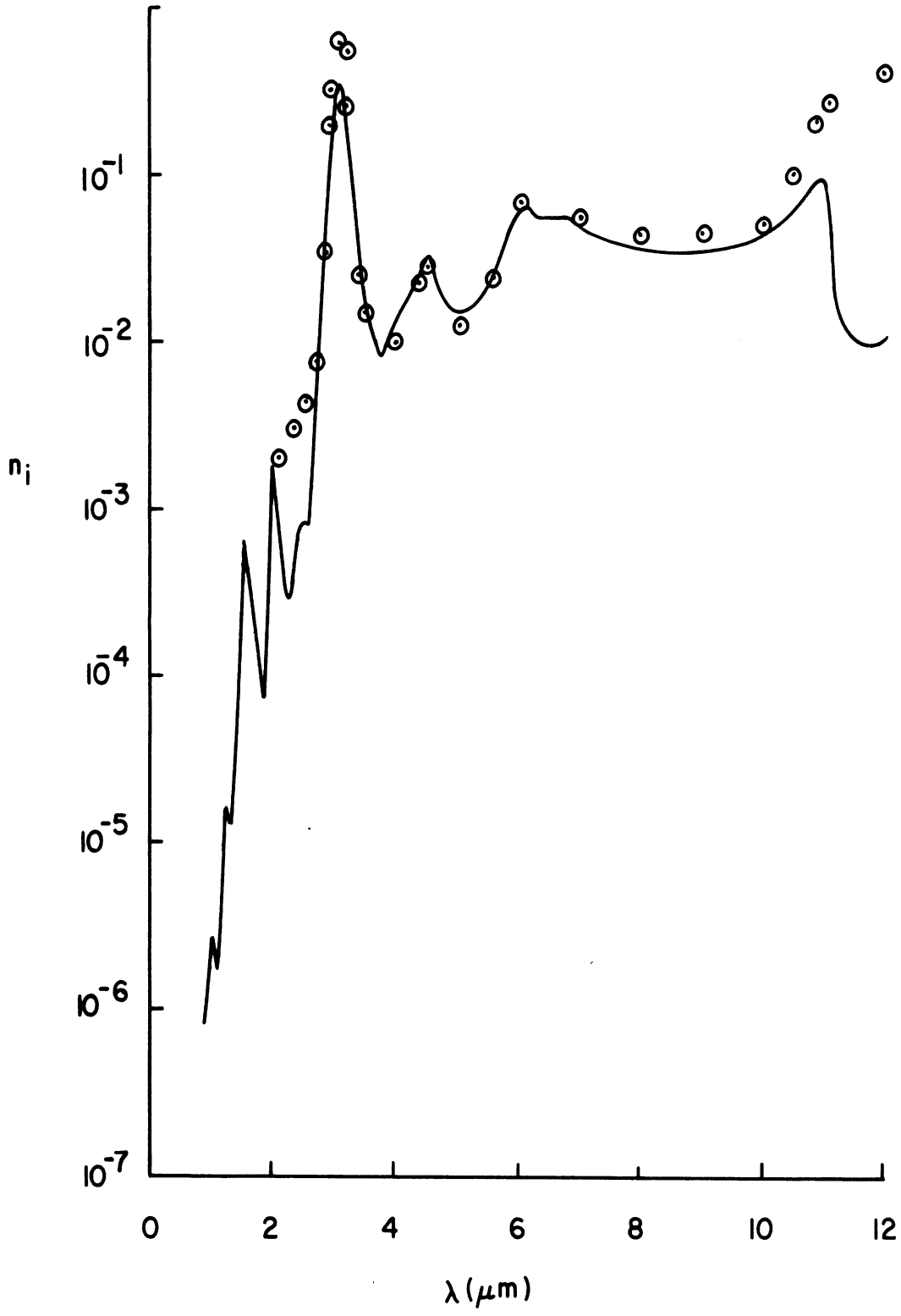

Fig. 2: Data for the imaginary part of the refractive index of ice: —— (Irvine and Pollack, 1968), • • • (Schaaf and Williams, 1973).

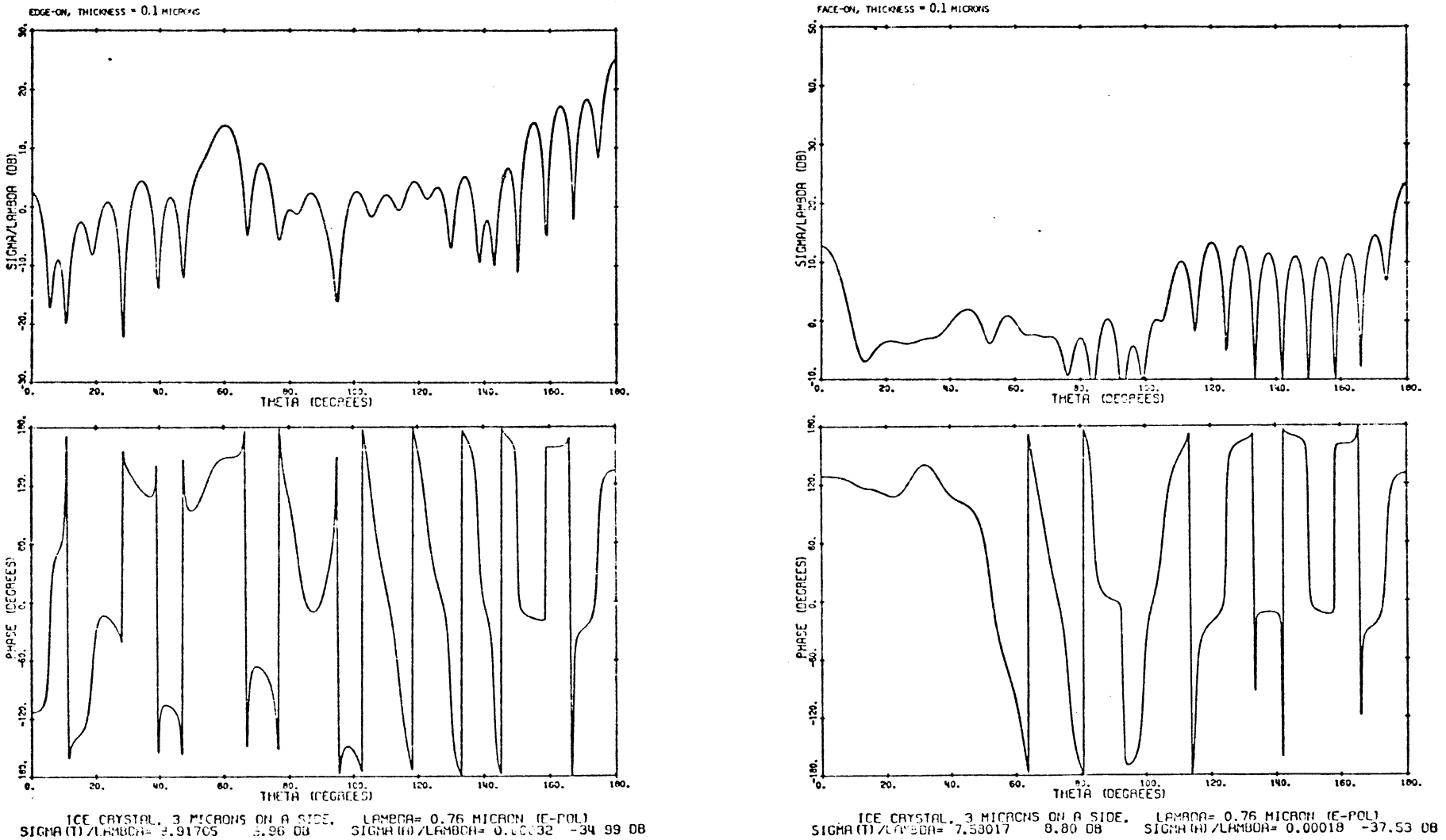
EDGE-ON, THICKNESS = 0.1 MICRONS
SIGMA/LAMBDA (DB)
THETA (DEGREES)
PHASE (DEGREES)
THETA (DEGREES)
ICE CRYSTAL, 3 MICRONS ON A SIDE. LAMBDA= 0.76 MICRON (E-POL)
SIGMA(T)/LAMBDA= 9.91705 9.96 DB SIGMA(N)/LAMBDA= 0.00032 -34.99 DB
FACE-ON, THICKNESS = 0.1 MICRONS
SIGMA/LAMBDA (DB)
THETA (DEGREES)
PHASE (DEGREES)
THETA (DEGREES)
ICE CRYSTAL, 3 MICRONS ON A SIDE. LAMBDA= 0.76 MICRON (E-POL)
SIGMA(T)/LAMBDA= 7.58017 8.80 DB SIGMA(N)/LAMBDA= 0.00018 -37.53 DB

Fig. 3

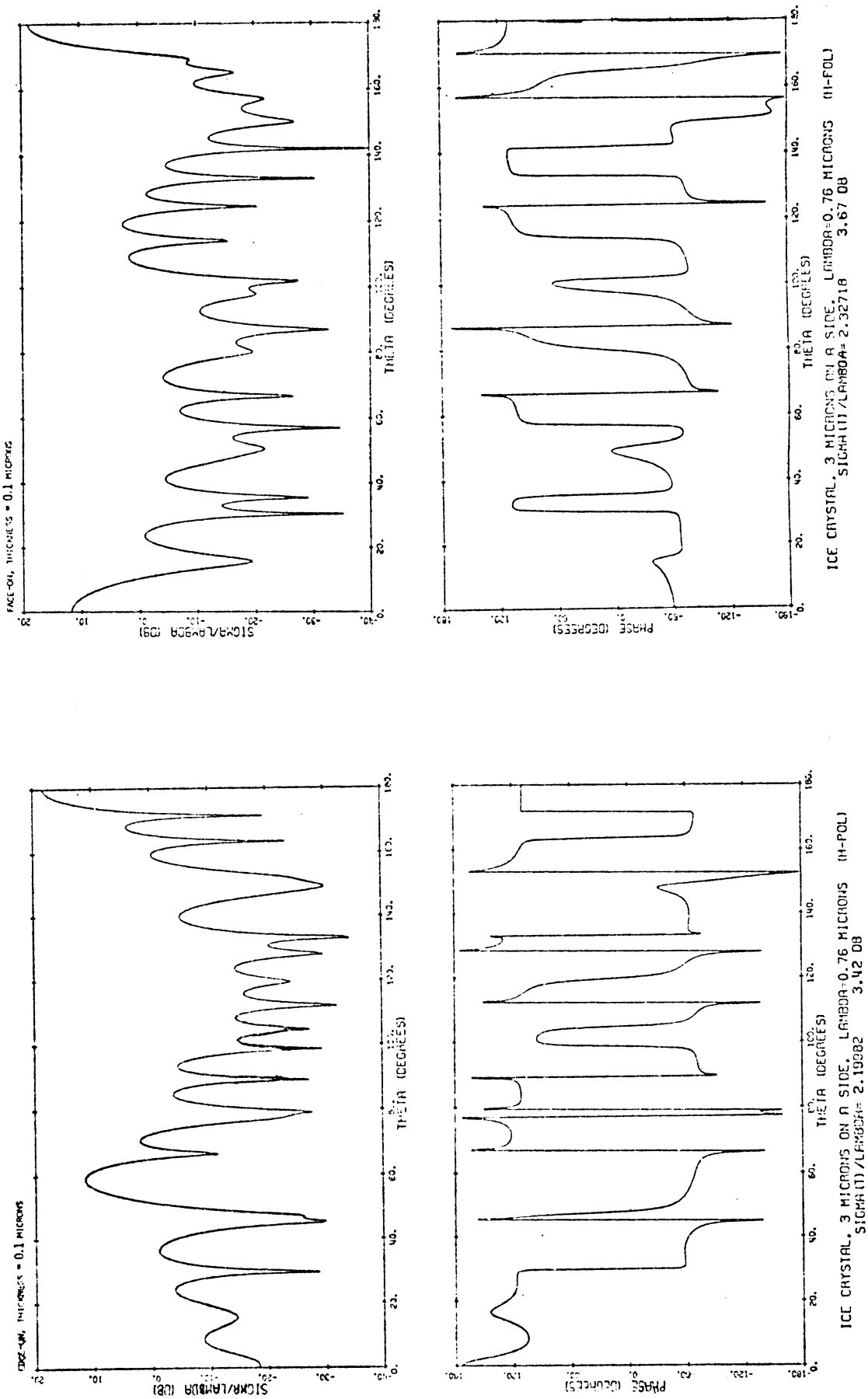
FACE-ON, THICKNESS = 0.1 MICRONS
SIGMA/LAMBDA (DB)
THETA (DEGREES)
PHASE (DEGREES)
ICE CRYSTAL, 3 MICRONS ON A SIDE, LAMBDA=0.76 MICRONS (H-POL)
SIGMA(I)/LAMBDA= 2.19382 3.42 DB
ICE CRYSTAL, 3 MICRONS ON A SIDE, LAMBDA=0.76 MICRONS (H-POL)
SIGMA(I)/LAMBDA= 2.32718 3.67 DB

Fig. 4

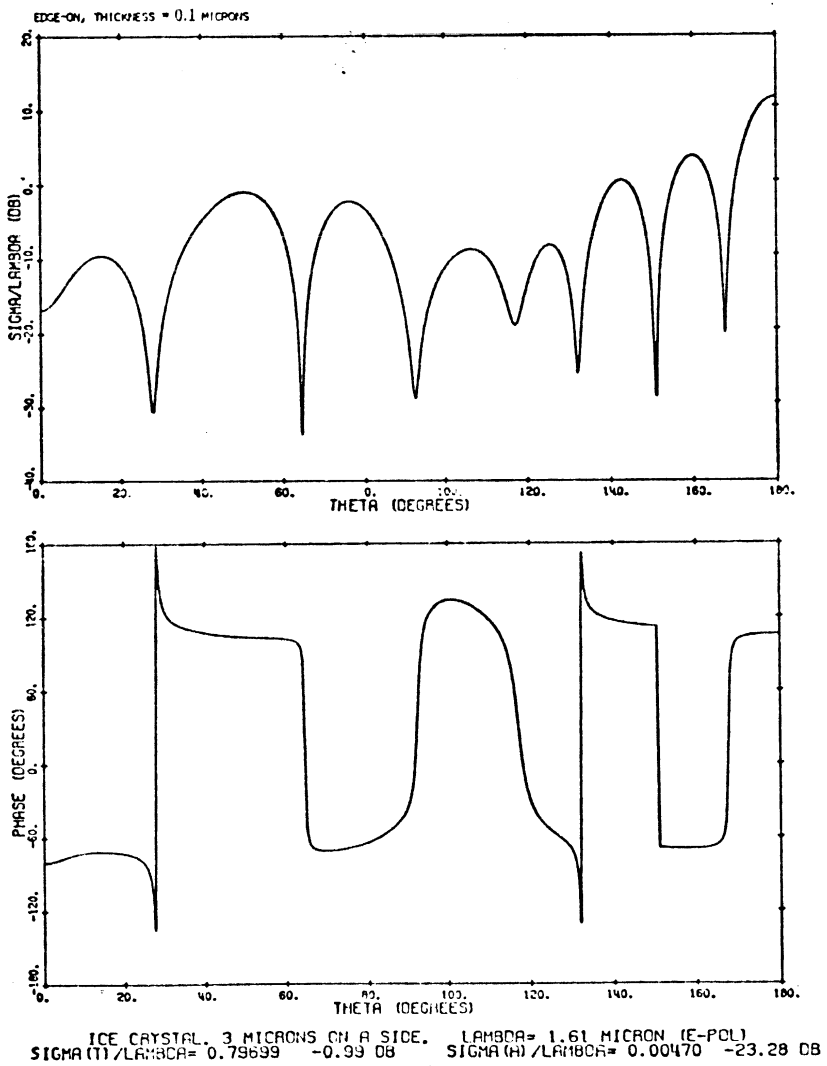
EDGE-ON, THICKNESS = 0.1 MICRONS
SIGMA/LAMBDA (DB)
THETA (DEGREES)
PHASE (DEGREES)
THETA (DEGREES)
ICE CRYSTAL. 3 MICRONS ON A SIDE. LAMBDA= 1.61 MICRON (E-POL)
SIGMA(T)/LAMBDA= 0.79699 -0.99 DB SIGMA(A)/LAMBDA= 0.00470 -23.28 DB

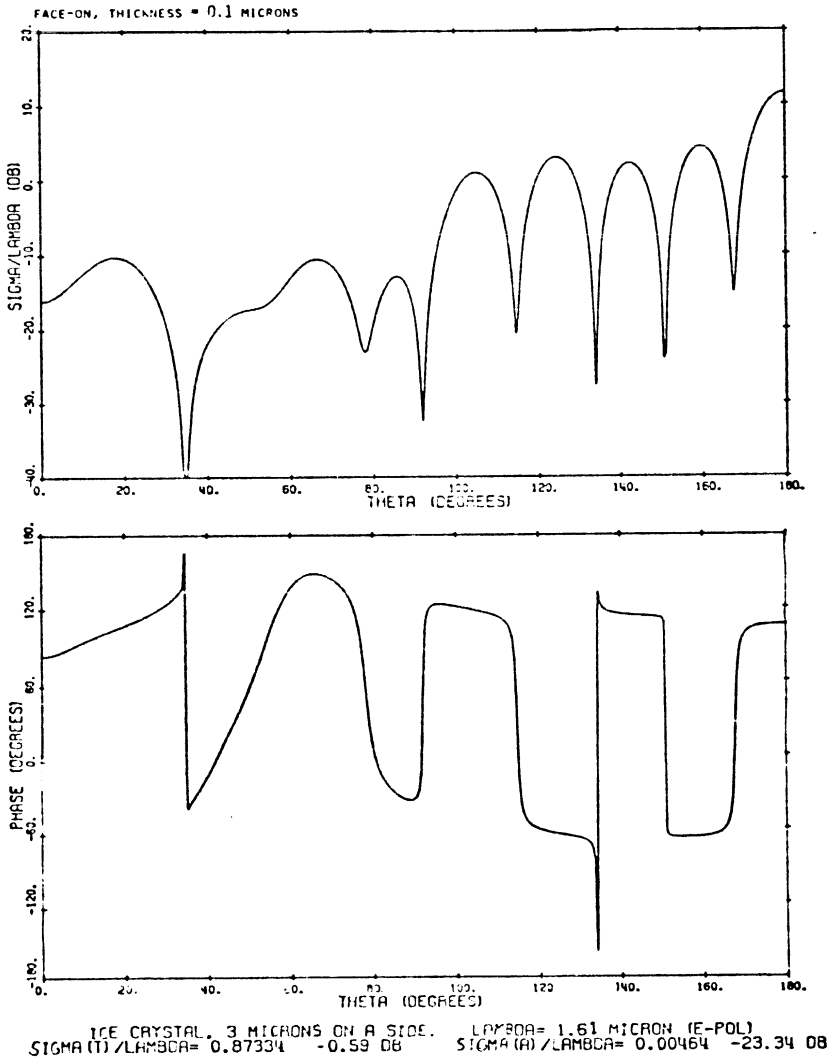
FACE-ON, THICKNESS = 0.1 MICRONS
SIGMA/LAMBDA (DB)
THETA (DEGREES)
PHASE (DEGREES)
THETA (DEGREES)
ICE CRYSTAL. 3 MICRONS ON A SIDE. LAMBDA= 1.61 MICRON (E-POL)
SIGMA(T)/LAMBDA= 0.87334 -0.59 DB SIGMA(A)/LAMBDA= 0.00464 -23.34 DB

Fig. 5

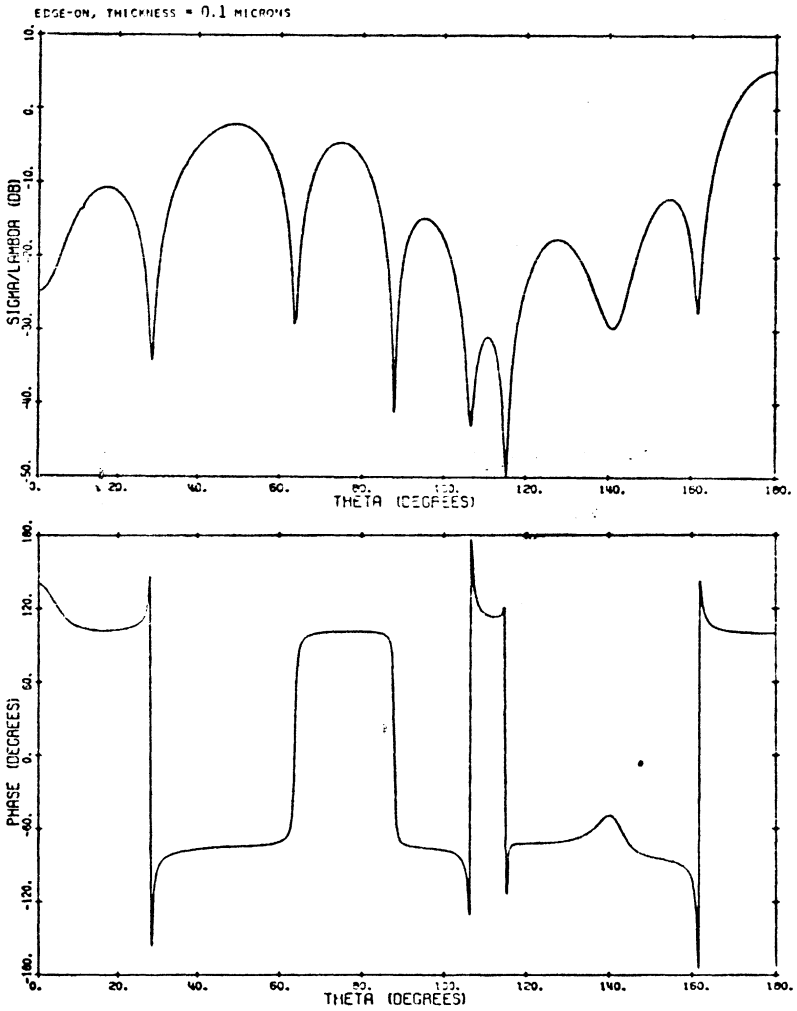

ICE CRYSTAL, 3 MICRONS ON A SIDE. LAMBDA= 1.61 MICRON (H-POL)
SIGMA(T)/LAMBDA= 0.24004 -6.20 DB SIGMA(A)/LAMBDA= 0.00336 -30.63 DB

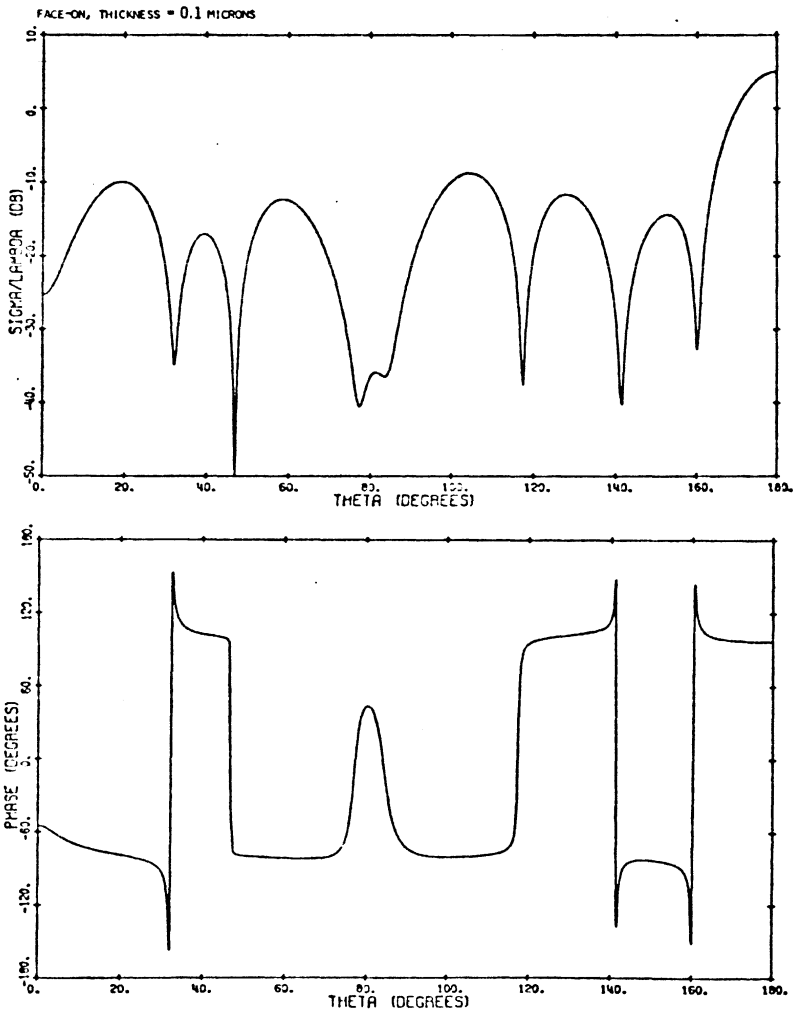

ICE CRYSTAL, 3 MICRONS ON A SIDE. LAMBDA= 1.61 MICRON (H-POL)
SIGMA(T)/LAMBDA= 0.17285 -7.62 DB SIGMA(A)/LAMBDA= 0.00182 -27.39 DB

Fig. 6

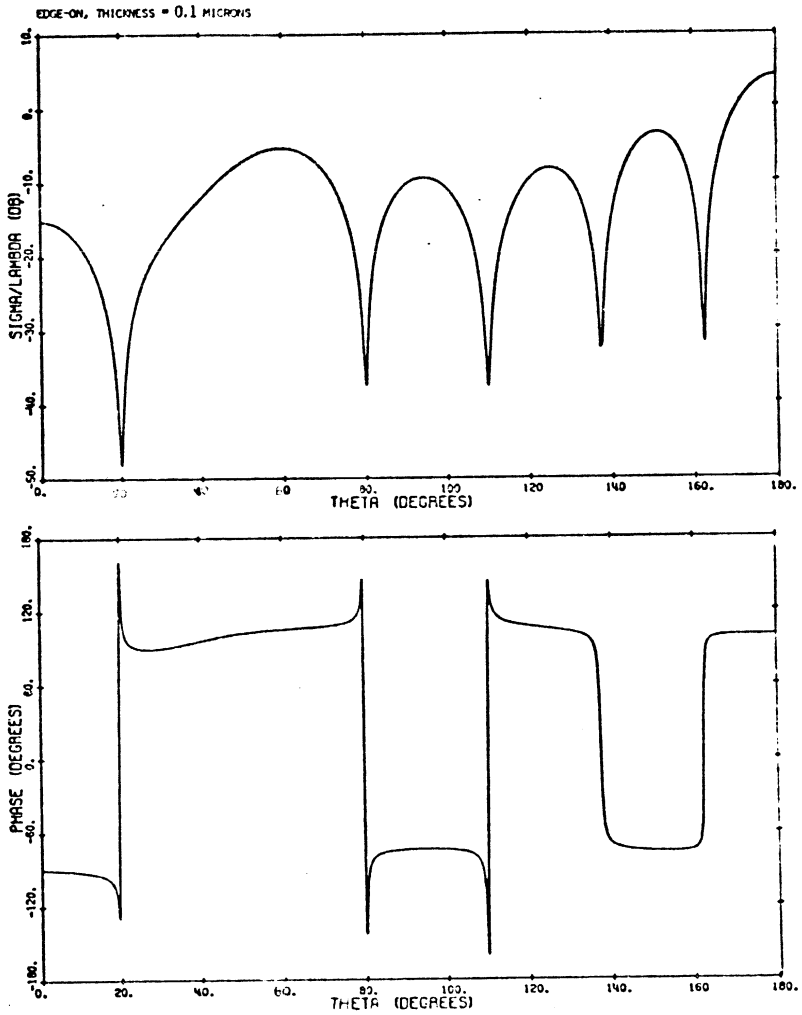

ICE CRYSTAL, 3 MICRONS ON A SIDE. LAMBDA= 2.25 MICRON (E-POL)
SIGMA(T)/LAMBDA= 0.21646 -6.65 DB SIGMA(A)/LAMBDA= 0.00585 -22.33 DB

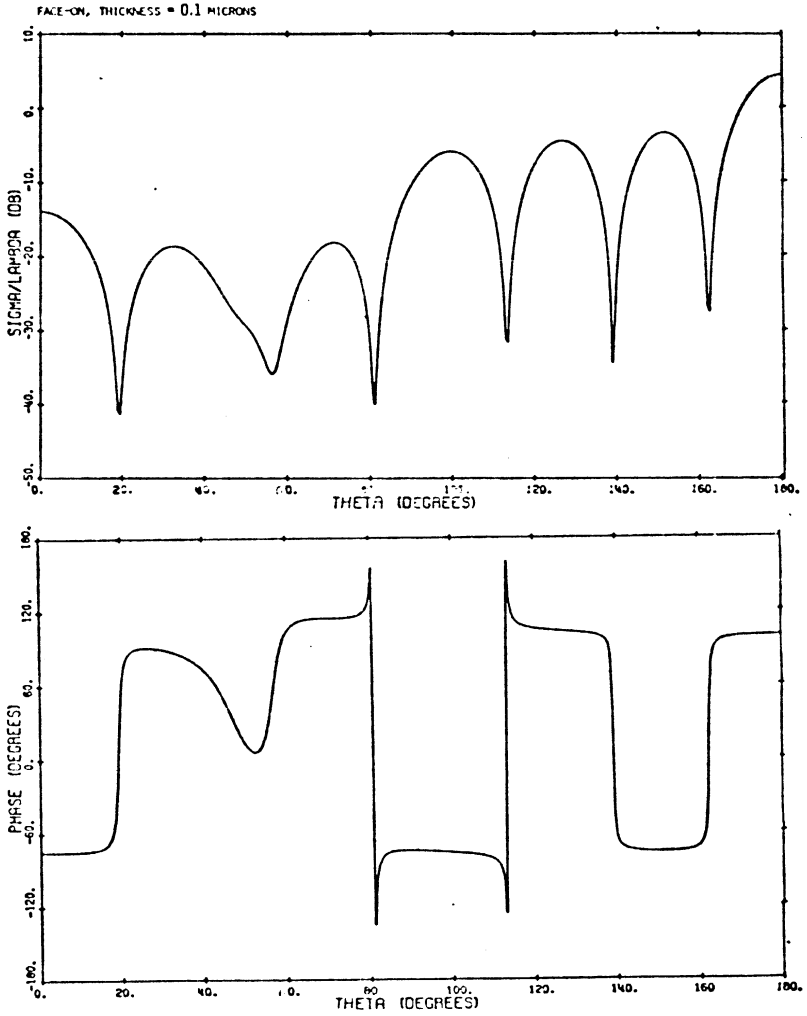

ICE CRYSTAL, 3 MICRONS ON A SIDE. LAMBDA= 2.25 MICRON (E-POL)
SIGMA(T)/LAMBDA= 0.21207 -6.74 DB SIGMA(A)/LAMBDA= 0.00616 -22.10 DB

Fig. 7

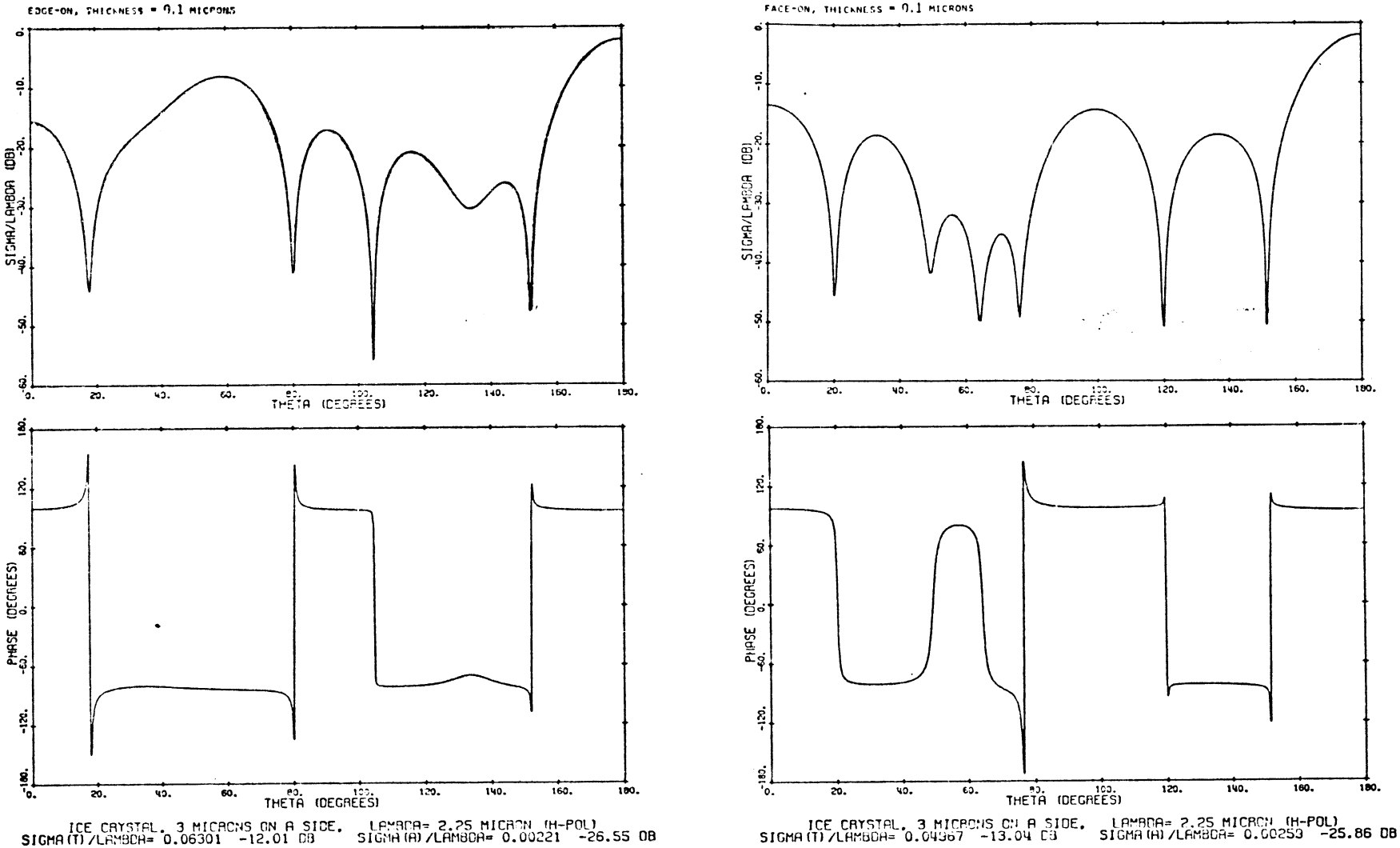

ICE CRYSTAL, 3 MICRONS ON A SIDE, LAMBDA= 2.25 MICRON (H-POL)
SIGMA(T)/LAMBDA= 0.06301 -12.01 DB SIGMA(A)/LAMBDA= 0.00221 -26.55 DB

ICE CRYSTAL, 3 MICRONS ON A SIDE, LAMBDA= 2.25 MICRON (H-POL)
SIGMA(T)/LAMBDA= 0.04967 -13.04 DB SIGMA(A)/LAMBDA= 0.00259 -25.86 DB

Fig. 8

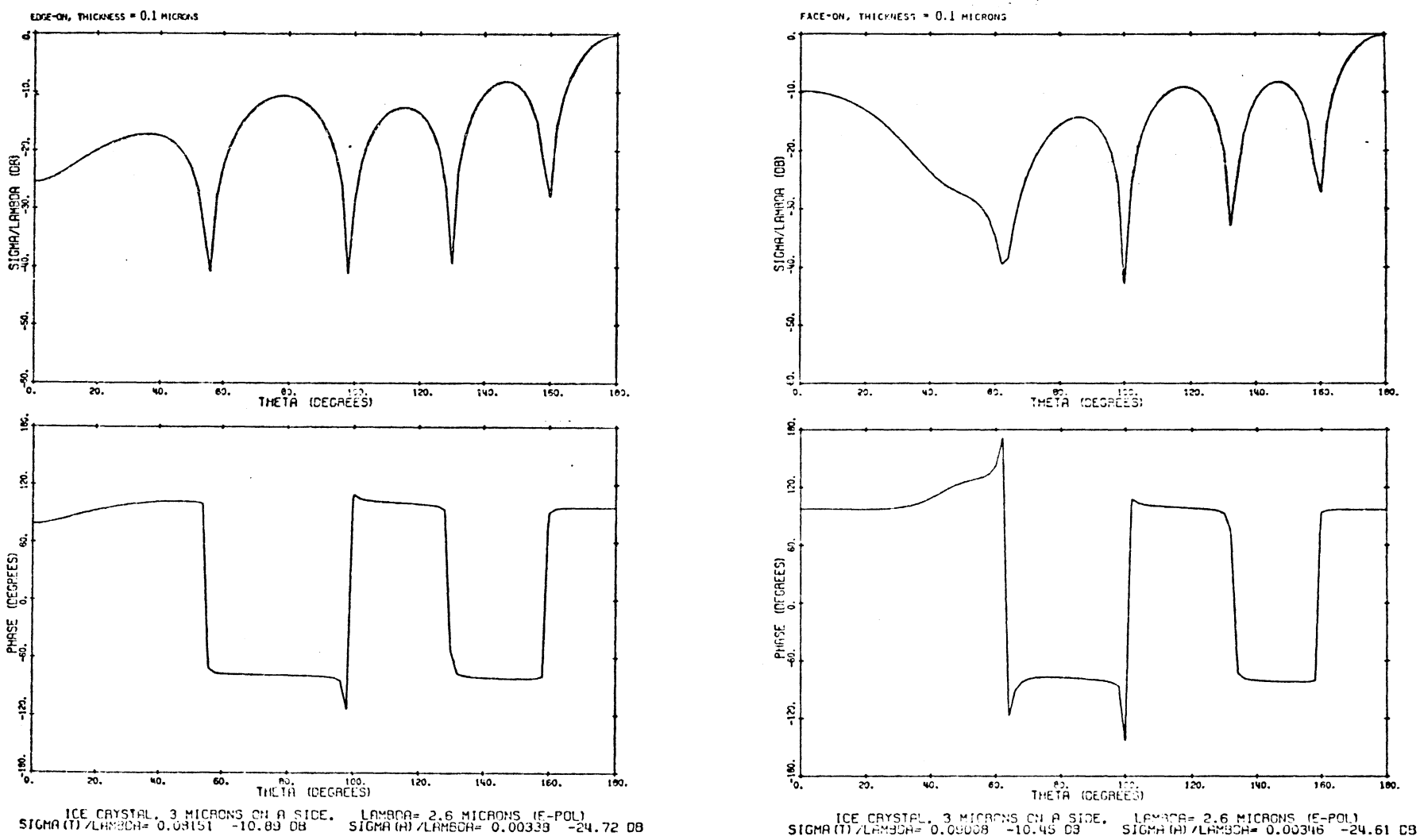
EDGE-ON, THICKNESS = 0.1 MICRONS
SIGMA/LAMBDA (DB)
THETA (DEGREES)
PHASE (DEGREES)
THETA (DEGREES)
ICE CRYSTAL, 3 MICRONS ON A SIDE. LAMBDA= 2.6 MICRONS (E-POL)
SIGMA(T)/LAMBDA= 0.08151 -10.89 DB SIGMA(A)/LAMBDA= 0.00338 -24.72 DB
FACE-ON, THICKNESS = 0.1 MICRONS
SIGMA/LAMBDA (DB)
THETA (DEGREES)
PHASE (DEGREES)
THETA (DEGREES)
ICE CRYSTAL, 3 MICRONS ON A SIDE. LAMBDA= 2.6 MICRONS (E-POL)
SIGMA(T)/LAMBDA= 0.09008 -10.45 DB SIGMA(A)/LAMBDA= 0.00346 -24.61 DB

Fig. 9

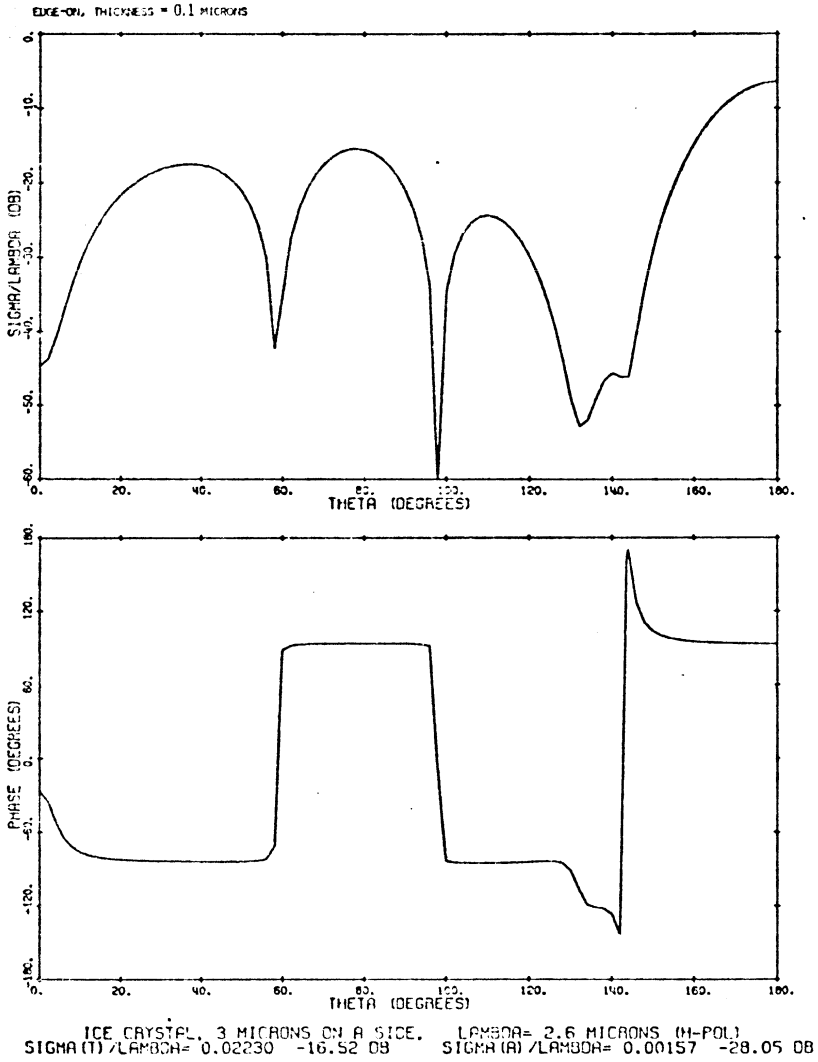
EDGE-ON, THICKNESS = 0.1 MICRONS
SIGMA/LAMBDA (DB)
THETA (DEGREES)
PHASE (DEGREES)
THETA (DEGREES)
ICE CRYSTAL, 3 MICRONS ON A SIDE, LAMBDA= 2.6 MICRONS (H-POL)
SIGMA(T)/LAMBDA= 0.02230 -16.52 DB SIGMA(A)/LAMBDA= 0.00157 -28.05 DB

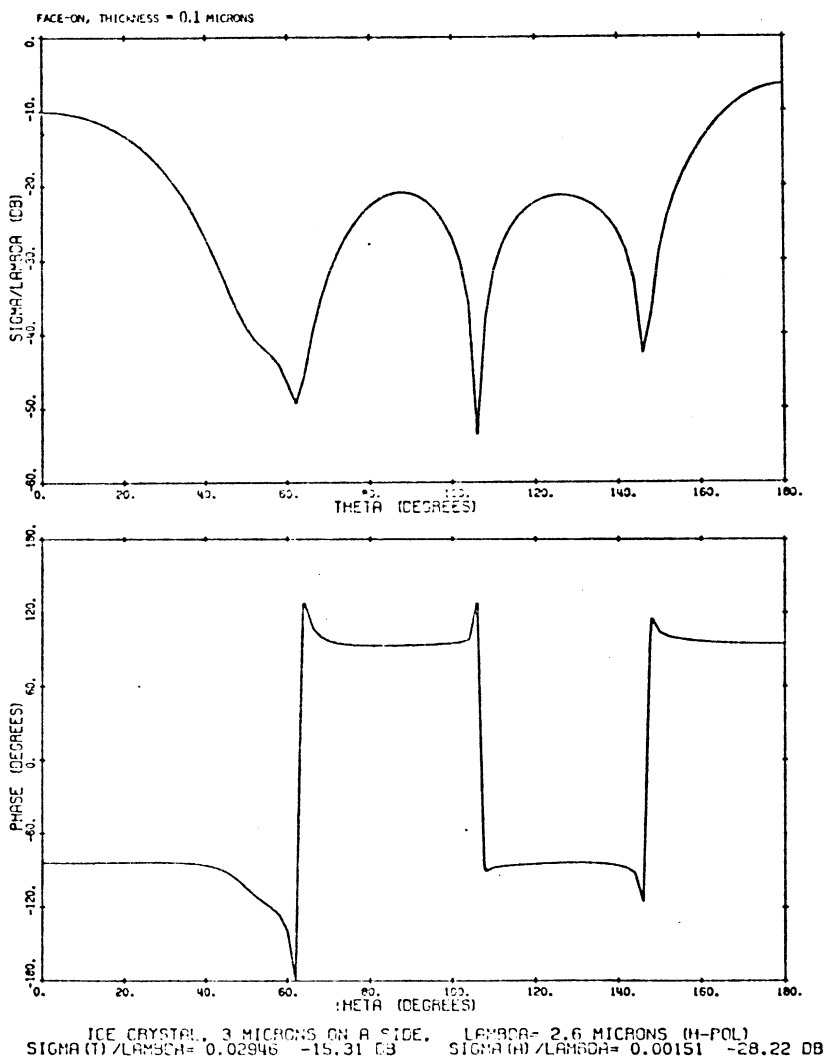
FACE-ON, THICKNESS = 0.1 MICRONS
SIGMA/LAMBDA (DB)
THETA (DEGREES)
PHASE (DEGREES)
THETA (DEGREES)
ICE CRYSTAL, 3 MICRONS ON A SIDE, LAMBDA= 2.6 MICRONS (H-POL)
SIGMA(T)/LAMBDA= 0.02946 -15.31 DB SIGMA(A)/LAMBDA= 0.00151 -28.22 DB

Fig. 10

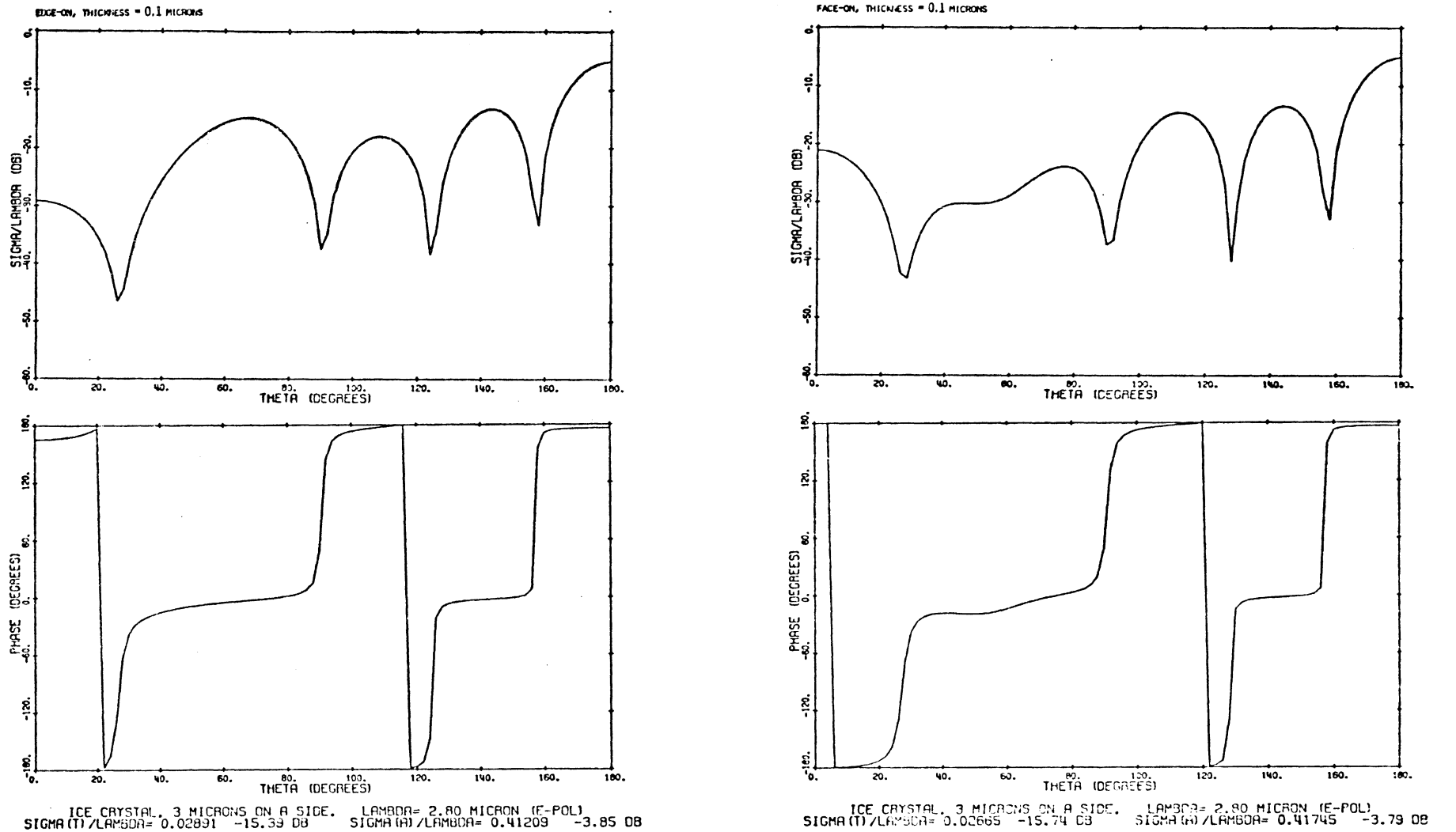
EDGE-ON, THICKNESS = 0.1 MICRONS
SIGMA/LAMBDA (DB)
THETA (DEGREES)
PHASE (DEGREES)
THETA (DEGREES)
ICE CRYSTAL, 3 MICRONS ON A SIDE. LAMBDA= 2.80 MICRON (E-POL)
SIGMA(T)/LAMBDA= 0.02891 -15.39 DB SIGMA(A)/LAMBDA= 0.41209 -3.85 DB
FACE-ON, THICKNESS = 0.1 MICRONS
SIGMA/LAMBDA (DB)
THETA (DEGREES)
PHASE (DEGREES)
THETA (DEGREES)
ICE CRYSTAL, 3 MICRONS ON A SIDE. LAMBDA= 2.80 MICRON (E-POL)
SIGMA(T)/LAMBDA= 0.02665 -15.74 DB SIGMA(A)/LAMBDA= 0.41745 -3.79 DB

Fig. 11

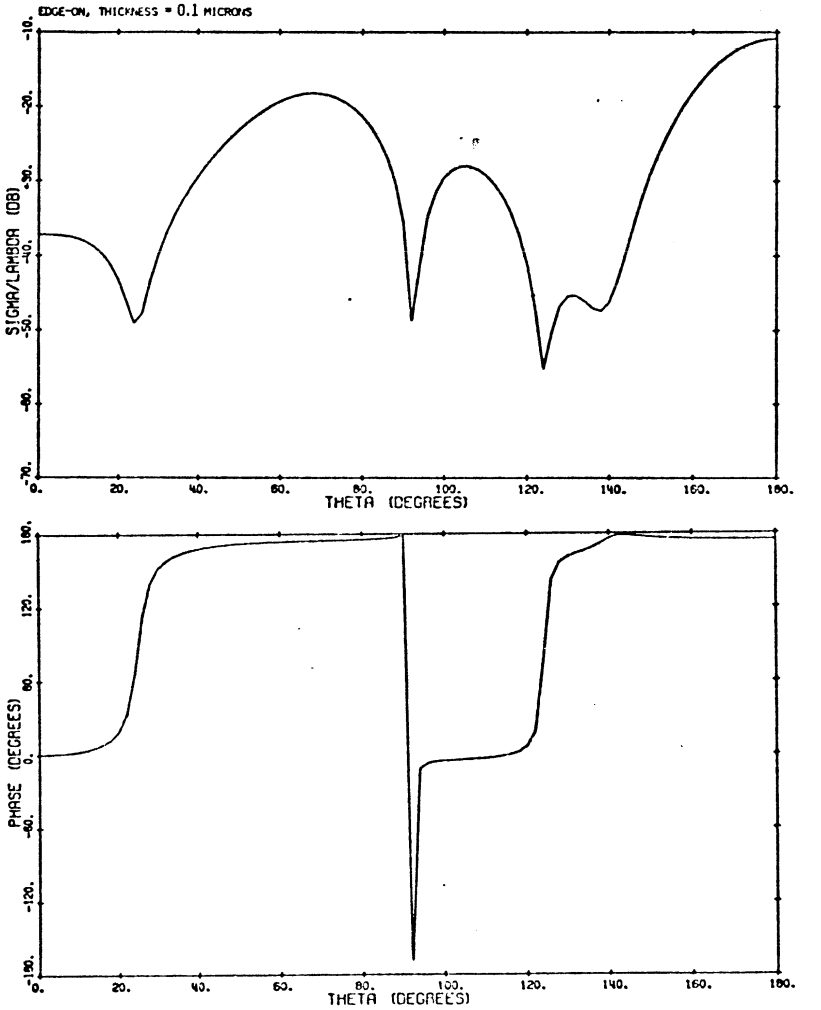

ICE CRYSTAL, 3 MICRONS ON A SIDE. LAMBDA= 2.80 MICRON (H-POL)
SIGMA(T)/LAMBDA= 0.00863 -20.64 DB SIGMA(A)/LAMBDA= 0.21783 -6.62 DB

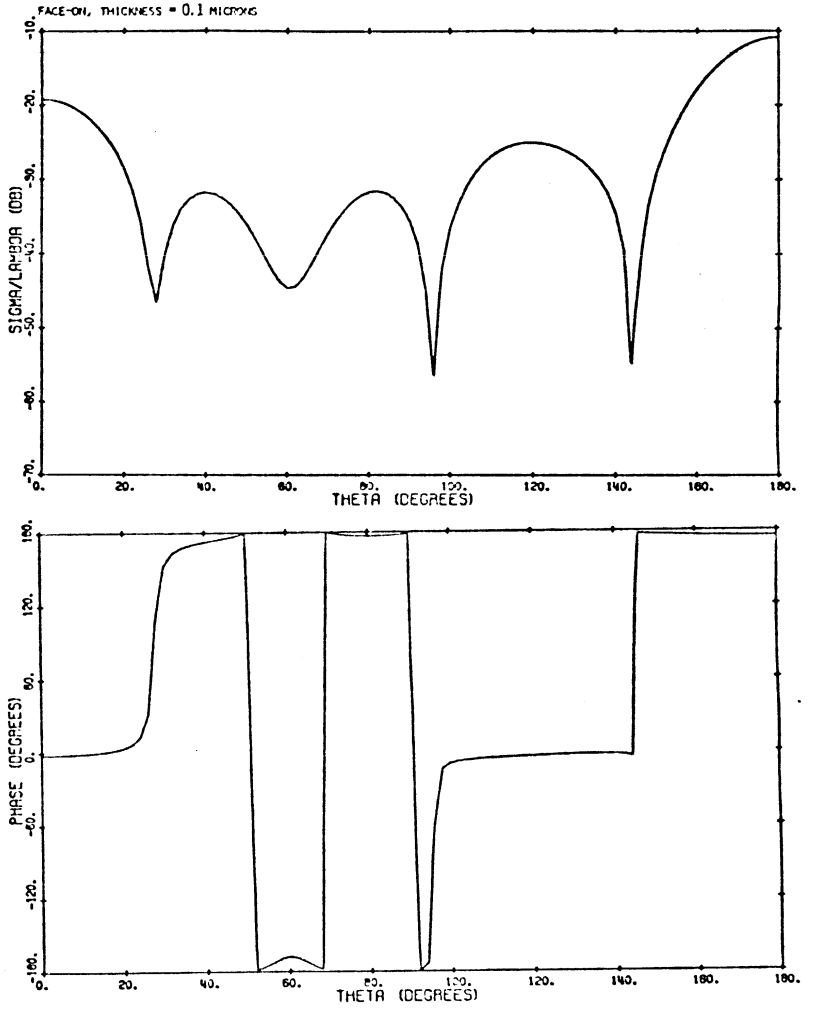

ICE CRYSTAL, 3 MICRONS ON A SIDE. LAMBDA= 2.80 MICRON (H-POL)
SIGMA(T)/LAMBDA= 0.00776 -21.10 DB SIGMA(A)/LAMBDA= 0.21999 -6.58 DB

Fig. 12

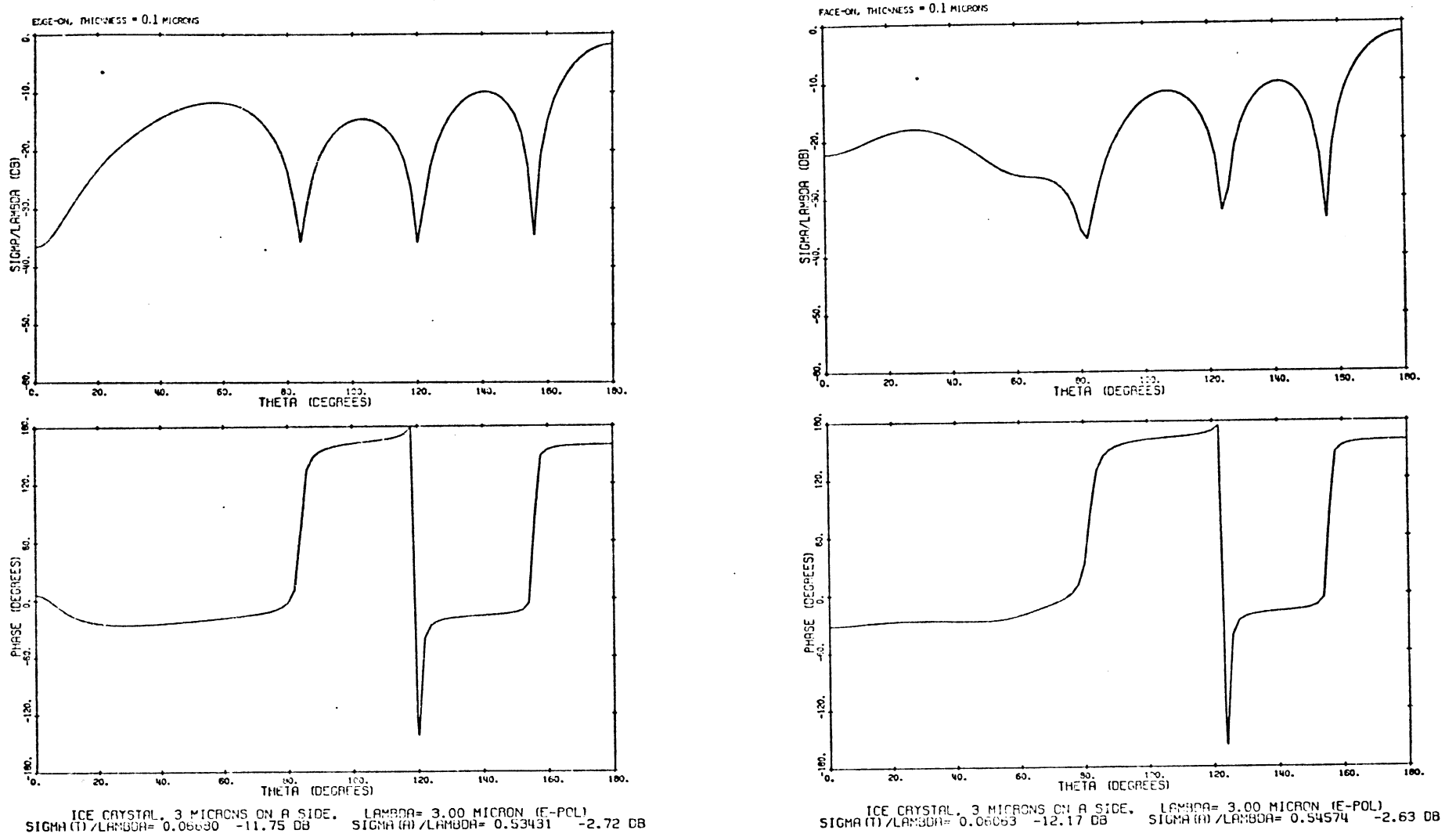
EDGE-ON, THICKNESS = 0.1 MICRONS
SIGMA/LAMBDA (DB)
THETA (DEGREES)
PHASE (DEGREES)
THETA (DEGREES)
ICE CRYSTAL, 3 MICRONS ON A SIDE. LAMBDA= 3.00 MICRON (E-POL)
SIGMA(T)/LAMBDA= 0.06630 -11.75 DB SIGMA(A)/LAMBDA= 0.53431 -2.72 DB
FACE-ON, THICKNESS = 0.1 MICRONS
SIGMA/LAMBDA (DB)
THETA (DEGREES)
PHASE (DEGREES)
THETA (DEGREES)
ICE CRYSTAL, 3 MICRONS ON A SIDE. LAMBDA= 3.00 MICRON (E-POL)
SIGMA(T)/LAMBDA= 0.06063 -12.17 DB SIGMA(A)/LAMBDA= 0.54574 -2.63 DB

Fig. 13

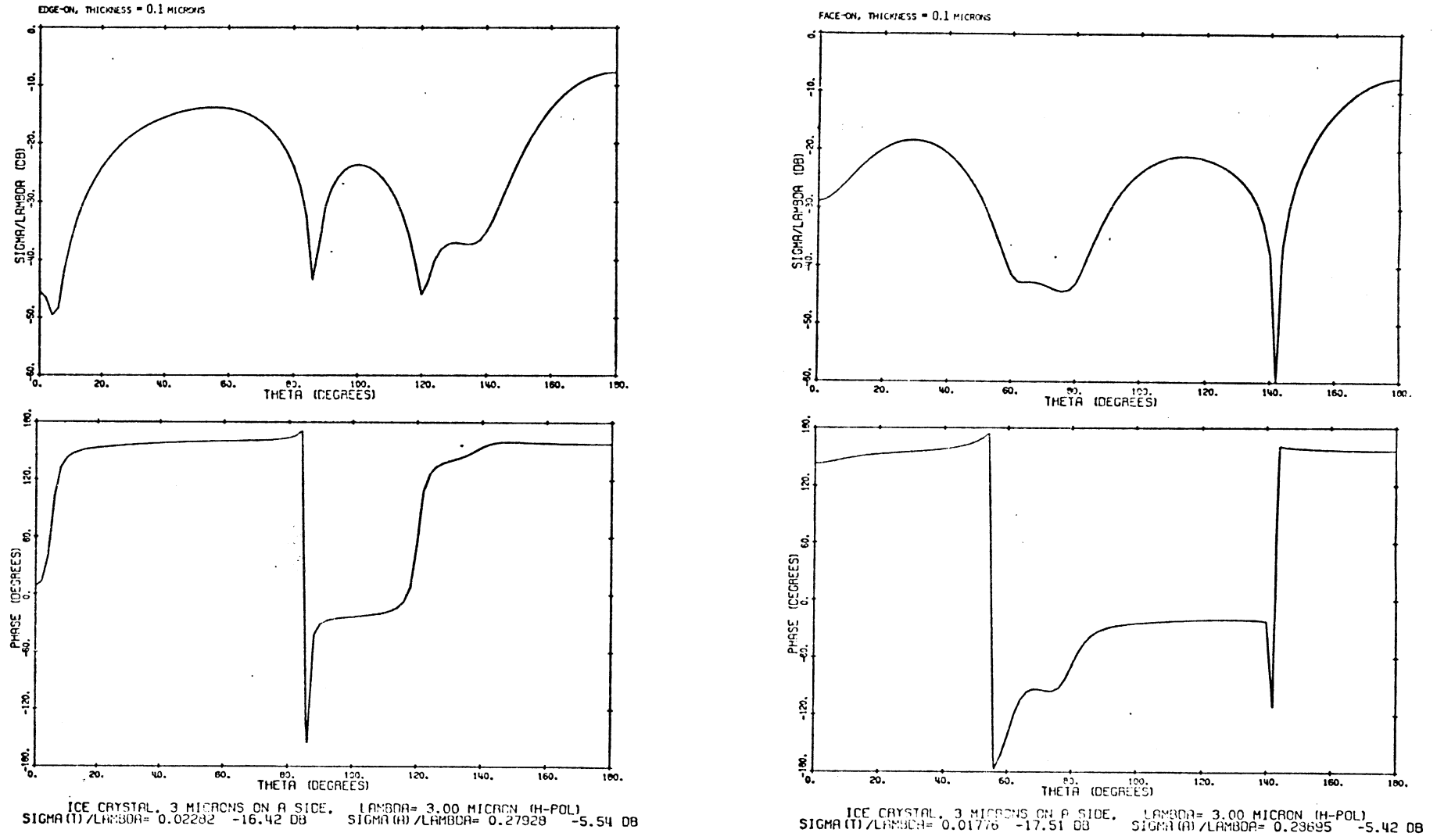
EDGE-ON, THICKNESS = 0.1 MICRONS
SIGMA/LAMBDA (DB)
THETA (DEGREES)
PHASE (DEGREES)
THETA (DEGREES)
ICE CRYSTAL, 3 MICRONS ON A SIDE, LAMBDA= 3.00 MICRON (H-POL)
SIGMA(T)/LAMBDA= 0.02282 -16.42 DB SIGMA(A)/LAMBDA= 0.27928 -5.54 DB
FACE-ON, THICKNESS = 0.1 MICRONS
SIGMA/LAMBDA (DB)
THETA (DEGREES)
PHASE (DEGREES)
THETA (DEGREES)
ICE CRYSTAL, 3 MICRONS ON A SIDE, LAMBDA= 3.00 MICRON (H-POL)
SIGMA(T)/LAMBDA= 0.01776 -17.51 DB SIGMA(A)/LAMBDA= 0.28695 -5.42 DB

Fig. 14

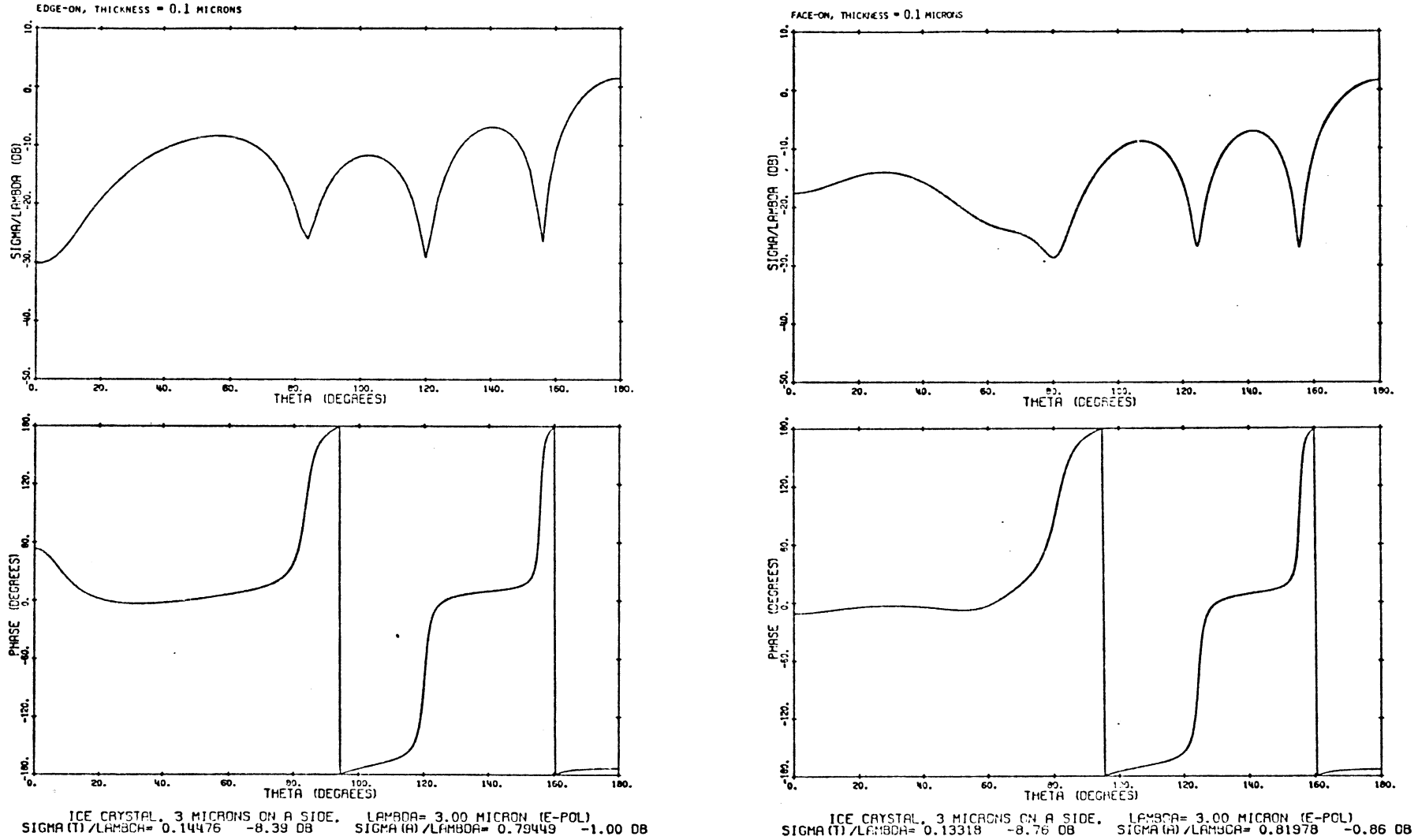
EDGE-ON, THICKNESS = 0.1 MICRONS
SIGMA/LAMBDA (DB)
THETA (DEGREES)
PHASE (DEGREES)
THETA (DEGREES)
ICE CRYSTAL, 3 MICRONS ON A SIDE. LAMBDA= 3.00 MICRON (E-POL)
SIGMA(T)/LAMBDA= 0.14476 -8.39 DB SIGMA(A)/LAMBDA= 0.79449 -1.00 DB
FACE-ON, THICKNESS = 0.1 MICRONS
SIGMA/LAMBDA (DB)
THETA (DEGREES)
PHASE (DEGREES)
THETA (DEGREES)
ICE CRYSTAL, 3 MICRONS ON A SIDE. LAMBDA= 3.00 MICRON (E-POL)
SIGMA(T)/LAMBDA= 0.13318 -8.76 DB SIGMA(A)/LAMBDA= 0.81978 -0.86 DB

Fig. 15

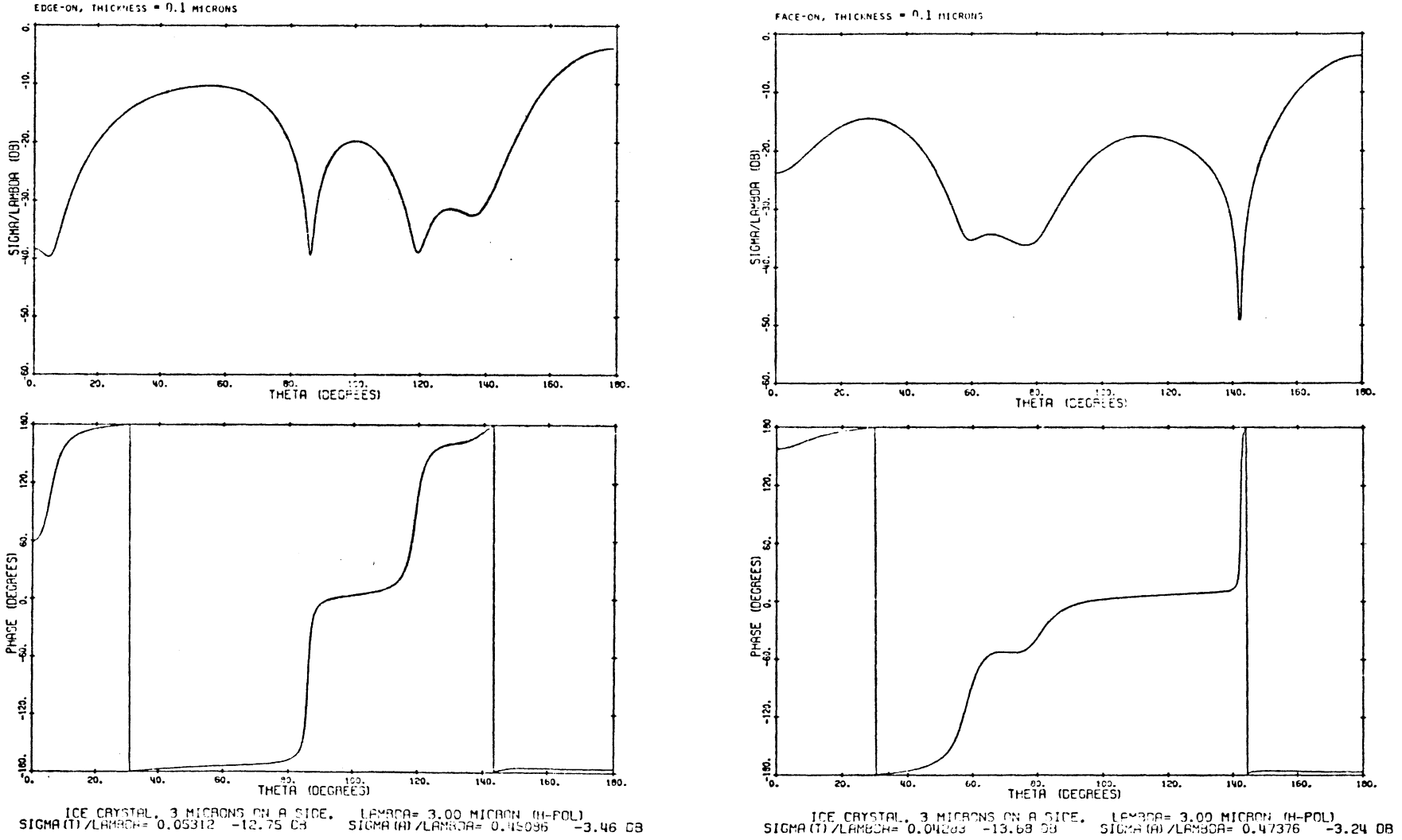
EDGE-ON, THICKNESS = 0.1 MICRONS
SIGMA/LAMBDA (DB)
THETA (DEGREES)
PHASE (DEGREES)
THETA (DEGREES)
ICE CRYSTAL, 3 MICRONS ON A SIDE. LAMBDA= 3.00 MICRON (H-POL)
SIGMA(T)/LAMBDA= 0.05312 -12.75 DB SIGMA(A)/LAMBDA= 0.45096 -3.46 DB
FACE-ON, THICKNESS = 0.1 MICRONS
SIGMA/LAMBDA (DB)
THETA (DEGREES)
PHASE (DEGREES)
THETA (DEGREES)
ICE CRYSTAL, 3 MICRONS ON A SIDE. LAMBDA= 3.00 MICRON (H-POL)
SIGMA(T)/LAMBDA= 0.04283 -13.68 DB SIGMA(A)/LAMBDA= 0.47376 -3.24 DB

Fig. 16

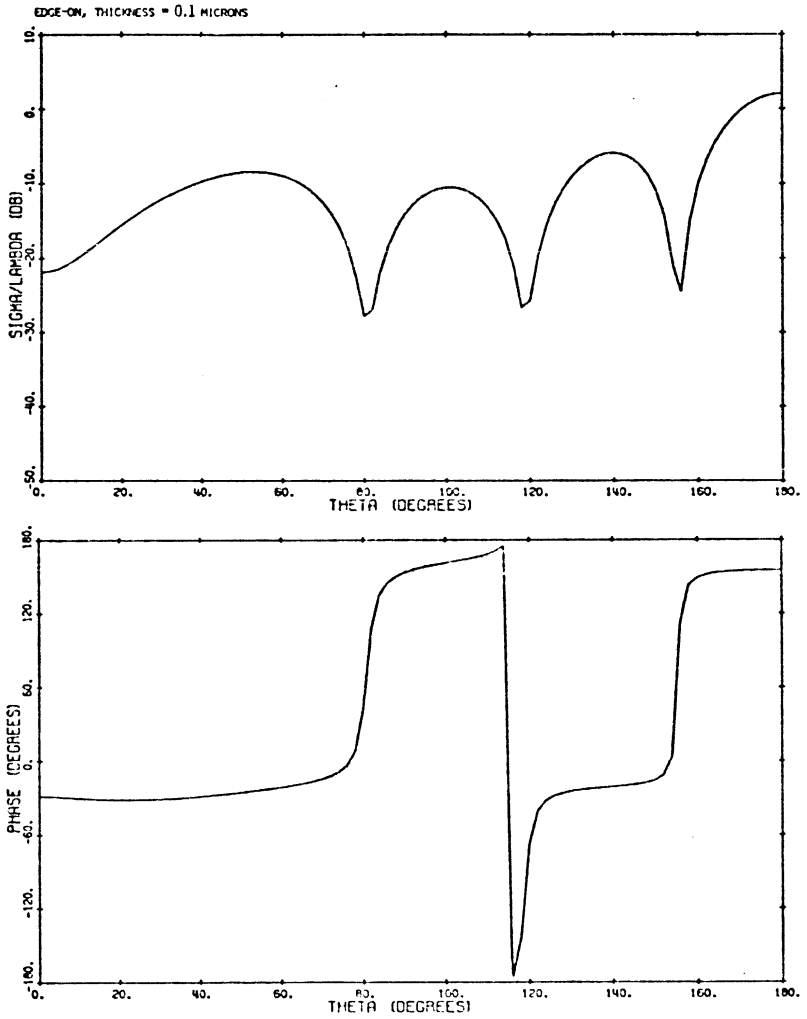

ICE CRYSTAL, 3 MICRONS ON A SIDE. LAMBDA= 3.10 MICRON (E-POL)
SIGMA(T)/LAMBDA= 0.16844 -7.74 DB SIGMA(A)/LAMBDA= 0.74370 -1.29 DB

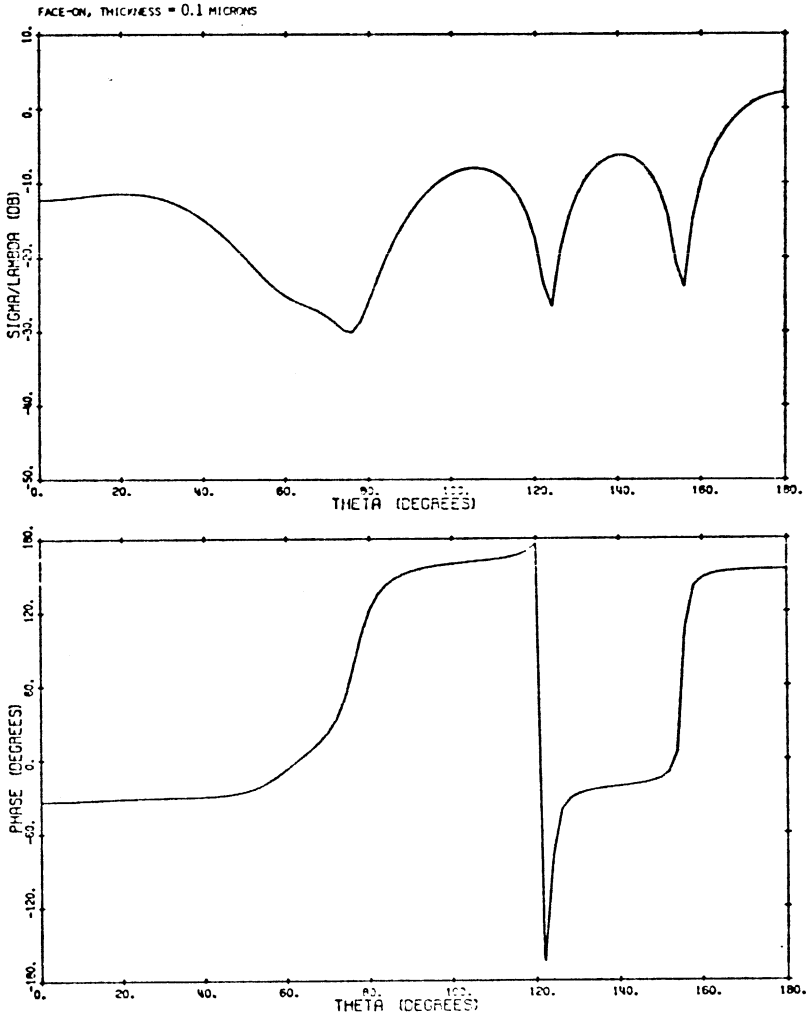

ICE CRYSTAL, 3 MICRONS ON A SIDE. LAMBDA= 3.10 MICRON (E-POL)
SIGMA(T)/LAMBDA= 0.15068 -7.97 DB SIGMA(A)/LAMBDA= 0.75425 -1.22 DB

Fig. 17

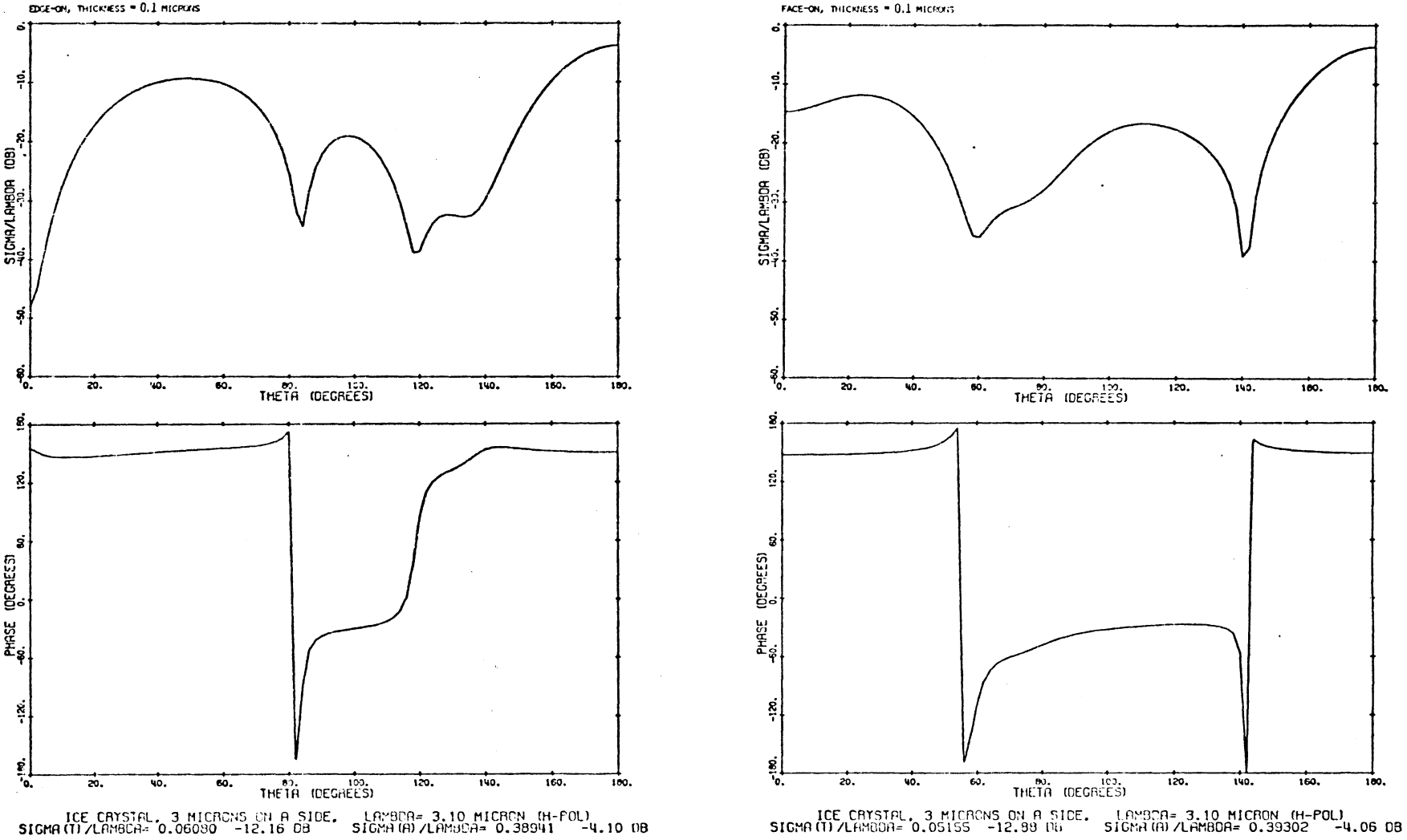

ICE CRYSTAL, 3 MICRONS ON A SIDE. LAMBDA= 3.10 MICRON (H-POL)
SIGMA(T)/LAMBDA= 0.06080 -12.16 DB SIGMA(A)/LAMBDA= 0.38941 -4.10 DB

ICE CRYSTAL, 3 MICRONS ON A SIDE. LAMBDA= 3.10 MICRON (H-POL)
SIGMA(T)/LAMBDA= 0.05155 -12.88 DB SIGMA(A)/LAMBDA= 0.39302 -4.06 DB

Fig. 18

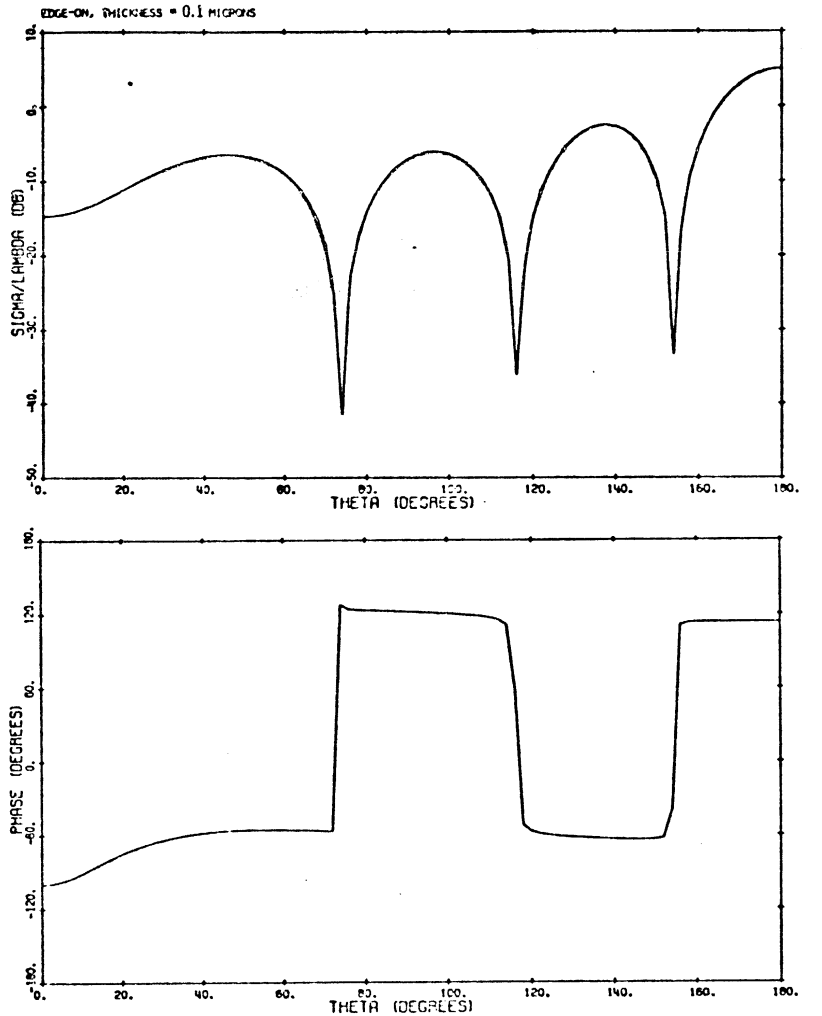
EDGE-ON, THICKNESS = 0.1 MICRONS
SIGMA/LAMBDA (DB)
THETA (DEGREES)
PHASE (DEGREES)
THETA (DEGREES)
ICE CRYSTAL, 3 MICRONS ON A SIDE. LAMBDA= 3.30 MICRON (E-POL)
SIGMA(T)/LAMBDA= 0.34629 -4.61 DB SIGMA(A)/LAMBDA= 0.20730 -6.83 DB

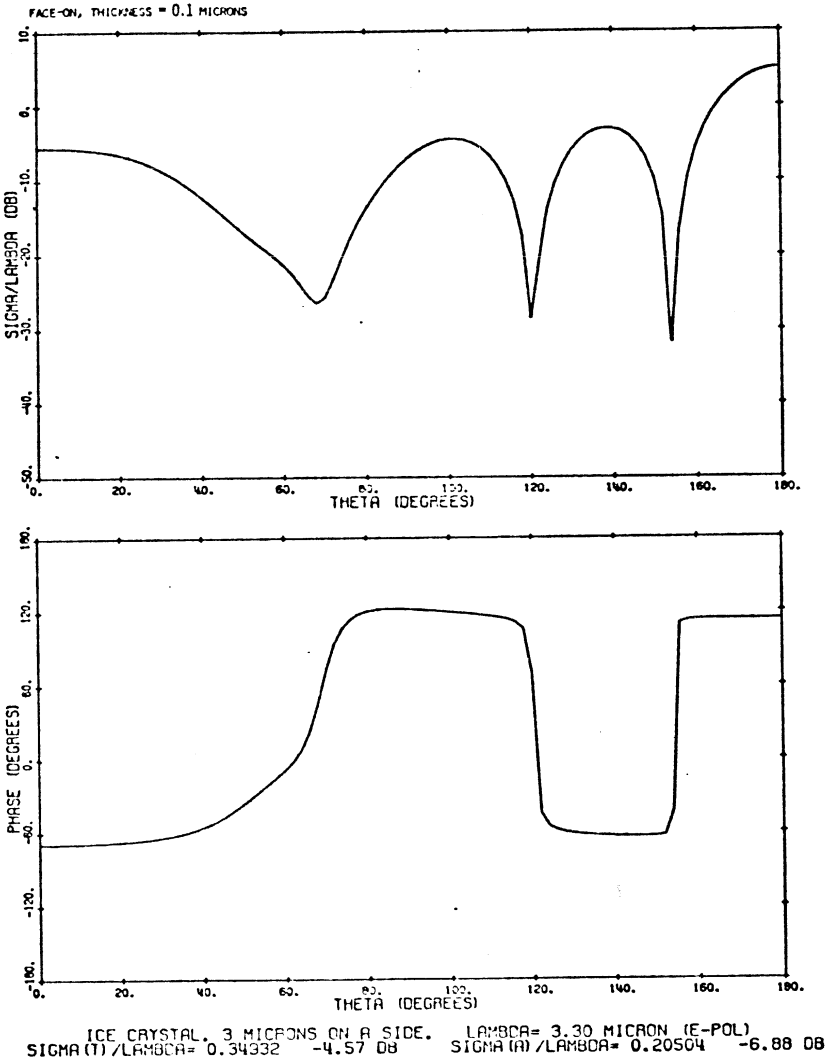
FACE-ON, THICKNESS = 0.1 MICRONS
SIGMA/LAMBDA (DB)
THETA (DEGREES)
PHASE (DEGREES)
THETA (DEGREES)
ICE CRYSTAL, 3 MICRONS ON A SIDE. LAMBDA= 3.30 MICRON (E-POL)
SIGMA(T)/LAMBDA= 0.34332 -4.57 DB SIGMA(A)/LAMBDA= 0.20504 -6.88 DB

Fig. 19

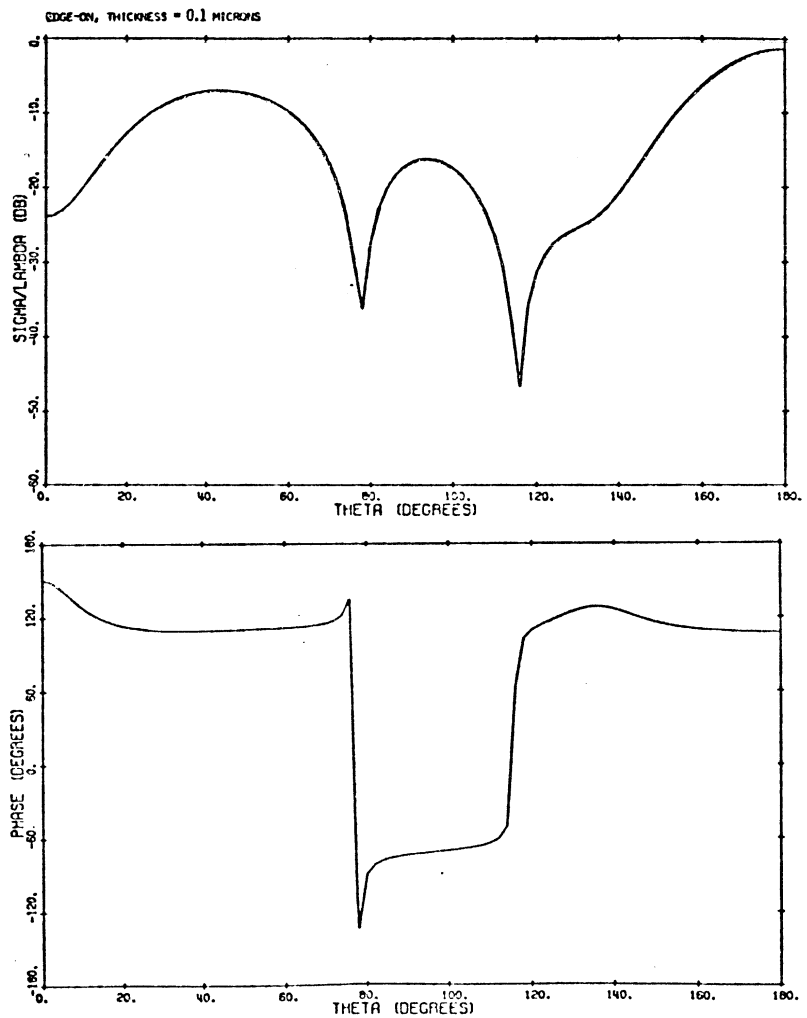

ICE CRYSTAL, 3 MICRONS ON A SIDE. LAMBDA= 3.30 MICRON (H-POL)
SIGMA(T)/LAMBDA= 0.10351 -9.61 DB SIGMA(A)/LAMBDA= 0.09484 -10.23 DB

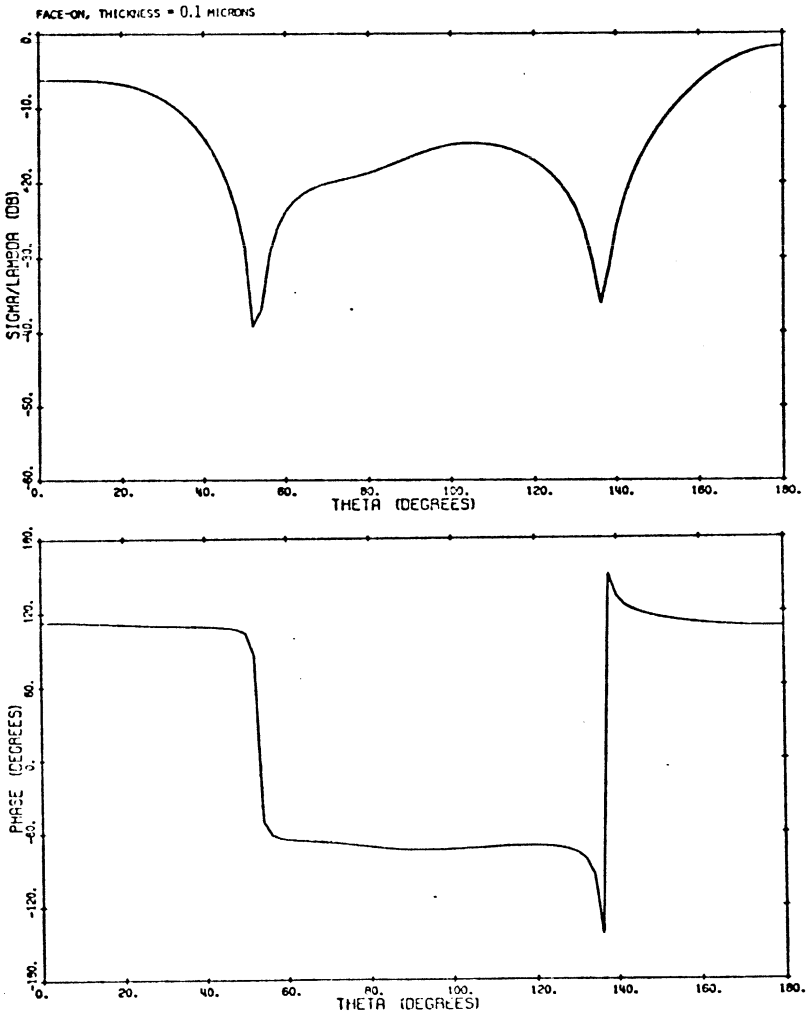

ICE CRYSTAL, 3 MICRONS ON A SIDE. LAMBDA= 3.30 MICRON (H-POL)
SIGMA(T)/LAMBDA= 0.11204 -9.51 DB SIGMA(A)/LAMBDA= 0.08622 -10.64 DB

Fig. 20

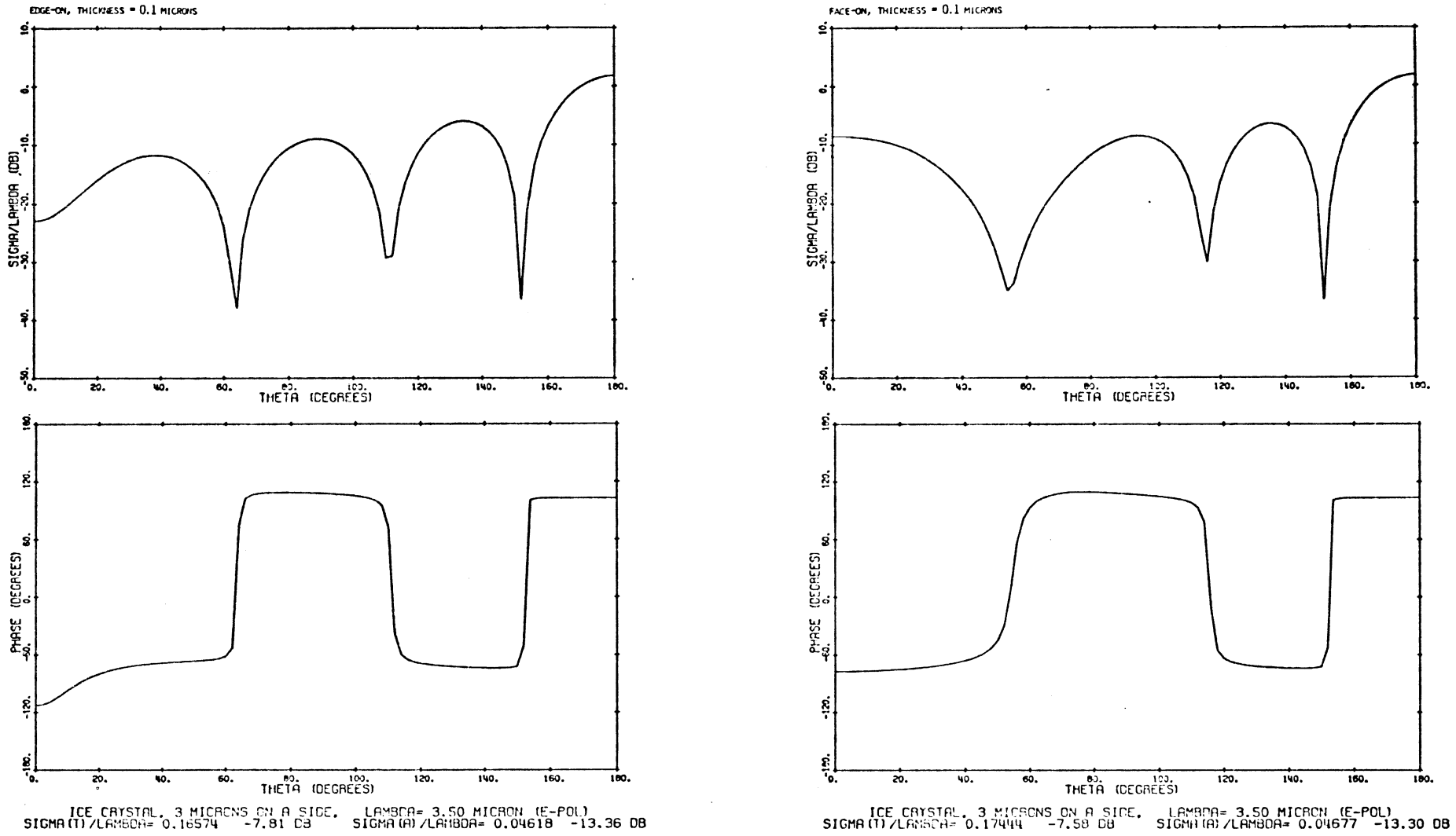
EDGE-ON, THICKNESS = 0.1 MICRONS
SIGMA/LAMBDA (DB)
THETA (DEGREES)
PHASE (DEGREES)
THETA (DEGREES)
ICE CRYSTAL, 3 MICRONS ON A SIDE, LAMBDA= 3.50 MICRON (E-POL)
SIGMA(T)/LAMBDA= 0.16574 -7.81 DB SIGMA(A)/LAMBDA= 0.04618 -13.36 DB
FACE-ON, THICKNESS = 0.1 MICRONS
SIGMA/LAMBDA (DB)
THETA (DEGREES)
PHASE (DEGREES)
THETA (DEGREES)
ICE CRYSTAL, 3 MICRONS ON A SIDE, LAMBDA= 3.50 MICRON (E-POL)
SIGMA(T)/LAMBDA= 0.17414 -7.59 DB SIGMA(A)/LAMBDA= 0.04677 -13.30 DB

Fig. 21

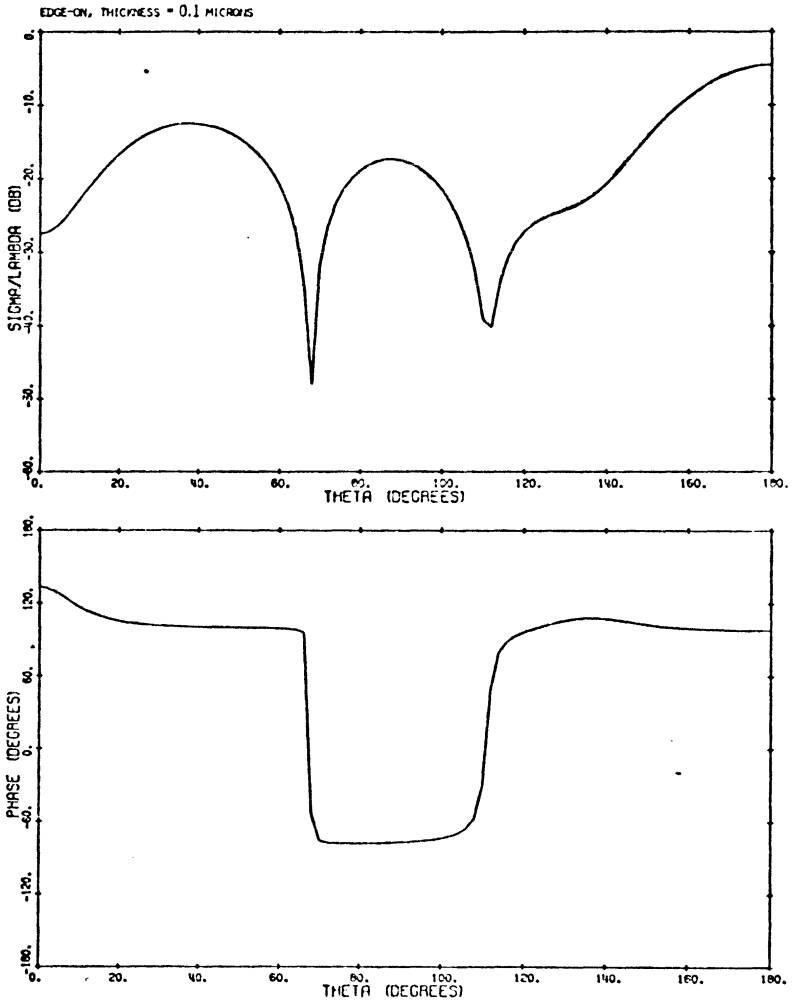

ICE CRYSTAL, 3 MICRONS ON A SIDE. LAMBDA= 3.50 MICRON (H-POL)
SIGMA(T)/LAMBDA= 0.04656 -13.32 DB SIGMA(A)/LAMBDA= 0.02126 -16.72 DB

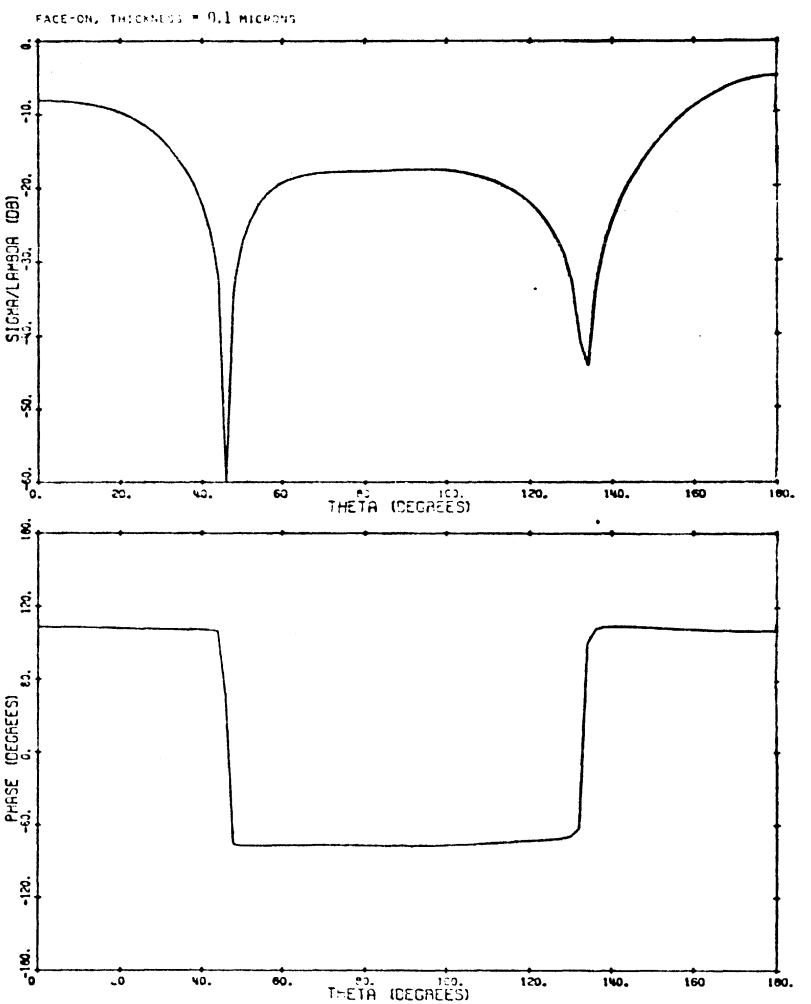

ICE CRYSTAL, 3 MICRONS ON A SIDE. LAMBDA= 3.50 MICRONS (H-POL)
SIGMA(T)/LAMBDA= 0.0607[illegible] -12.16 DB SIGMA(A)/LAMBDA= 0.0207[illegible] -16.83 DB

Fig. 22

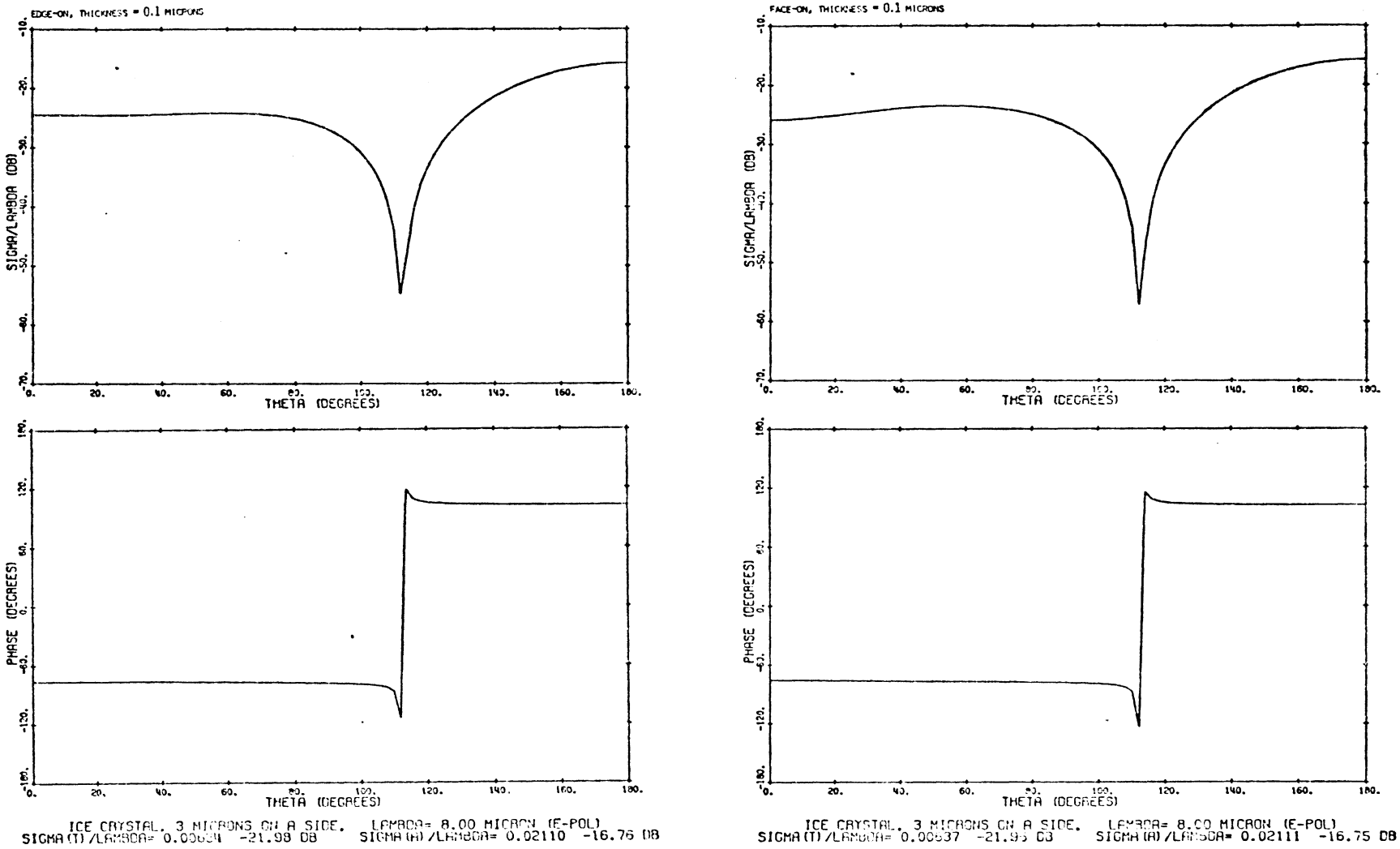
EDGE-ON, THICKNESS = 0.1 MICRONS
SIGMA/LAMBDA (DB)
THETA (DEGREES)
PHASE (DEGREES)
THETA (DEGREES)
ICE CRYSTAL, 3 MICRONS ON A SIDE. LAMBDA= 8.00 MICRON (E-POL)
SIGMA(T)/LAMBDA= 0.00634 -21.98 DB SIGMA(A)/LAMBDA= 0.02110 -16.76 DB
FACE-ON, THICKNESS = 0.1 MICRONS
SIGMA/LAMBDA (DB)
THETA (DEGREES)
PHASE (DEGREES)
THETA (DEGREES)
ICE CRYSTAL, 3 MICRONS ON A SIDE. LAMBDA= 8.00 MICRON (E-POL)
SIGMA(T)/LAMBDA= 0.00637 -21.95 DB SIGMA(A)/LAMBDA= 0.02111 -16.75 DB

Fig. 23

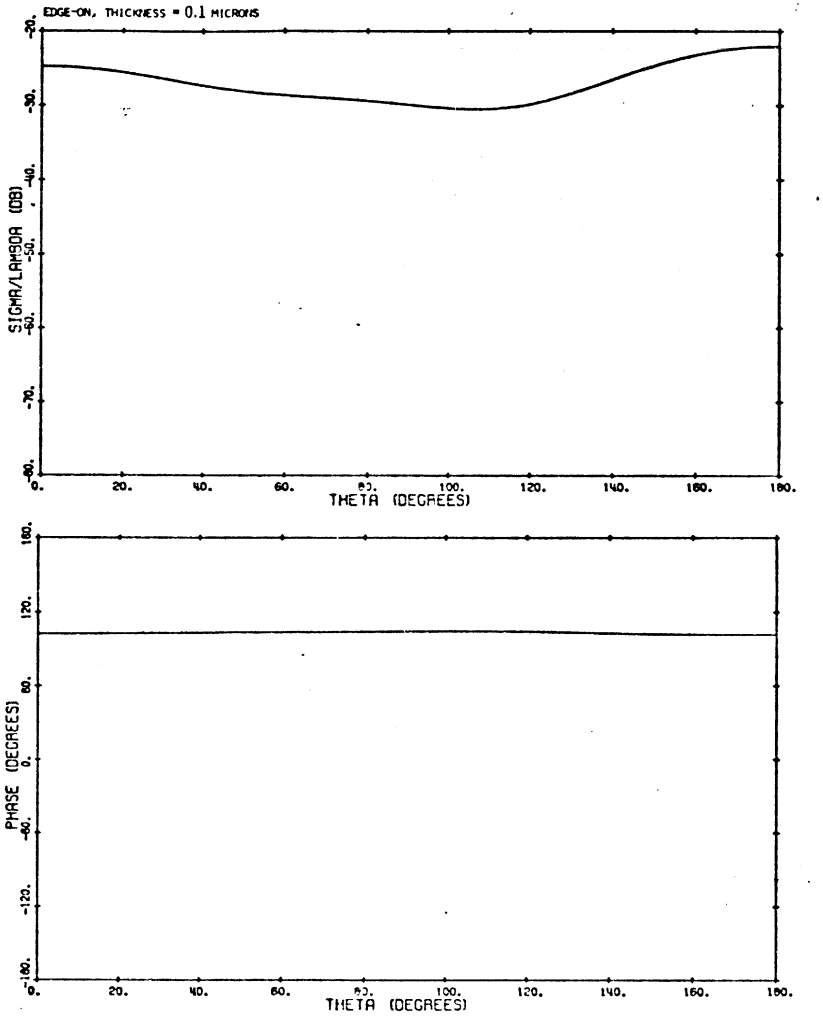

ICE CRYSTAL, 3 MICRONS ON A SIDE. LAMBDA= 8.00 MICRON (H-POL)
SIGMA(T)/LAMBDA= 0.00233 -26.33 DB SIGMA(A)/LAMBDA= 0.01007 -19.97 DB

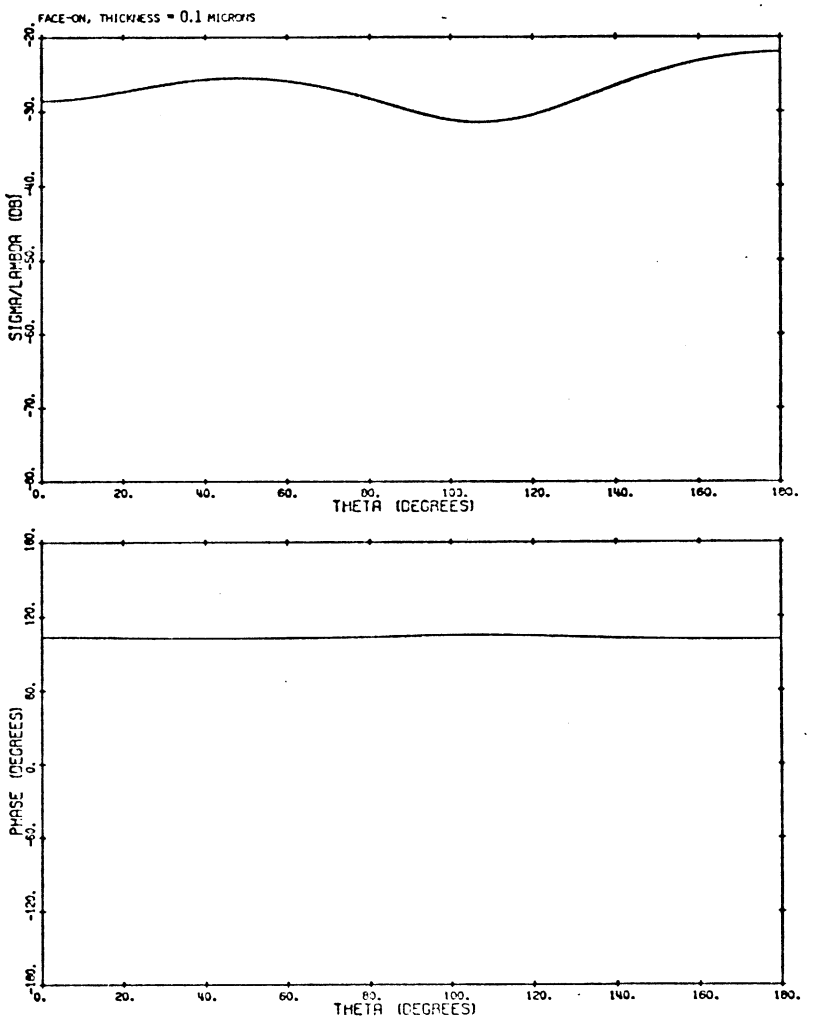

ICE CRYSTAL, 3 MICRONS ON A SIDE. LAMBDA= 8.00 MICRON (H-POL)
SIGMA(T)/LAMBDA= 0.00234 -26.32 DB SIGMA(A)/LAMBDA= 0.01009 -19.96 DB

Fig. 24

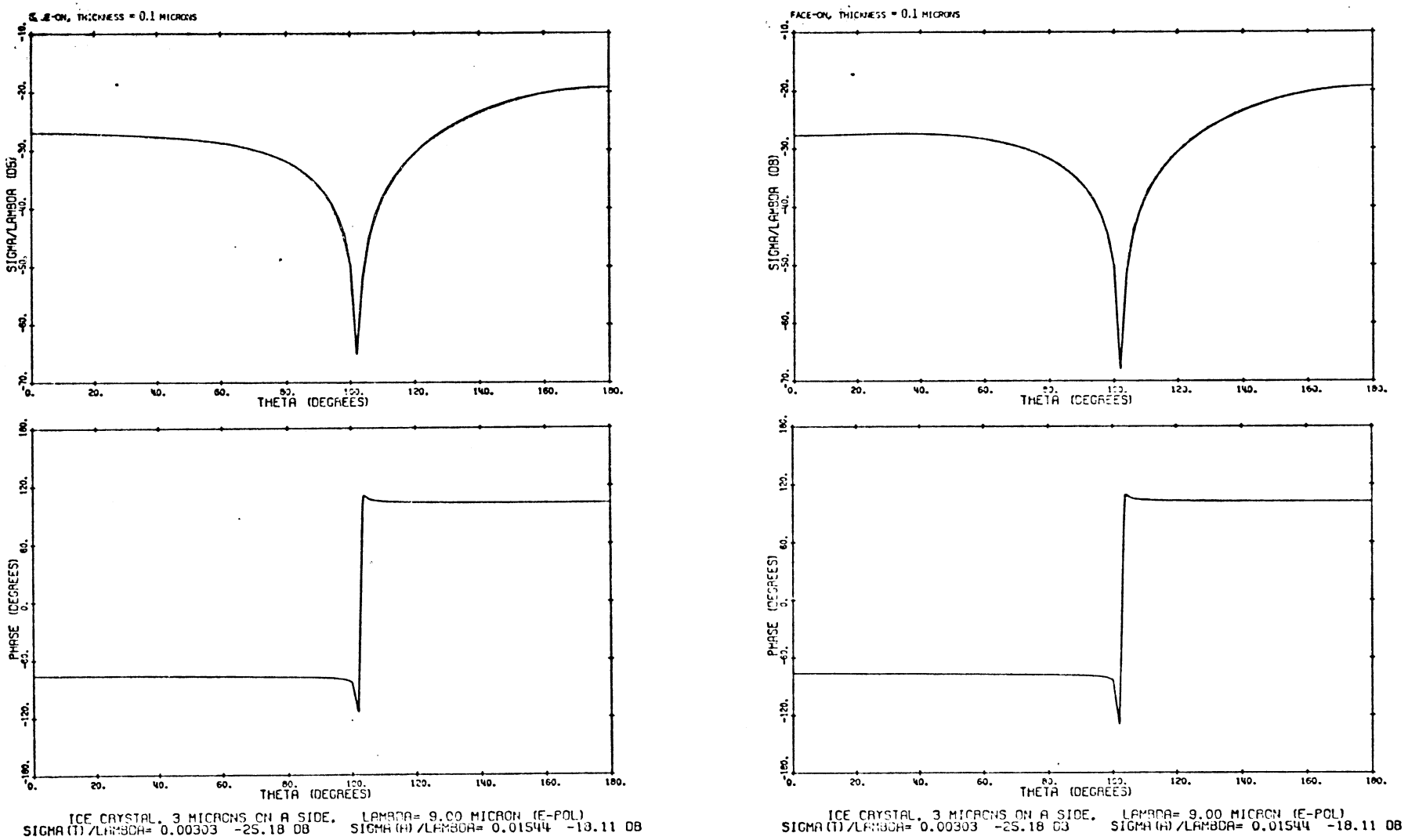
FACE-ON, THICKNESS = 0.1 MICRONS
SIGMA/LAMBDA (DB)
THETA (DEGREES)
PHASE (DEGREES)
THETA (DEGREES)
ICE CRYSTAL, 3 MICRONS ON A SIDE. LAMBDA= 9.00 MICRON (E-POL)
SIGMA(T)/LAMBDA= 0.00303 -25.18 DB SIGMA(A)/LAMBDA= 0.01544 -18.11 DB
FACE-ON, THICKNESS = 0.1 MICRONS
SIGMA/LAMBDA (DB)
THETA (DEGREES)
PHASE (DEGREES)
THETA (DEGREES)
ICE CRYSTAL, 3 MICRONS ON A SIDE. LAMBDA= 9.00 MICRON (E-POL)
SIGMA(T)/LAMBDA= 0.00303 -25.18 DB SIGMA(A)/LAMBDA= 0.01544 -18.11 DB

Fig. 25

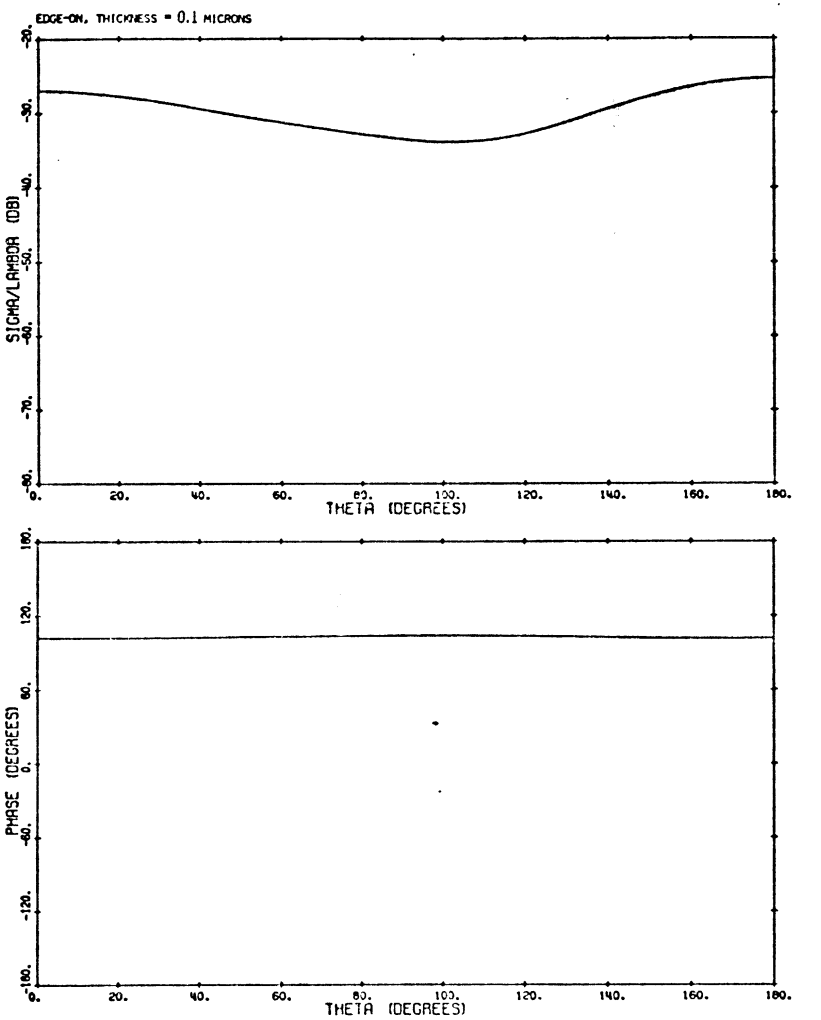

ICE CRYSTAL, 3 MICRONS ON A SIDE, LAMBDA= 9.00 MICRON (H-POL)
SIGMA(T)/LAMBDA= 0.00121 -29.18 DB SIGMA(A)/LAMBDA= 0.00748 -21.26 DB

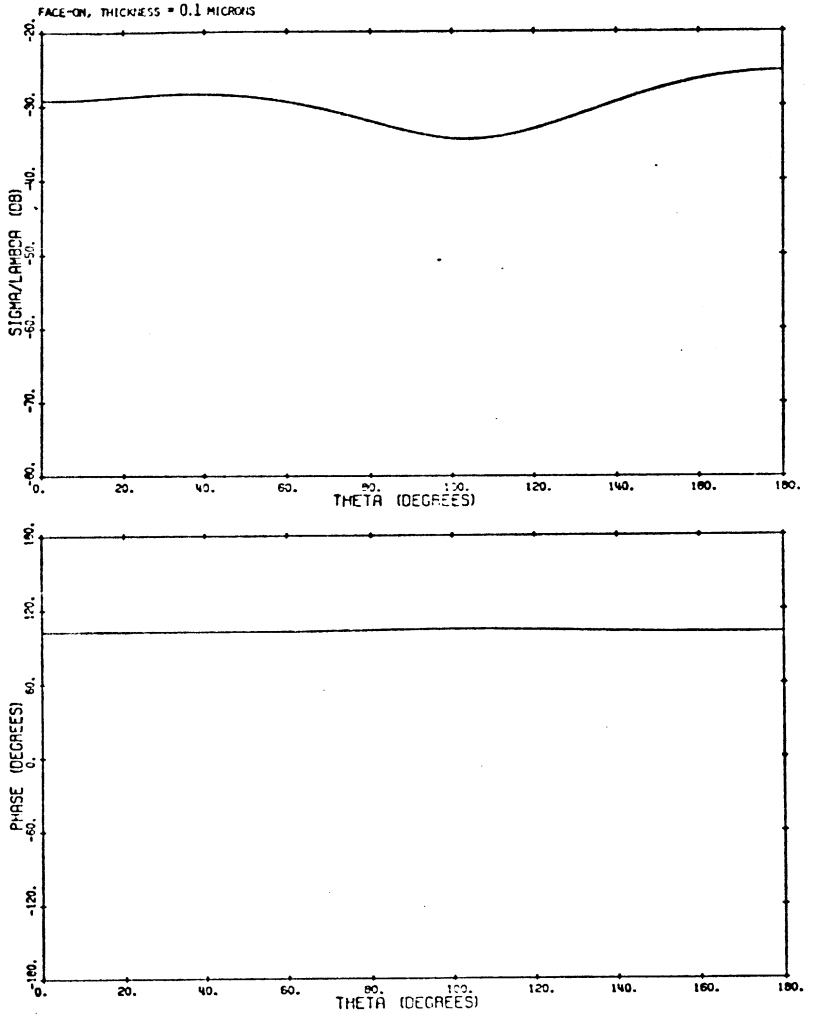

ICE CRYSTAL, 3 MICRONS ON A SIDE, LAMBDA= 9.00 MICRON (H-POL)
SIGMA(T)/LAMBDA= 0.00120 -29.22 DB SIGMA(A)/LAMBDA= 0.00748 -21.26 DB

Fig. 26

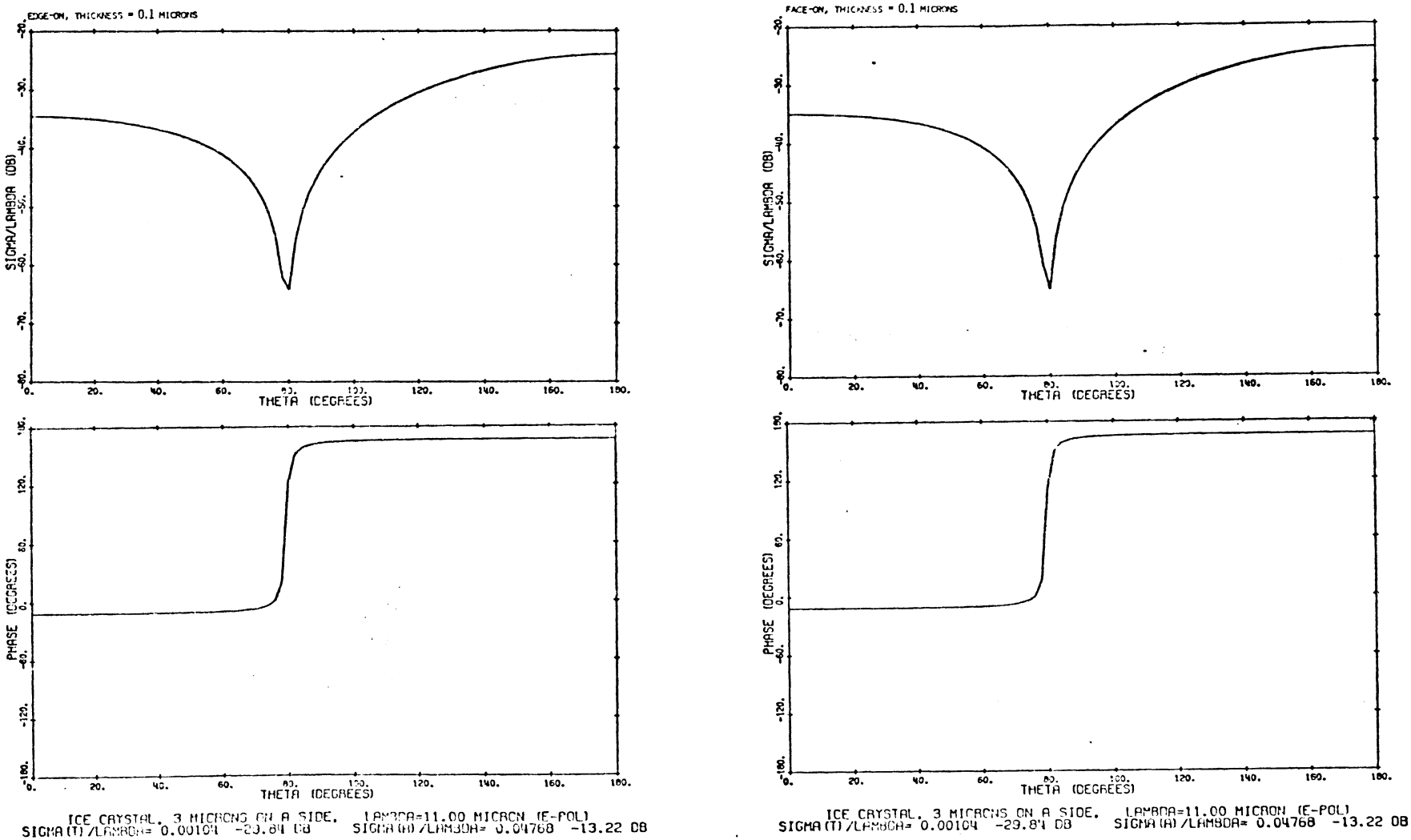
EDGE-ON, THICKNESS = 0.1 MICRONS
SIGMA/LAMBDA (DB)
THETA (DEGREES)
PHASE (DEGREES)
THETA (DEGREES)
ICE CRYSTAL, 3 MICRONS ON A SIDE, LAMBDA=11.00 MICRON (E-POL)
SIGMA(T)/LAMBDA= 0.00104 -29.84 DB SIGMA(A)/LAMBDA= 0.04768 -13.22 DB
FACE-ON, THICKNESS = 0.1 MICRONS
SIGMA/LAMBDA (DB)
THETA (DEGREES)
PHASE (DEGREES)
THETA (DEGREES)
ICE CRYSTAL, 3 MICRONS ON A SIDE, LAMBDA=11.00 MICRON (E-POL)
SIGMA(T)/LAMBDA= 0.00104 -29.84 DB SIGMA(A)/LAMBDA= 0.04768 -13.22 DB

Fig. 27

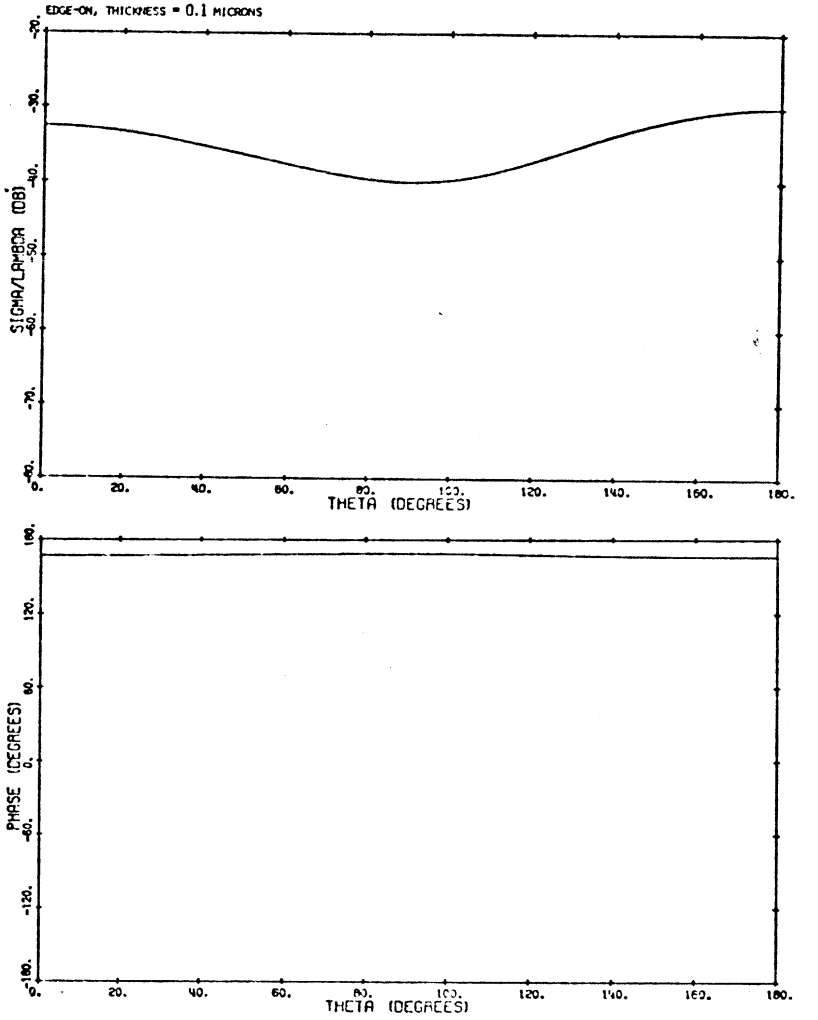

ICE CRYSTAL, 3 MICRONS ON A SIDE, LAMBDA=11.00 MICRON (H-POL)
SIGMA(T)/LAMBDA= 0.00037 -34.27 DB SIGMA(A)/LAMBDA= 0.02399 -16.20 DB

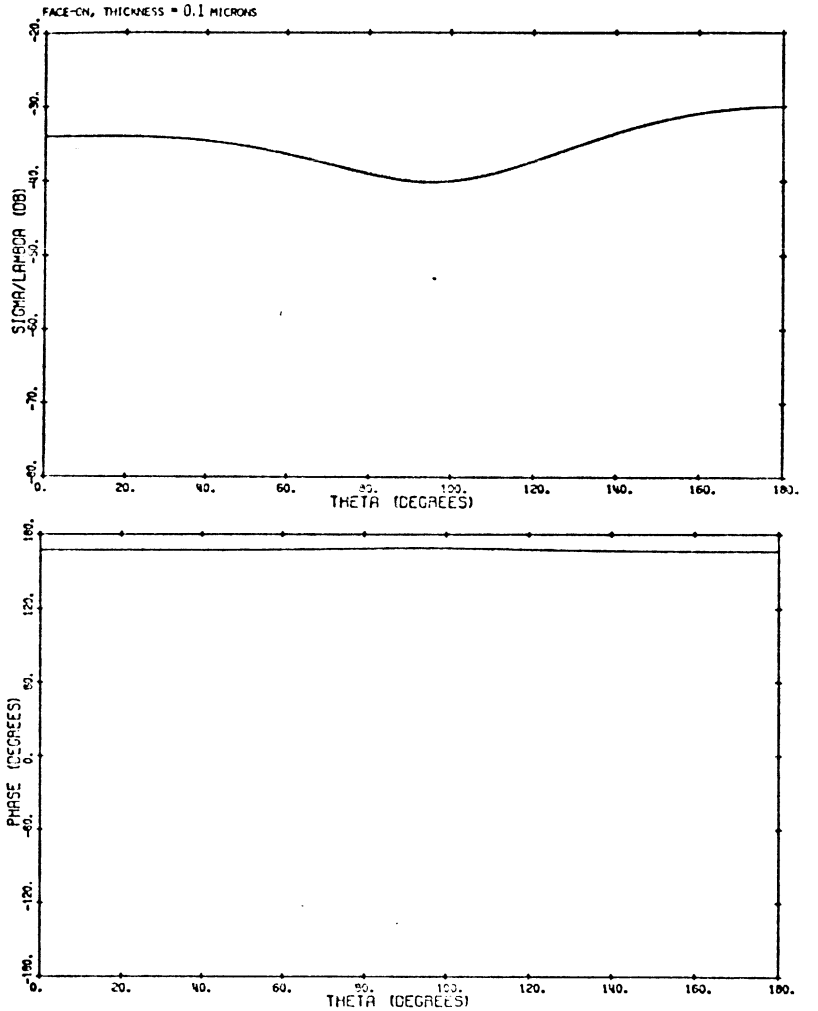

ICE CRYSTAL, 3 MICRONS ON A SIDE, LAMBDA=11.00 MICRON (H-POL)
SIGMA(T)/LAMBDA= 0.00037 -34.32 DB SIGMA(A)/LAMBDA= 0.02400 -16.20 DB

Fig. 28

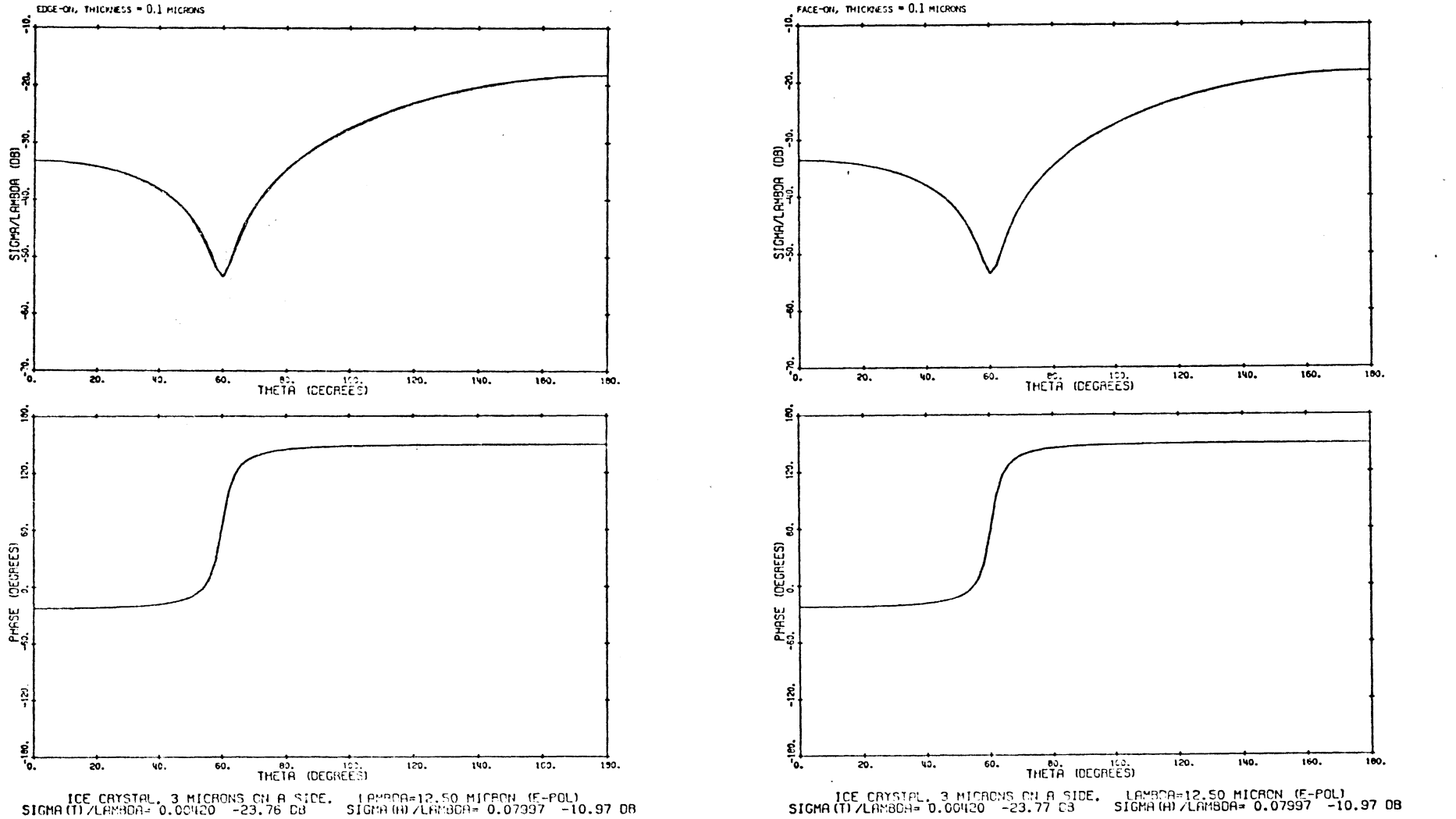
EDGE-ON, THICKNESS = 0.1 MICRONS
SIGMA/LAMBDA (DB)
THETA (DEGREES)
PHASE (DEGREES)
THETA (DEGREES)
ICE CRYSTAL, 3 MICRONS ON A SIDE. LAMBDA=12.50 MICRON (E-POL)
SIGMA(T)/LAMBDA= 0.00420 -23.76 DB SIGMA(A)/LAMBDA= 0.07997 -10.97 DB
FACE-ON, THICKNESS = 0.1 MICRONS
SIGMA/LAMBDA (DB)
THETA (DEGREES)
PHASE (DEGREES)
THETA (DEGREES)
ICE CRYSTAL, 3 MICRONS ON A SIDE. LAMBDA=12.50 MICRON (E-POL)
SIGMA(T)/LAMBDA= 0.00420 -23.77 DB SIGMA(A)/LAMBDA= 0.07997 -10.97 DB

Fig. 29

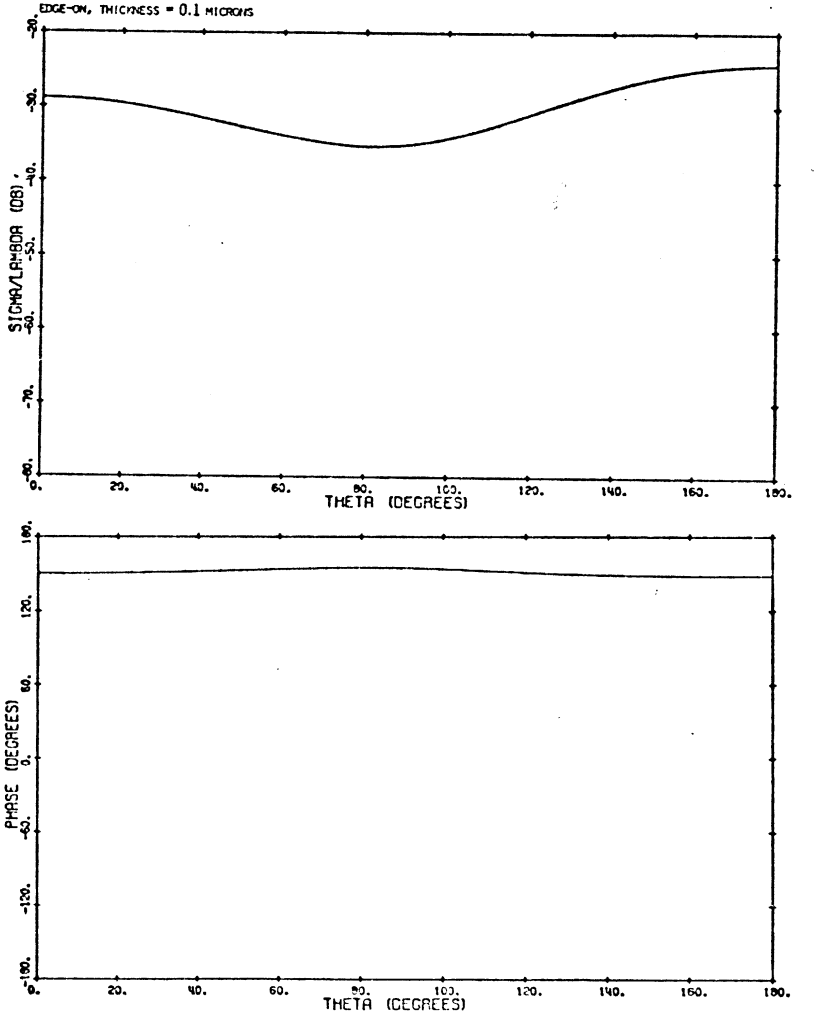

ICE CRYSTAL, 3 MICRONS ON A SIDE. LAMBDA=12.50 MICRON (H-POL)
SIGMA(T)/LAMBDA= 0.00123 -29.09 DB SIGMA(A)/LAMBDA= 0.04027 -13.95 DB

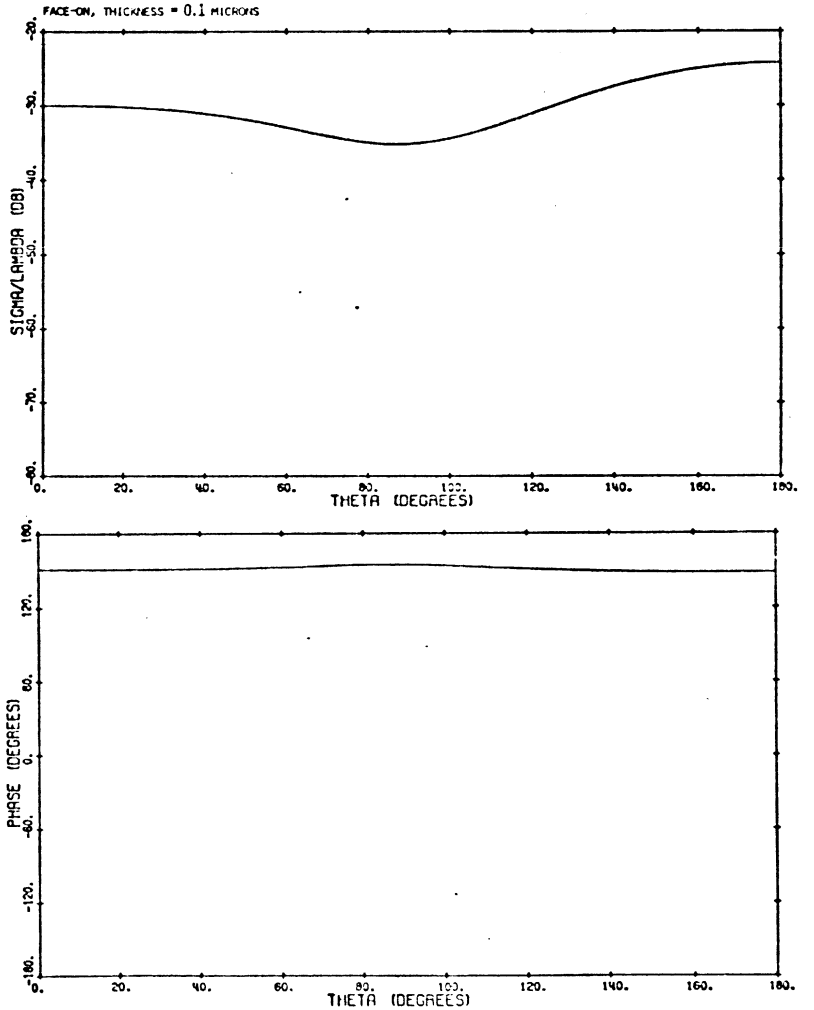

ICE CRYSTAL, 3 MICRONS ON A SIDE. LAMBDA=12.50 MICRON (H-POL)
SIGMA(T)/LAMBDA= 0.00122 -29.12 DB SIGMA(A)/LAMBDA= 0.04028 -13.95 DB

Fig. 30

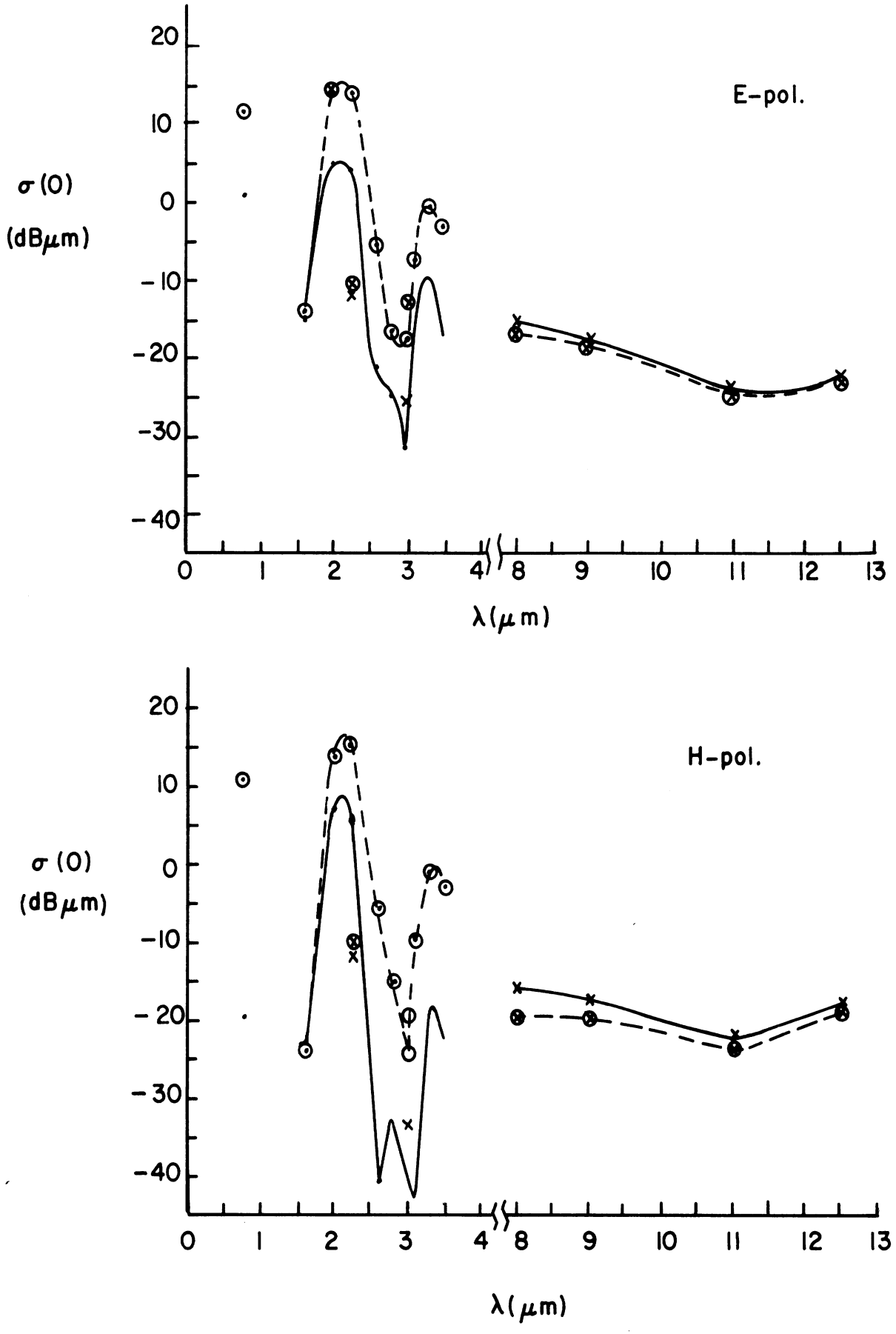

Fig. 31: Computed backscattering cross sections of hexagonal (shell) cylinders. In this and the following four figures, • and ⊙ show edge-on and face-on results respectively for IP data; similarly x and ⊗ are for SW data.

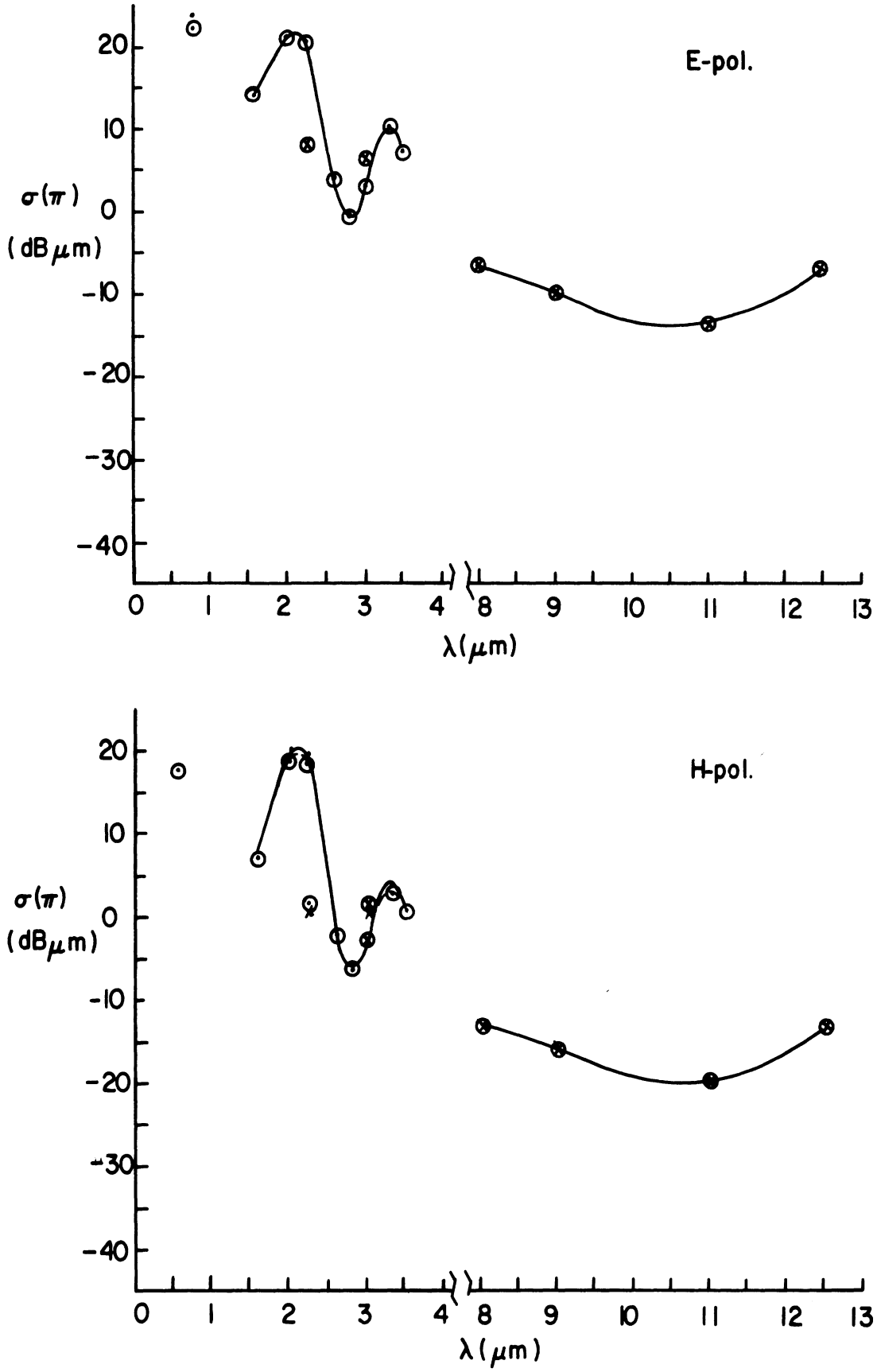

Fig. 32: Computed forward scattering cross sections of hexagonal (shell) cylinders.

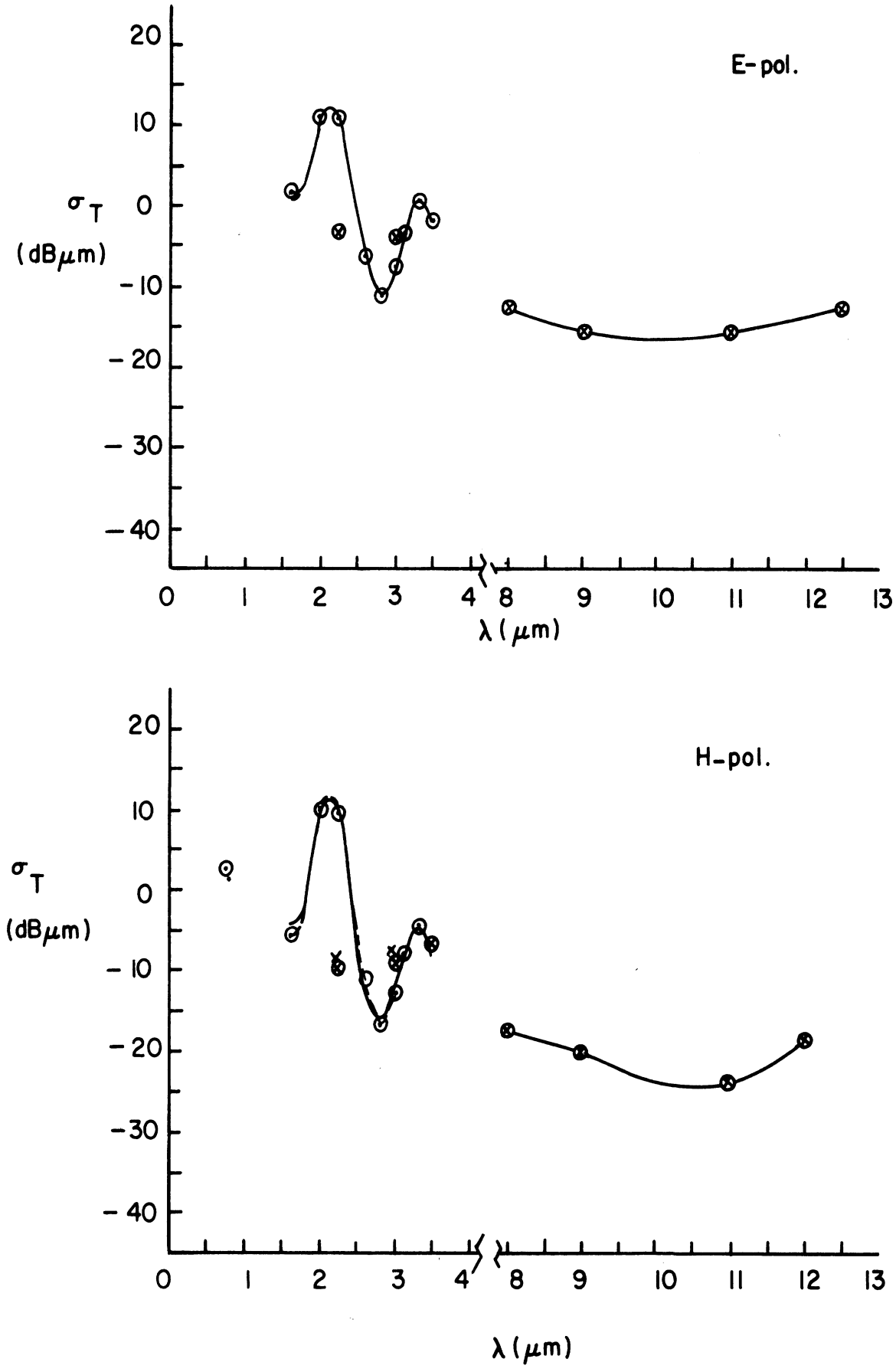

Fig. 33: Computed total scattering cross sections of hexagonal (shell) cylinders.

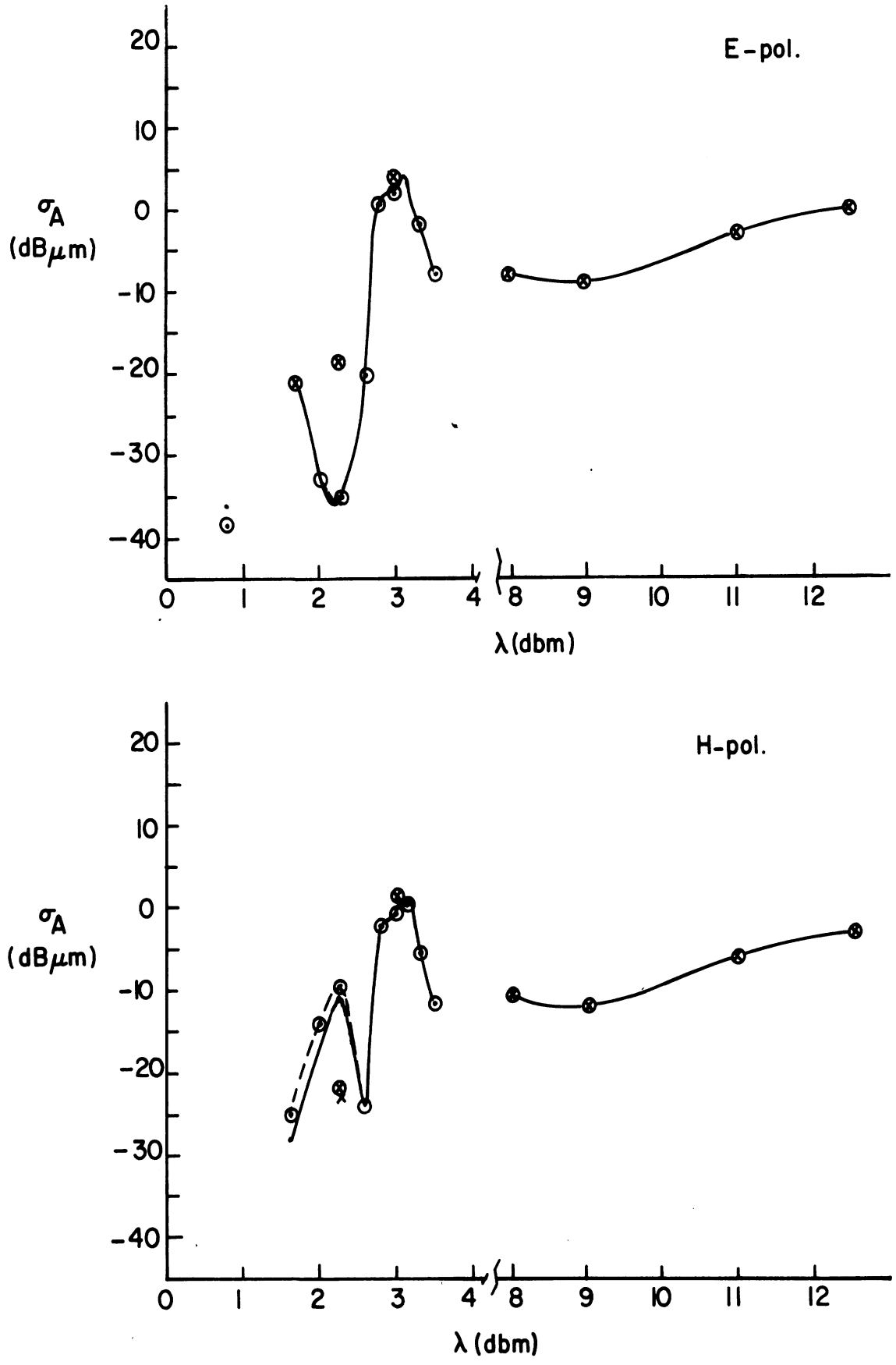

Fig. 34: Computed absorption cross sections of hexagonal (shell) cylinders.

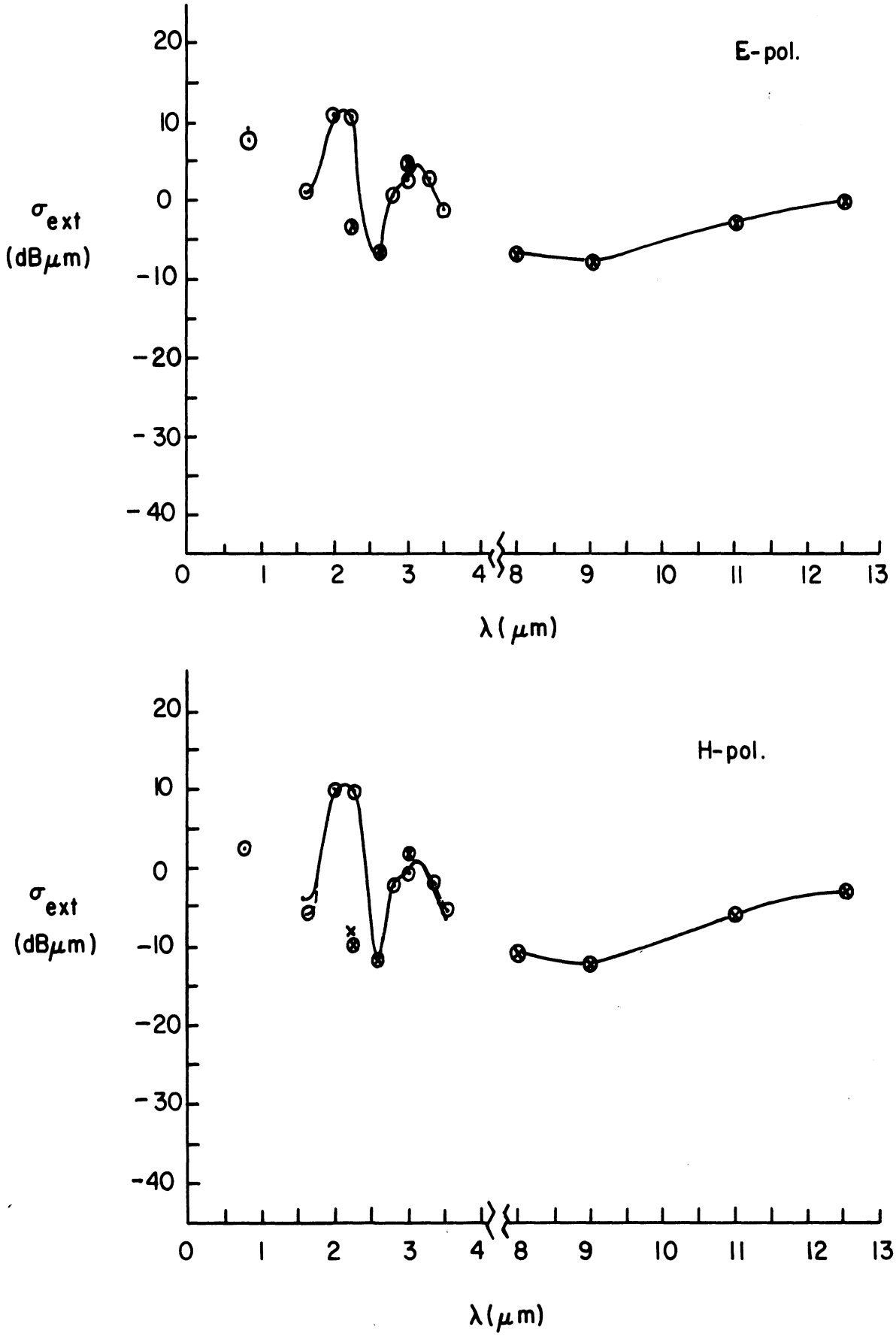

Fig. 35: Computed extinction cross sections of hexagonal (shell) cylinders.

Appendix: Scattering by a Cylindrical Resistive Shell

A-1 Formulation

The shell crystal is simulated by a hexagonal cylindrical shell of uniform thickness and constitution, which is in turn treated as an infinitesimally thin, electrically resistive membrane.

The concept of such a membrane arises naturally from a consideration of a thin sheet of highly conducting material whose permeability μ is that of free space. If σ is the conductivity and τ is the thickness, we can define a surface resistivity R as

$$R = \frac{1}{\sigma\tau} = \frac{i}{\omega\epsilon_0\chi_e\tau} \tag{1}$$

where χ_e is the electric susceptibility, ϵ_0 is the permittivity of free space and a time factor $e^{-i\omega t}$ has been assumed; and as $\tau \to 0$ we can imagine σ to be increased in such a manner that R is finite and non-zero in the limit. The result is an idealized (infinitesimally thin) electrically resistive sheet whose electromagnetic properties are specified by the single quantity R. In terms of the (complex) refractive index n of the layer material

$$R = \frac{iZ}{(n^2 - 1)k\tau} \quad , \tag{2}$$

where k and Z are the propagation constant and intrinsic impedance of free space, respectively.

Mathematically at least, the membrane is simply an electric current sheet whose strength is related to the tangential electric field via the resistivity R ohms/m^2, which may be a function of position. Since $\mu = \mu_0$, there is no magnetic current present and

$$\hat{n} \times (\underline{E}^+ - \underline{E}^-) = 0 \tag{3}$$

where the affices $\pm$ refer to the positive (upper or outer) and negative (lower or inner) sides of the sheet and $\hat{n}$ is the outward normal to the positive side. If $\underline{J}$ is the total current

$$\hat{n} \wedge (\underline{H}^{+} - \underline{H}^{-}) = \underline{J} \tag{4}$$

and from the definition of the surface resistivity

$$\hat{n} \wedge (\hat{n} \wedge \underline{E}^{\pm}) = -R\underline{J} \quad . \tag{5}$$

The tangential components of the electric field are therefore continuous across the sheet, whereas the tangential components of the magnetic field have a jump discontinuity $\underline{J}$ directly related to the electric field via the resistivity R. With R specified, the conditions (3) - (5) define a transition problem for the electromagnetic field and were first used by Levi-Cività (see Bateman, 1915) in studies of charges and currents close to a conducting sheet.

A-2 Scattering by a Resistive Membrane

It is convenient to start by considering a general resistive membrane in three space dimensions illuminated by an arbitrary electromagnetic field. We treat first an open sheet for which a representation of the scattered field was obtained by Knott and Senior (1974) and then examine the case of a closed resistive shell.

If S is an open electrically resistive sheet and we surround it by a closed surface S_1, the scattered field at any point $\underline{r}$ outside S_1 can be written as

$$\begin{aligned} \underline{E}^{S}(\underline{r}) &= \nabla \wedge \nabla \wedge \underline{\pi} + ikZ\nabla \wedge \underline{\pi}^{*} \\ \underline{H}^{S}(\underline{r}) &= \nabla \wedge \nabla \wedge \underline{\pi}^{*} - ikY\nabla \wedge \underline{\pi} \end{aligned} \tag{6}$$

where $Y = Z^{-1}$ and $\underline{\pi}$ and $\underline{\pi}^*$ are the electric and magnetic Hertz vectors defined as

$$\underline{\pi}(\underline{r}) = \frac{iZ}{k} \iint_{S_1} \hat{n} \wedge \underline{H} g \, dS'$$

$$\underline{\pi}^*(\underline{r}) = -\frac{iY}{k} \iint_{S_1} \hat{n} \wedge \underline{E} g \, dS' \quad , \tag{7}$$

and

$$g = g(\underline{r} \,|\, \underline{r}') = \frac{e^{ikd}}{4\pi d} \tag{8}$$

with $d = |\underline{r} - \underline{r}'|$ is the free space Green function. On collapsing S_1 to the two sides of S, the expression for $\underline{\pi}(\underline{r})$ reduces to

$$\underline{\pi}(\underline{r}) = \frac{iZ}{k} \iint_{S} \hat{n} \wedge (\underline{H}^+ - \underline{H}^-) g \, dS'$$

i.e., $$\underline{\pi}(\underline{r}) = \frac{iZ}{k} \iint_{S} \underline{J}(\underline{r}') g \, dS' \tag{9}$$

where the integration is now a one-sided integration along S. Since $\hat{n} \wedge (\underline{E}^+ - \underline{E}^-) = 0$, we have similarly

$$\underline{\pi}^*(\underline{r}) = 0 \quad , \tag{10}$$

and eqs. and (10) are precisely those which would have been obtained by starting with the concept of an electric current sheet. Hence

$$\underline{E}(\underline{r}) = \underline{E}^i(\underline{r}) + \nabla \wedge \nabla \wedge \underline{\pi}$$

$$\underline{H}(\underline{r}) = \underline{H}^i(\underline{r}) - ikY \nabla \wedge \underline{\pi} \tag{11}$$

where $\underline{E}^i$, $\underline{H}^i$ are the incident field vectors.

If $\underline{r}$ is not on S, the derivative operations can be applied directly to the integrand of (9) giving

$$\underline{E}(\underline{r}) = \underline{E}^i(\underline{r}) + ikZ \iint_S \left\{ \underline{J}(\underline{r}')g + \frac{1}{k^2}\left[\underline{J}(\underline{r}')\cdot\nabla'\right]\nabla' g \right\} dS' \tag{12}$$

$$\underline{H}(\underline{r}) = \underline{H}^i(\underline{r}) + \iint_S \underline{J}(\underline{r}') \wedge \nabla' g \, dS' \quad . \tag{13}$$

In the particular case when the incident field and the surface S are both independent of a Cartesian coordinate z, eq.(12) was the starting point for the analysis of resistive sheets by Knott and Senior (1974). Integral equations for the tangential components of $\underline{J}$ were developed by taking the limit $\underline{r} \rightarrow S$, and similar results can be obtained even in three dimensions.

On the other hand, a somewhat different expression for the electric field is also possible. By applying standard vector identities to the second term in the integrand of (12), we have (Senior, 1975)

$$\underline{E}(\underline{r}) = \underline{E}^i(\underline{r}) + ikZ \iint_S \left\{ \underline{J}(\underline{r}')g - \frac{1}{k^2}(\nabla'_s \cdot \underline{J})\nabla' g \right\} dS'$$

$$- \frac{iZ}{k} \oint_L \nabla' g \, \underline{J}(\underline{r}') \cdot \hat{n}' \wedge d\underline{\ell} \tag{14}$$

where ∇'_s. is the surface divergence operator and the line integral is in the positive direction around the edge L of S. For a perfectly conducting surface the line integral vanishes by virtue of the edge condition. The electric field expression (14) is then identical to that given by Poggio and Miller (1973) for a closed surface S, and since

$$\nabla'_s \cdot \underline{J} = ikY\rho_s/\epsilon_0 = ikY\hat{n}' \cdot (\underline{E}^+ - \underline{E}^-) \quad , \tag{15}$$

it is also identical to that produced by application of the appropriate Stratton-Chu formula (Stratton, 1941) to the closed surface consisting of the two sides of S. For a nonmetallic surface, however, the line integral is in general nonzero. The Stratton-Chu formulas are no longer valid and to avoid the occurrence of a line integral it is necessary to use the representation (12).

If S is a closed resistive shell, the Stratton-Chu formulas can be used to give the following expressions for the total field at a point $\underline{r}$ outside S:

$$\underline{E}(\underline{r}) = \underline{E}^i(\underline{r}) + \iint_S \left\{ ikZ(\hat{n}' \wedge \underline{H}^+)g + (\hat{n}' \wedge \underline{E}^+) \wedge \nabla' g + (\hat{n}' \cdot \underline{E}^+)\nabla' g \right\} dS' \qquad (16)$$

$$\underline{H}(\underline{r}) = \underline{H}^i(\underline{r}) + \iint_S \left\{ -ikY(\hat{n}' \wedge \underline{E}^+)g + (\hat{n}' \wedge \underline{H}^+) \wedge \nabla' g + (\hat{n}' \cdot \underline{H}^+)\nabla' g \right\} dS' \qquad (17)$$

where the unit vector normal is directed into the space containing $\underline{r}$. In contrast to (12) and (13), the surface integrals now involve the fields on one side of S alone, rather than their jump discontinuities across S. We recall, however, that (16) and (17) are obtained by application of the vector Green's theorem to the volume exterior to S containing the observation point. If, instead, we apply the theorem to the volume interior to S with the observation point still outside S, g will be regular throughout the entire volume of integration, implying

$$0 = \iint_S \left\{ ikZ(\hat{n}' \wedge \underline{H}^-)g + (\hat{n}' \wedge \underline{E}^-) \wedge \nabla' g + (\hat{n}' \cdot \underline{E}^-)\nabla' g \right\} dS' \qquad (18)$$

$$0 = \iint_S \left\{ -ikY(\hat{n}' \wedge \underline{E}^-)g + (\hat{n} \wedge \underline{H}^-) \wedge \nabla' g + (\hat{n}' \cdot \underline{H}^-)\nabla' g \right\} dS' \quad . \qquad (19)$$

By choosing $\underline{r}$ the same as in eqs. (16) and (17), subtraction of (18) from (16) gives

$$\underline{E}(\underline{r}) = \underline{E}^i(\underline{r}) + \iint_S \left\{ ikZ(\hat{n}' \wedge [\underline{H}])g + (\hat{n}' \wedge [\underline{E}]) \wedge \nabla' g + (\hat{n}' \cdot [\underline{E}])\nabla' g \right\} dS'$$

where $[\underline{E}] = \underline{E}^+ - \underline{E}^-$ and $[\underline{H}] = \underline{H}^+ - \underline{H}^-$. Similarly

$$\underline{H}(\underline{r}) = \underline{H}^i(\underline{r}) + \iint_S \left\{-ikY(\hat{n}' \wedge [\underline{E}])g + (\hat{n}' \wedge [\underline{H}]) \wedge \nabla' g + (\hat{n}' \cdot [\underline{H}])\nabla' g \right\} dS'$$

and when the boundary conditions (3), (4) and the relation (15) are used, we have

$$\underline{E}(\underline{r}) = \underline{E}^i(\underline{r}) + ikZ \iint_S \left\{\underline{J}(\underline{r}')g - \frac{1}{k^2}(\nabla'_s \cdot \underline{J})\nabla g\right\} dS' \tag{20}$$

$$\underline{H}(\underline{r}) = \underline{H}^i(\underline{r}) + \iint_S \underline{J}(\underline{r}') \wedge \nabla' g \, dS' \, . \tag{21}$$

The above results could also have been obtained using a Hertz vector representation of the scattered field, and are identical to those for an open resistive sheet when the line integral contribution to the electric field is ignored. More to the point, when the steps leading from (12) to (14) are reversed and applied to (20), eq. (12) for an open sheet is recovered, thereby validating this integral representation for both open and closed resistive sheets.

For a closed shell either (12) or (20) can be used to generate an integral equation for $\underline{J}$, but the two equations are significantly different. On selecting the tangential components of (20) and then allowing the observation point to lie on either side of S, we have

$$\hat{n} \wedge \underline{E}(\underline{r}) = \hat{n} \wedge \underline{E}^i(\underline{r}) + ikZ \lim_{\underline{r} \to S} \iint_S \left\{\hat{n} \wedge \underline{J}(\underline{r}')g - \frac{1}{k^2}(\nabla'_s \cdot \underline{J})\hat{n} \wedge \nabla' g\right\} dS' \tag{22}$$

and since

$$\hat{n} \wedge \nabla' g = (\hat{n} - \hat{n}') \wedge \nabla' g + \hat{n}' \wedge \nabla' g,$$

the more singular term in the integrand contains only tangential derivations of the kernel at the self point $\underline{r}' = \underline{r}$. It follows that the integral in (22) is continuous as $\underline{r}$ approaches S, allowing us to apply the limit directly to the integrand, and imposition of the boundary condition (5) then gives

$$\hat{n}_\wedge \underline{E}^i(\underline{r}) = R\hat{n}_\wedge \underline{J}(\underline{r}) - ikZ \iint_S \left\{\hat{n}_\wedge \underline{J}(\underline{r}')g - \frac{1}{k^2}(\nabla'_s \cdot \underline{J})\hat{n}_\wedge \nabla' g\right\} dS' \tag{23}$$

for $\underline{r}$ on S. This is a valid integral equation whose only disadvantage is the occurrence of surface derivatives of $\underline{J}$.

This difficulty can be overcome if we use the integral representation (12). On paralleling the steps leading from (20 to (22), we have

$$\hat{n}_\wedge \underline{E}(\underline{r}) = \hat{n}_\wedge \underline{E}^i(\underline{r}) + ikZ \lim_{\underline{r}\to S} \iint_S \left\{\hat{n}_\wedge \underline{J}(\underline{r}')g + \frac{1}{k^2}\left[\underline{J}(\underline{r}')\cdot\nabla'\right]\hat{n}_\wedge \nabla' g\right\} dS' \tag{24}$$

and because of the higher order, non-integrable singularity of the integrand at the self point, it is no longer possible to apply the limit directly to the integrand. Since the contribution of the 'self cell' tends to infinity as the cell size tends to zero, even the limit shown in (24) does not exist, and though (24) differs from (22) only through an integration by parts applied to the second term in the integrand, it does not constitute an analytically valid integral equation. Nevertheless, it can be used as the basis of a numerical solution provided the segmentation of the integral which is inherent in such a method is performed prior to the limiting operation, with the segment size remaining non-zero. The resulting equation is in some respects preferable to (22) and has been found more convenient for our present purposes.

A-3 Scattering by a Cylindrical Resistive Shell

We now turn to the problem of a closed cylindrical shell illuminated by a plane wave at oblique incidence, and consider the form which the above integral equations take in this particular case.

Since the shell is independent of the z coordinate, the entire dependence on z is that produced by the incident field. If, therefore,

$$\underline{E}^i(\underline{r}) = \underline{E}^i(\underline{\rho})\exp(ik_z z), \qquad \underline{H}^i(\underline{r}) = \underline{H}^i(\underline{\rho})\exp(ik_z z) \tag{25}$$

where $\underline{r} = \underline{\rho} + z\hat{z}$, the total fields admit the same decomposition and, in particular,

$$\underline{J}(\underline{r}) = \underline{J}(s)\exp(ik_z z) \tag{26}$$

where s is the circumferential distance around the shell in the plane $z = 0$. Thus

$$\iint_S \underline{J}(\underline{r}')g\,dS' = \frac{i}{4}\exp(ik_z z)\int_C \underline{J}(s')H_0^{(1)}(\kappa d)ds'$$

where (now)

$$\underline{d} = \underline{\rho} - \underline{\rho}'$$

and

$$\kappa = \sqrt{k^2 - k_z^2} \quad . \tag{27}$$

The remaining integration is with respect to the circumferential distance s around the (closed) perimeter of the shell in the plane $z = 0$. Also

$$\nabla_s' \cdot \underline{J} = \exp(ik_z z')\left\{\frac{\partial}{\partial s'}J_s(s') + ik_z J_z(s')\right\}$$

and since

$$\iint_S f(\underline{\rho}')\exp(ik_z z')\nabla' g\,dS' = \frac{i}{4}\exp(ik_z z)\int_C f(s')(\nabla_t' - ik_z\hat{z})H_0^{(1)}(\kappa d)\,ds'$$

where ∇_t' is the two-dimensional (transverse) del operator in the plane $z = 0$,

eq. (23) becomes

$$\hat{n}\wedge\underline{E}^i(s) = R\hat{n}\wedge\underline{J}(s) + \frac{kZ}{4}\hat{n}\wedge\int_C\left\{\underline{J}(s')H_0^{(1)}(\kappa d) - \frac{1}{2k}\left[\frac{\partial J_s}{\partial s'} + ik_z J_z(s')\right]\cdot(\nabla_t' - ik_z\hat{z})H_0^{(1)}(\kappa d)\right\}ds' \tag{28}$$

The $\hat{s}$ component is simply

$$YE_z^i(s) = YRJ_z(s) + \frac{\kappa^2}{4k}\int_C\left\{J_z(s') + i\frac{k_z}{\kappa^2}\frac{\partial J_s}{\partial s'}\right\}H_0^{(1)}(\kappa d)\,ds' \quad . \tag{29}$$

which is a coupled integral equation involving the longitudinal and circumferential components of the current. Likewise, from the $\hat{z}$ component of (28) we obtain the second coupled equation

$$YE_z^i(s) = YRJ_z(s) + \frac{k}{4}\int_C \left\{ J_z(s')(\hat{s}\cdot\hat{s}')H_0^{(1)}(\kappa d) - \frac{\kappa}{k^2}\left[\frac{\partial J_s}{\partial s'} + ik_z J_z(s')\right](\hat{s}\cdot\hat{d})H_1^{(1)}(\kappa d)\right\} ds' . \qquad (30)$$

and though it is not in general possible to decouple (29) and (30), we can eliminate J_z from the integral portion of (30). Differentiating (29) with respect to s, we have

$$\int_C J_z(s')(\hat{s}\cdot\hat{d})H_1^{(1)}(\kappa d)ds' = \frac{4kY}{\kappa^3}\frac{\partial}{\partial s}\left\{RJ_z(s) - E_z^i(s)\right\} - i\frac{k_z}{\kappa^2}\int_C \frac{\partial J_s}{\partial s'}(\hat{s}\cdot\hat{d})H_1^{(1)}(\kappa d)ds' ,$$

and when this is substituted into (30), **the integral equation becomes**

$$Y\left\{E_s^i(s) - i\frac{k_z}{\kappa^2}\frac{\partial}{\partial s}E_z^i(s)\right\} = Y\left\{RJ_s(s) - i\frac{k_z}{\kappa^2}\frac{\partial}{\partial s}RJ_z(s)\right\} + \frac{k}{4}\int_C \left\{J_s(s')(\hat{s}\cdot\hat{s}')H_0^{(1)}(\kappa d) - \frac{1}{\kappa}\frac{\partial J_s}{\partial s'}(\hat{s}\cdot\hat{d})H_1^{(1)}(\kappa d)\right\} ds' . \qquad (31)$$

which now involves J_z only as a pseudo excitation term.

Formally at least, the corresponding equations resulting from (24) can be obtained from (20) and (30) by integrating by parts the terms involving $\partial J_z/\partial s'$. Equation (29) is then replaced by

$$YE_z^i(s) = YRJ_z(s) + \frac{\kappa^2}{4k} \int_C \left\{ J_z(s') H_0^{(1)}(\kappa d) - i \frac{k_z}{\kappa} J_s(s')(\hat{s}' \cdot \hat{d}) H_1^{(1)}(\kappa d) \right\} dS' \quad (32)$$

and (30) by

$$YE_s^i(s) = YRJ_s(s) + \frac{k}{4} \int_C J_s(s')(\hat{s} \cdot \hat{s}') H_0^{(1)}(\kappa d) ds'$$

$$+ \frac{\kappa}{4k} \lim_{\rho \to C} \int_C J_s(s') \frac{\partial}{\partial s'} \left\{ (\hat{s} \cdot \hat{d}) H_1^{(1)}(\kappa d) \right\} ds' \quad (33)$$

$$- i \frac{\kappa k_z}{4k} \int_C J_z(s')(\hat{s} \cdot \hat{d}) H_1^{(1)}(\kappa d) ds' .$$

The latter is meaningful only if the second integral on the right hand side is handled in the manner described earlier. With this proviso, however, (32) and (33) are adequate for a numerical determination of the currents and we can, of course, eliminate $J_z(s')$ from the integral portion of (33) if we so desire.

The case considered now is that in which the plane wave is incident in a plane perpendicular to the z axis of the cylindrical shell. Then $k_z = 0$ implying $\kappa = k$, and (32) and (33) reduce to

$$YE_z^i(s) = YRJ_z(s) + \frac{k}{4} \int_C J_z(s') H_0^{(1)}(kd) ds' \quad (34)$$

$$YE_s^i(s) = YRJ_s(s) + \frac{k}{4} \int_C J_s(s')(\hat{s} . \hat{s}') H_0^{(1)}(kd) ds'$$

$$+ \frac{1}{4} \lim_{\rho \to C} \int_C J_s(s') \frac{\partial}{\partial s'} \left\{ (\hat{s} \cdot \hat{d}) H_1^{(1)}(kd) \right\} ds' , \quad (35)$$

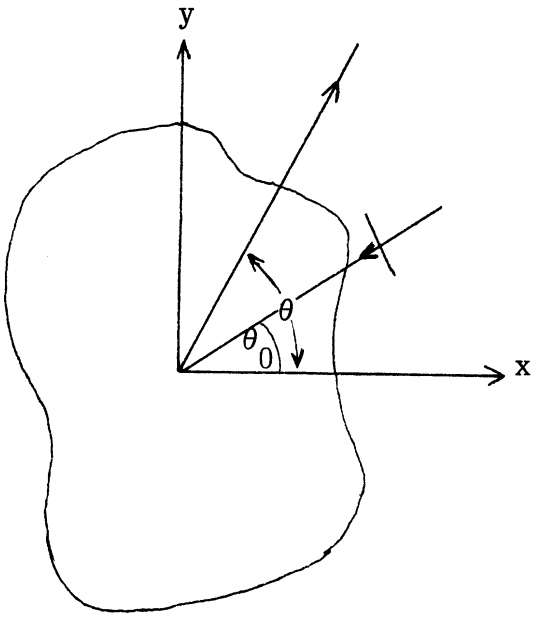

Fig. A-1. Geometry.

which are two uncoupled integral equations for the longitudinal and transverse current components $J_z(s)$ and $J_s(s)$ respectively.

If the incident field is E - polarized, i.e.

$$\underline{E}^i = \hat{z} e^{-ik(x\cos\theta_0 + y\sin\theta_0)}$$

where θ_0 is the angle of incidence with respect to the negative x axis (see Fig. A-1), only the component $J_z(s)$ is excited and we shall refer to (34) as the E - polarized equation. Once $J_z(s)$ has been found, the scattered electric field in the far zone is

$$\underline{E}^s = \hat{z} \sqrt{\frac{2}{\pi k\rho}}\, e^{i(k\rho - \pi/4)} P_E(\theta, \theta_0)$$

where the complex scattering amplitude P_E is given by

$$P_E(\theta, \theta_0) = -\frac{kZ}{4} \int_C J_z(s') e^{-ik\hat{\rho}\cdot\underline{\rho}'} ds' \tag{36}$$

with $$\hat{\rho} = \hat{x}\cos\theta + \hat{y}\sin\theta$$

and in terms of P, the two dimensional scattering cross section is

$$\sigma(\theta, \theta_0) = \frac{4}{k} \left| P(\theta, \theta_0) \right|^2 . \tag{37}$$

If, on the other hand, the incident field is H - polarized, i.e.

$$\underline{H}^i = \hat{z} e^{-ik(x\cos\theta_0 + y\sin\theta_0)}$$

the only component excited is $J_s(s)$ and this can be obtained from the H - polarized equation (35). In the far zone

$$\underline{H}^s = \hat{z} \sqrt{\frac{2}{\pi k\rho}}\, e^{i(k\rho - \pi/4)} P_H(\theta, \theta_0)$$

where $$P_H(\theta, \theta_0) = -\frac{k}{4} \int_C \hat{\rho}\cdot\hat{n}' J_s(s') e^{-ik\hat{\rho}\cdot\underline{\rho}'} ds' , \tag{38}$$

from which the H - polarized cross section can be found using (37).

Two quantities of particular interest are the total (integrated) scattering and the absorption cross sections σ_T and σ_A respectively. The former is given by

$$\sigma_T(\theta_0) = \frac{1}{2\pi} \int_0^{2\pi} \sigma(\theta, \theta_0) d\theta \tag{39}$$

and from the forward scattering theorem the absorption cross section is

$$\sigma_A(\theta_0) = - \sigma_T(\theta_0) - \frac{4}{k} \text{Re. } P(\theta_0 + \pi, \theta_0). \tag{40}$$

We remark that for a finite shell of length ℓ ($>>\lambda$) each three dimensional cross section $\sigma^{(3)}$ for incidence in a plane perpendicular to the length and computed on the assumption that the surface field is the same as for the infinite shell is related to the corresponding two dimensional cross section by

$$\sigma^{(3)} = \frac{2\ell^2}{\lambda} \sigma \tag{41}$$

where λ is the free space wavelength.

A-4 Computer Programs

The integral equations (34) and (35) are special cases of those solved by computer program RAMVS (Liepa et al., 1974), and because of the availability of this general program we chose to concentrate on these equations rather than the ones involving the derivatives of the currents. While seeking to refine RAMVS and to make it more efficient for a polygonal shell, we became aware of certain errors and/or deficiencies in the program which are most apparent when the resistivity is small. These had not shown up in the testing and verification done earlier, and it proved quite time consuming to locate the errors and rectify them. We believe this has now been done. In addition, the program has been extended to compute the normalized two dimensional cross sections and to plot the normalized bistatic scattering cross section, where the normalization is with respect to the free space wavelength to make the quantities dimensionless. The two programs that resulted are designated RICE and RICH and are based on eqs. (34) and (35) for E- and H- polarization respectively.

Both equations are solved by breaking up the integrals into N equal segments or cells within each of which the current is assumed constant, but because the kernels are infinite when the integration and observation points coincide, the self cells must be treated analytically. This is a rather trivial matter in the case of eq. (34) whose kernel has an integrable singularity. From the small argument expansion of the the Hankel function we have

$$H_0^{(1)}(kd) \simeq \left\{1 + \frac{2i}{\pi}\left(\ell n \frac{kd}{2} + \gamma\right)\right\}\left\{1 - \left(\frac{kd}{2}\right)^2\right\} + \frac{2i}{\pi}\left(\frac{kd}{2}\right)^2$$

where $\gamma = 0.577215...$ is Euler's constant, and hence, for the self cell Δ of width 2δ,

$$\int_\Delta J_z(s')H_0^{(1)}(kd)ds' \simeq 2\delta J_z(s)\left\{1 + \frac{2i}{\pi}\left(\ell n \frac{2\delta}{\lambda} + 0.028798...\right)\right\}.$$

Equation (34) now becomes

$$YE_z^i(s) = \left[YR + \frac{\pi\delta}{\lambda}\left\{1 + \frac{2i}{\pi}\left(\ell n \frac{2\delta}{\lambda} + 0.028798...\right)\right\}\right] J_z(s) + \frac{\pi}{2\lambda}\int_{C-\Delta} J_z(s')H_0^{(1)}(kd)ds' \tag{42}$$

and this is the equation used in program RICE.

The same reasoning applied to the first integral in (35) gives

$$\int_\Delta J_s(s')(\hat{s}\cdot\hat{s}')H_0^{(1)}(kd)\,ds' \simeq 2\delta J_s(s)\left\{1 + \frac{2i}{\pi}\left(\ell n \frac{2\delta}{\lambda} + 0.028798...\right)\right\},$$

but the second integral is more difficult to treat. When the self cell is excluded from the range of integration, the limiting operation can be applied to the integrand directly, and since $J_s(s')$ is assumed constant over each cell,

$$\lim_{\underline{\rho}\to C} \int_{C-\Delta} J_s(s') \frac{\partial}{\partial s'} \left\{ (\hat{s}\cdot\hat{d}) H_1^{(1)}(kd) \right\} ds' = \sum_{\substack{j=1 \\ j\neq i}}^{N} J_s(s_j) \left[(\hat{s}\cdot\hat{d}) H_1^{(1)}(kd) \right]_{\rho' = \rho_j - \delta}^{\rho' = \rho_j + \delta}$$

where the subscripts j and i denote the integration and observation points respectively. To evaluate the self cell contribution we first use the fact that

$$\frac{\partial}{\partial s'} \left\{ (\hat{s}\cdot\hat{d}) H_1^{(1)}(kd) \right\} = k \left\{ (\hat{n}'\cdot\hat{d})(\hat{n}\cdot\hat{d}) - (\hat{s}'\cdot\hat{d})(\hat{s}\cdot\hat{d}) \right\} H_1^{(1)'}(kd)$$
$$- k(\hat{n}'\cdot\hat{d})(\hat{n}\cdot\hat{d}) H_0^{(1)}(kd)$$

with the prime attached to the Hankel function denoting differentiation to express the contribution as

$$J_s(s) \lim_{\underline{\rho}\to C} I$$

where
$$I = k \int_{\Delta} \left\{ (\hat{n}'\cdot\hat{d})(\hat{n}\cdot\hat{d}) - (\hat{s}'\cdot\hat{d})(\hat{s}\cdot\hat{d}) \right\} H_1^{(1)'}(kd) ds'.$$

For a locally plane element with the observation point a small distance y above its midpoint,

$$I = 2k \int_0^{\delta} \frac{y^2 - t^2}{y^2 + t^2} H_1^{(1)'}(k\sqrt{y^2 + t^2})\, dt$$

and on inserting the small argument expansion of the Hankel function, we have

$$I \simeq \frac{4i\delta}{\pi k} \frac{1}{y^2 + \delta^2} + k \int_0^{\delta} \frac{y^2 - t^2}{y^2 + t^2} \left\{ 1 + \frac{2i}{\pi} \left(\ln\left[\frac{k}{2} \sqrt{y^2 + t^2} \right] + \gamma + \frac{1}{2} \right) \right\} dt \,.$$

Hence

$$\lim_{y \to 0} I = \frac{4i}{\pi k \delta} - k \int_0^{\delta} \left\{ 1 + \frac{2i}{\pi} \left(\ell n \frac{kt}{2} + \gamma + \frac{1}{2} \right) \right\} dt$$

$$= \frac{4i}{\pi k \delta} - k\delta \left\{ 1 + \frac{2i}{\pi} \left(\ell n \frac{2\delta}{\lambda} + 0.528798\ldots \right) \right\}$$

the first term of which becomes infinite as the cell size tends to zero. Equation (35) now has the form

$$YE_s^i(s) = \left[YR + \frac{i}{\pi} \frac{\lambda}{2} \frac{}{2\delta} + \frac{\pi\delta}{2\lambda} \left\{ 1 + \frac{2i}{\pi} \left(\ell n \frac{2\delta}{\lambda} + 0.028798\ldots - 0.5 \right) \right\} \right] J_s(s)$$

$$+ \frac{\pi}{2\lambda} \int_{c-\Delta} J_s(s')(\hat{s} \cdot \hat{s}') H_0^{(1)}(kd) ds' \qquad (43)$$

$$+ \frac{1}{4} \sum_{\substack{j=1 \\ j \neq i}}^{N} J_s(s_j) \left[(\hat{s} \cdot \hat{d}) H_1^{(1)}(kd) \right]_{\rho' = \rho_j - \delta}^{\rho' = \rho_j + \delta}$$

whose solution is computed by program RICH.

Of the two programs it is evident that RICH is the more complicated, and to obtain a feeling for the rapidity of convergence as a function of the cell size, the program was run for edge-on incidence on a hexagonal shell 3μ on the side at a wavelength 2.6μ. The normalised resistivity employed was

$$YR = 0.03876 + i9.10650$$

corresponding to a shell 0.1μ thick and the refractive index

$$n = 1.206 + i0.00080$$

for ice at 2.6μ quoted by Irvine and Pollack (1968). The results of decreasing the total number N of cells from 72 down to 24 are listed in Table A-1, and we observe that the total scattering and absorption cross sections are relatively insensitive to

TABLE A - 1: Effect of Cell Size

N	cells per wavelength	time used (sec.)	$\sigma(\theta_0, \theta_0)/\lambda$ (dB)	$\sigma(\pi+\theta_0, \theta_0)/\lambda$ (dB)	$\sigma_T(\theta_0)/\lambda$	$\sigma_A(\theta_0)/\lambda$
72	10.4	10.911	-44.83	-6.45	0.02229	0.00158
60	8.7	6.645	-44.70	-6.45	0.02230	0.00157
48	6.9	3.768	-44.48	-6.45	0.02233	0.00155
36	5.2	1.948	-44.04	-6.46	0.02241	0.00153
30	4.3	1.332	-43.63	-6.46	0.02250	0.00151
24	3.5	0.895	-42.91	-6.46	0.02272	0.00149

N, as is the forward scattering cross section, but the backscattering changes noticeably on decreasing the sampling rate below (about) 9 cells per wavelength. In running the program we have therefore used 9 or more cells per wavelength whenever possible consistent with the maximum of N = 100 allowed by the matrix inversion routine used.

Listings of the two programs follow.

```
C*****************************************************************************C
C    INPUT FORMAT FOR PROGRAM RICE     SEPT, 1975                              C
C*****************************************************************************C
C  CARD 1   FORMAT (18A4)              TITLE CARD: USE UP TO 72 COLUMNS        C
C                                                                              C
C CARD 2    FORMAT (I2,I3,5F10.5)    MORE,KODE,ZFAC,WAVE,FIRST,LAST,INK       C
C           MORE=0         THIS WILL BE THE LAST RUN FOR THIS DATA SET         C
C           MORE=1         THERE ARE MORE DATA TO BE READ AFTER THIS SET       C
C           KODE=0         COMPUTES BISTATIC SCATTERING PATTERN                C
C           KODE=1         COMPUTES BACKSCATTERING PATTERN                     C
C           ZFAC           A COMPLEX FACTOR MULTIPLYING ALL ELEMENT            C
C           WAVE           WAVELENGTH                                          C
C           FIRST          INITIAL SCATTERING AND INCIDENCE ANGLE              C
C           LAST           FINAL ANGLE                                         C
C           INK            ANGULAR INCREMENT                                   C
C                                                                              C
C  CARD 3   FORMAT (I2,5X,7F10.5) N,Z,XA,YA,XB,YB,ANG                          C
C           N              NUMBER OF SAMPLING POINTS ON THIS SEGMENT           C
C           Z              NORMALIZED IMPEDANCE OF THE SEGMENT                 C
C           XA,YA,XB,YB    SEGMENT ENDPOINTS                                   C
C           ANG            ANGLE SUBTENDED BY THE SEGMENT                      C
C                                ZERO IN COL 2 SHUTS OFF                       C
C                                READING OF SEGMENTS                           C
C                                                                              C
C  CARD 4   FORMAT (I2,I3,F10.5)    MORE,KODE,ZFAC,FIRST,LAST,INK             C
C                                THIS CARD IS USED ONLY IF,                    C
C                                ON CARD 2, MORE=1                             C
C*****************************************************************************C
C                                                                              C
C    IO SPECIFICATIONS:                                                        C
C      5:INPUT DATA: 6:OUTPUT(PRINTER): 7:OUTPUT(GRAPHICS)                     C
C                                                                              C
C*****************************************************************************C
```

```
      COMPLEX*8 A(100,101),PHI(100),PINK(100),ZS(10)
      COMPLEX*8 DEL,SUM,ZFAC
      REAL*4 LAST,INK
      REAL*4 X(200),Y(200),XN(200),YN(200),S(200),DSQ(10),ASUM(361),RSUM(361)
      INTEGER*4 ID(18),LUMP(200),IPOL(2),LV(100),MM(100)
      DATA MH/100/
      COMMON /PIES/ PI,TPI, PIT, PIPI, YZ,RED,DIG
      DATA IPOL /'EEEE', 'HHHH'/
      DATA IPP/1/
C.....READ INPUT DATA AND GENERATE BODY PROFILE
    5 READ (5,100) ID
      READ (5,200) MORE,KODE,ZFAC,WAVE,FIRST,LAST,INK
      WRITE(7,100) ID
      WRITE(7,101) WAVE
      WRITE(7,199) FIRST,LAST,INK,IPP
  101 FORMAT(' LAMBDA=',F5.2,' MICRONS')
  199 FORMAT(1X,3F10.5,I3)
      IWHICH=1
      IF(REAL(ZFAC).EQ.0.AND.AIMAG(ZFAC).EQ.0.)
     &ZFAC=(1.E-20,1.E-20)
      WRITE (6,150) ID
      WRITE (6,300)
      CALL GEOM(LUMP,X,Y,XN,YN,S,DSQ,ZS,M)
      MT=M/2
      LL=LUMP(M)

   20 IF (KODE.NE.0) GO TO 25
      NINC=1
      NBIT=1+IFIX((LAST-FIRST)/INK)
      GO TO 30
   25 NBIT=0
      NINC=1+IFIX((LAST-FIRST)/INK)
   30 WRITE (6,150) ID
      WRITE (6,400) IPOL(IPP),LL,MT,NINC,NBIT,WAVE,ZFAC
      WRITE (6,425) FIRST
   38 DO 35 I=1,LL
      ZS(I)=ZS(I)*ZFAC
   35 DSQ(I)=DSQ(I)/WAVE
      XK=TPI/WAVE
C.....CONSTRUCT MATRIX ELEMENTS
      IF(IWHICH.EQ.2) GO TO 37
      CALL MTX(M,MH,XK,X,Y,XN,YN,DSQ,LUMP,ZS,A)
C.....COMPUTE INCIDENT FIELD AND INVERT MATRIX
   37 TETA=RED*FIRST
      CT=COS(TETA)
      ST=SIN(TETA)
      DO 60 I=2,M,2
      HOLD=-XK*(CT*X(I)+ST*Y(I))
      DEL=CMPLX(COS(HOLD),SIN(HOLD))
   60 PINK(I/2)=DEL
      CALL FLIP(A,MT,MH,LV,MM,PINK,PHI,IWHICH)
```

```
C.....PRINT OUT CURRENTS AND ELEMENT PROPERTIES FOR FIRST ANGLE
      WRITE (6,500)
      IT=0
      DO 65 I=2,M,2
      IT=IT+1
      AMP=CABS(PHI(IT))
      PHASE=DIG*ATAN2(AIMAG(PHI(IT)),REAL(PHI(IT)))
      ISEG=LUMP(I)
   65 WRITE (6,250) IT,ISEG,X(I),Y(I),S(I),DSQ(ISEG),ZS(ISEG),AMP,PHASE
C.....DOPE OUT THE APPROPRIATE FIELD FACTORS
      THE=FIRST-INK
      K=0
      IF (KODE.EQ.1) GO TO 70
      WRITE (6,800) FIRST
      GO TO 75
   70 WRITE (6,600)
   75 THE=THE+INK
      IF (THE.GT.LAST) GO TO 105
      IF (THE.EQ.FIRST) GO TO 85
C.....IN THE FOLLOWING LOOP, PINK IS NOT NECESSARILY THE INCIDENT FIELD
      TETA=RED*THE
      CT=COS(TETA)
      ST=SIN(TETA)
      DO 80 J=2,M,2
      HOLD=-XK*(CT*X(J)+ST*Y(J))
      DEL=CMPLX(COS(HOLD),SIN(HOLD))
   80 PINK(J/2)=DEL
      IF (KODE.EQ.0) GO TO 85
      CALL FLIP(A,MT,MH,LV,MM,PINK,PHI,2)
   85 SUM=CMPLX(0.0,0.0)
C.....ADD UP THE CURRENTS
      DO 95 J=2,M,2
      JT=J/2
   95 SUM=SUM+PHI(JT)*PINK(JT)*DSQ(LUMP(J))
      SUM=-SUM
      SUMR=REAL(SUM)
      SUMI=AIMAG(SUM)
      SUMSQ=SUMR*SUMR+SUMI*SUMI
      SCAT=10.*ALOG10(SUMSQ)+1.9612
      K=K+1
      ASUM(K)=SUMSQ
      RSUM(K)=REAL(SUM)
      PHASE=DIG*ATAN2(SUMI,SUMR)
      WRITE(6,901) THE,SCAT,PHASE
      WRITE(7,900) THE,SCAT,PHASE
      GO TO 75
  105 DIFF=LAST-FIRST
      IF(DIFF .NE. 180.0 .AND. DIFF .NE. 360.0) GO TO 205
      IODD=MOD(K,2)
      IF(DIFF .EQ. 360.0 .AND. IODD .NE. 1) GO TO 205
      IF(DIFF .EQ. 180.0) FAC=2.0
      IF(DIFF .EQ. 360.0) FAC=1.0
```

```
C*** SIMPSON INTEGRATION OF CROSSECTIONS
      KLAST=K
      IF(IODD .EQ. 0) KLAST=KLAST-3
      SIGT=ASUM(1)+ASUM(KLAST)
      SIG=0.0
      DO 203 I=2,KLAST,2
  203 SIG=SIG+ASUM(I)
      SIGT=SIGT+4.0*SIG
      SIG=0.0
      KLAST=K-2
      DO 210 I=3,KLAST,2
  210 SIG=SIG+ASUM(I)
      SIGT=SIGT+2.0*SIG
      SIGT=SIGT*INK/3.0
      IF(IODD .EQ. 0) SIGT=SIGT+3./8.*INK*
     &(ASUM(K-3)+ASUM(K)+3.*(ASUM(K-2)+ASUM(K-1)))
      SIGT=SIGT*FAC*RED/4.
C*** END SIMPSON INTEGRATION
      KF=K
      IF(FAC .EQ. 1) KF=(K+1)/2
      SIGF=-RSUM(KF)
      SIGA=-SIGT+SIGF
      IF(KODE) 220,220,240
  220 SIGTDB=10.0*ALOG10(SIGT)
      IF(SIGA .LE. 0.0) GO TO 225
      SIGADB=10.0*ALOG10(SIGA)
      GO TO 230
  225 WRITE(6,825) SIGT,SIGA,SIGF
      WRITE(7,825) SIGT,SIGA,SIGF
      GO TO 205
  230 SIGTDB=10.0*ALOG10(SIGT)
      WRITE(6,850) SIGT,SIGTDB,SIGA,SIGADB
      WRITE(7,851) SIGT,SIGTDB,SIGA,SIGADB
      GO TO 205
  240 SIGTDB=10.0*ALOG10(SIGT)
      WRITE(6,875) SIGT,SIGTDB
  825 FORMAT(///,5X,40H*FOUL*   NEGATIVE ABSORPTION CROSSECTION,//,
     &15X,5HSIGT=,F8.5,5X,5HSIGA=,F8.5,5X,5HSIGF=,F8.5)
  850 FORMAT(///,15X,5HSIGT=,F8.5,F8.2,3H DB,5X,5HSIGA=,F8.5,F8.2,
     &3H DB)
  851 FORMAT(///,15X,'SIGMA(T)/LAMBDA=',F8.5,F8.2,' DB',5X,
     &'SIGMA(A)/LAMBDA=',F8.5,F8.2,' DB')
  875 FORMAT(///,15X,7HSIGAVE=,F8.5,F8.2,3H DB)

  205 IF (MORE.EQ.0) GO TO 5
      DO 103 I=1,LL
      ZS(I)=ZS(I)/ZFAC
  103 DSQ(I)=DSQ(I)*WAVE
      DEL=ZFAC
      PWAVE=WAVE
```

```
      READ (5,200) MORE,KODE,ZFAC,WAVE,FIRST,LAST,INK
      WRITE(7,100) ID
      WRITE(7,101) WAVE
      WRITE(7,199) FIRST,LAST,INK,IPP
      IWHICH=1
      IF(REAL(ZFAC).EQ.0.AND.AIMAG(ZFAC).EQ.0.)
     &ZFAC=(1.E-20,1.E-20)
      IF(REAL(ZFAC).EQ.REAL(DEL).AND.AIMAG(ZFAC).EQ.AIMAG(DEL)
     &.AND.WAVE.EQ.PWAVE) IWHICH=2
      GO TO 20
  100 FORMAT (18A4)
  150 FORMAT (1H1,18A4)
  200 FORMAT (I2,I3,6F10.5)
  250 FORMAT (2I5,7F10.5,F10.3)
  300 FORMAT (10HOSEG   NUM,11X,24HENDPOINTS OF THE SEGMENT,19X,
     &18HSEGMENT PARAMETERS/11H NUM  CELLS,6X,2HXA,8X,2HYA,8X,2HXB,8X,
     &2HYB,6X,24HANGLE   RADIUS    LENGTH,4X,14HRE-Z       IM-Z//)
  400 FORMAT (//31X,14HKEY PARAMETERS//
     &16X,21HINCIDENT POLARIZATION,22X,1A1/
     &16X,23HNUMBER OF SEGMENTS USED,I21/
     &16X,33HTOTAL NUMBER OF CELLS ON THE BODY,I11/
     &16X,35HNUMBER OF INCIDENT FIELD DIRECTIONS,I9/
     &16X,29HNUMBER OF BISTATIC DIRECTIONS,I15/
     &16X,10HWAVELENGTH,F34.5/
     &16X,16HIMPEDANCE FATOR,F16.5,' ,',F10.5)
  425 FORMAT (////,36X,18HSURFACE FIELD DATA/,27X,
     &29HFOR INCIDENT FIELD DIRECTION=,F7.2)
  500 FORMAT (11HO   I   SEG,4X,4HX(I),6X,4HY(I),6X,4HS(I),5X,6HDSO(I),
     &4X,6HRS(I) ,4X,6HXS(I) ,4X,6HMOD(J),4X,6HARG(J))
  600 FORMAT (1H1,27X,28HBACKSCATTERING CROSS SECTION//23X,
     &36HTHETA    SIGMA/LAMBDA,DB   PHASE,DEG)
  800 FORMAT (1H1,23X,33HBISTATIC SCATTERING CROSS SECTION/23X,
     &29HFOR INCIDENT FIELD DIRECTION=,F7.2//23X,
     &36HTHETA    SIGMA/LAMBDA,DB   PHASE,DEG)
  900 FORMAT (15X,F13.2,F14.2,F16.1)
  901 FORMAT (15X,F13.2,F14.2,F15.1)
      END
      SUBROUTINE MTX(M,MH,XK,X,Y,XN,YN,DSO,LUMP,ZS,A)
C   RICE VERSION, F-POLARIZATION
      REAL*4 X(1),Y(1),XN(1),YN(1),DSO(1)
      INTEGER*4 LUMP(1)
      COMPLEX*8 A(MH,1),ZS(1),HZ,DUM
      COMMON /PIES/ PI,TPI, PIT, PIPI, YZ,RED,DIG
      IH=0
      DO 10 I=2,M,2
      IH=IH+1
      XI=X(I)
      YI=Y(I)
      JH=0
      DO 10 J=2,M,2
      JH=JH+1
      ISEG=LUMP(J)
      DS=DSO(ISEG)
      IF(IH.EQ.JH)GO TO 50
```

```
      RX=XI-X(J)
      RY=YI-Y(J)
      R=SQRT(RX*RX+RY*RY)
      RK=R*XK
      CALL HANKZ1(RK,0,HZ,DUM)
      A(IH,JH)=PIT*HZ*DS
      GO TO 10
   50 A(IH,JH)=ZS(ISEG)+
     &DS*CMPLX(PIT,ALOG(DS)+.02879837)
   10 CONTINUE
      RETURN
      END
      SUBROUTINE GEOM(LUMP,X,Y,XN,YN,S,DSQ,ZS,M)
C    THIS VERSION READS AND GENETATES SEGMENTS IN COUNTER-CLOCKWISE DIRECTION.
C    THE SURFACE MUST BE CLOSED.
C    POINTS ARE GENERETED AT  THE START AND MIDPOINTS OF EACH CELL;
C    THE START POINT OF THE FIRST CELL EVENTUALLY COINCIDES
C    WITH THE END POINT OF THE LAST CELL.
      COMPLEX*8 ZS(1),Z
      REAL*4 X(1),Y(1),XN(1),YN(1),S(1),DSQ(1)
      INTEGER*4 LUMP(1)
      COMMON /PIES/ PI,TPI, PIT, PIPI, YZ,RED,DIG
      I=0
      L=0
C.....READ INPUT PARAMETERS AND PREPARE TO GENERATE SAMPLING POINTS
   10 READ (5,200) N,Z,XA,YA,XB,YB,ANG
      IF(N.LT.1) GO TO 120
      LIM=2*N
      TX=XA-XB
      TY=YA-YB
      D=SQRT(TX*TX+TY*TY)
      L=L+1
      ZS(L)=Z
      IF (ANG.EQ.0.0) GO TO 20
      T=0.5*RED*ANG
      TRX=TX+TY*COTAN(T)
      TRY=TY-TX*COTAN(T)
      RAD=0.5*D/SIN(T)
      ARC=2.0*RAD*T
      ALF=T/N
      DSQ(L)=2.0*RAD*ALF
      GO TO 30
   20 RAD=999.999
      ARC=D
      DSQ(L)=D/N
C.....START GENERATING
   30 DSS=0.
      DS=DSQ(L)/2.
      DO 50 JJ=1,LIM
      I=I+1
      J=JJ-1
      S(I)=DSS
      DSS=DSS+DS
```

```
      LUMP(I)=L
      IF (ANG.EQ.0.0) GO TO 40
      ARG=J*ALF
      SINQ=SIN(ARG)
      COSQ=COS(ARG)
      X(I)=XA-0.5*(TRX*(1.0-COSQ)-TRY*SINQ)
      Y(I)=YA+0.5*(TRX*SINQ+TRY*(1.0-COSQ))
      XN(I)=+0.5*(TRX*COSQ+TRY*SINQ)/RAD
      YN(I)= 0.5*(TRX*SINQ-TRY*COSQ)/RAD
      GO TO 50
   40 X(I)=XA-0.5*J*TX/N
      Y(I)=YA-0.5*J*TY/N
      XN(I)=-TY/D
      YN(I)= TX/D
   50 CONTINUE
  100 WRITE(6,300)L,N,XA,YA,XB,YB,ANG,RAD,ARC,Z
      GO TO 10
  120 M=I
      LL=L
  200 FORMAT(I2,3X,7F10.5)
  300 FORMAT(I3,I6,4X,4F10.5,F7.2,4F10.5)
      RETURN
      END
      SUBROUTINE HANKZ1(R,N,HZERO,HONE)
C.....HANKEL FUNCTIONS ARE OF FIRST KIND--J+IY
C.....   N=0 RETURNS HZERO
C.....   N=1 RETURNS HONE
C.....   N=2 RETURNS HZERO AND HONE
C.....SUBROUTINE REQUIRES R>0
C.....SUBROUTINE ADAM MUST BE SUPPLIED BY USER
      DIMENSION A(7),B(7),C(7),D(7),E(7),F(7),G(7),H(7)
      COMPLEX HZERO,HONE
      DATA A,B,C,D,E,F,G,H/1.0,-2.2499997,1.2656208,-0.3163866,
     &0.0444479,-0.0039444,0.00021,0.36746691,0.60559366,-0.74350384,
     &0.25300117,-0.04261214,0.00427916,-0.00024846,0.5,-0.56249985,
     &0.21093573,-0.03954289,0.00443319,-0.00031761,-0.00001109,
     &-0.6366198,0.2212091,2.1682709,-1.3164827,0.3123951,-0.0400976,
     &0.0027873,0.79788456,-0.00000077,-0.0055274,-0.00009512,
     &0.00137237,-0.00072805,0.00014476,-0.78539816,-0.04166397,
     &-0.00003954,0.00262573,-0.00054125,-0.00029333,0.00013558,
     &0.79788456,0.00000156,0.01659667,0.00017105,-0.00249511,
     &0.00113653,-0.00020033,-2.35619449,0.12499612,0.0000565,
     &-0.00637879,0.00074348,0.00079824,-0.00029166/
      IF (R.LE.0.0) GO TO 50
      IF (N.LT.0.OR.N.GT.2) GO TO 50
      IF (R.GT.3.0) GO TO 20
      X=R*R/9.0
      IF (N.EQ.1) GO TO 10
      CALL ADAM(A,X,BJ)
      CALL ADAM(B,X,Y)
      BY=0.6366198*ALOG(0.5*R)*BJ+Y
      HZERO=CMPLX(BJ,BY)
      IF (N.EQ.0) RETURN
```

```
10   CALL ADAM(C,X,Y)
     BJ=R*Y
     CALL ADAM(D,X,Y)
     BY=0.6366198*ALOG(0.5*R)*BJ+Y/R
     HONE=CMPLX(BJ,BY)
     RETURN
20   X=3.0/R
     IF (N.EQ.1) GO TO 30
     CALL ADAM(F,X,Y)
     FOOL=Y/SQRT(R)
     CALL ADAM(F,X,Y)
     T=R+Y
     BJ=FOOL*COS(T)
     BY=FOOL*SIN(T)
     HZERO=CMPLX(BJ,BY)
     IF (N.EQ.0) RETURN
30   CALL ADAM(G,X,Y)
     FOOL=Y/SQRT(R)
     CALL ADAM(H,X,Y)
     T=R+Y
     BJ=FOOL*COS(T)
     BY=FOOL*SIN(T)
     HONE=CMPLX(BJ,BY)
     RETURN
50   WRITE(6,90) N,R
90   FORMAT(32HOSICK DATA IN HANKZ1  *QUIT*  N=,I2,2X,2HR=,F11.3)
     CALL SYSTEM
     END
     SUBROUTINE ADAM(C,X,Y)
     DIMENSION C(7)
     Y=X*C(7)
     DO 10 I=1,5
10   Y=X*(C(7-I)+Y)
     Y=Y+C(1)
     RETURN
     END
     SUBROUTINE FLIP(A,N,MI,L,M,X,Y,IAT)
     COMPLEX A(MI,1),X(1),Y(1),D,BIGA,HOLD
     DIMENSION L(1),M(1)
     IF (IAT.GT.1) GO TO 150
     D=CMPLX(1.0,0.0)
     DO 80 K=1,N
     L(K)=K
     M(K)=K
     BIGA=A(K,K)
     DO 20 J=K,N
     DO 20 I=K,N
10   IF (CABS(BIGA).GE.CABS(A(I,J))) GO TO 20
     BIGA=A(I,J)
     L(K)=I
     M(K)=J
```

```
 20   CONTINUE
      J=L(K)
      IF (J.LE.K) GO TO 35
      DO 30 I=1,N
      HOLD=-A(K,I)
      A(K,I)=A(J,I)
 30   A(J,I)=HOLD
 35   I=M(K)
      IF (I.LE.K) GO TO 45
      DO 40 J=1,N
      HOLD=-A(J,K)
      A(J,K)=A(J,I)
 40   A(J,I)=HOLD
 45   IF (CABS(BIGA).NE.0.0) GO TO 50
      D=CMPLX(0.0,0.0)
      RETURN
 50   DO 55 I=1,N
      IF (I.EQ.K) GO TO 55
      A(I,K)=-A(I,K)/BIGA
 55   CONTINUE
      DO 65 I=1,N
      DO 65 J=1,N
      IF (I.EQ.K.OR.J.EQ.K) GO TO 65
      A(I,J)=A(I,K)*A(K,J)+A(I,J)
 65   CONTINUE
      DO 75 J=1,N
      IF (J.EQ.K) GO TO 75
      A(K,J)=A(K,J)/BIGA
 75   CONTINUE
      D=D*BIGA
 80   A(K,K)=1.0/BIGA
      K=N
100   K=K-1
      IF (K.LE.0) GO TO 150
      I=L(K)
      IF (I.LE.K) GO TO 120
      DO 110 J=1,N
      HOLD=A(J,K)
      A(J,K)=-A(J,I)
110   A(J,I)=HOLD
120   J=M(K)
      IF (J.LE.K) GO TO 100
      DO 130 I=1,N
      HOLD=A(K,I)
      A(K,I)=-A(J,I)
130   A(J,I)=HOLD
      GO TO 100
150   DO 200 I=1,N
      Y(I)=CMPLX(0.0,0.0)
      DO 200 J=1,N
200   Y(I)=A(I,J)*X(J)+Y(I)
      RETURN
      END
      BLOCK DATA
      COMMON/PIES/PI,TPI,PIT,PIPI,YZ,RED,DIG
      DATA PI,TPI,PIT,PIPI,YZ,RED,DIG/3.1415927,6.2831853,
     &1.5707963,9.8696044,0.0026525824,0.01745329,57.29578/
      END
```

```
C*************************************************************************C
C   INPUT FORMAT FOR PROGRAM RICH    SEPT, 1975                           C
C*************************************************************************C
C  CARD 1  FORMAT (18A4)          TITLE CARD: USE UP TO 72 COLUMNS       C
C                                                                         C
C CARD 2   FORMAT (I2,I3,5F10.5)   MORE,KODE,ZFAC,WAVE,FIRST,LAST,INK    C
C          MORE=0        THIS WILL BE THE LAST RUN FOR THIS DATA SET     C
C          MORE=1        THERE ARE MORE DATA TO BE READ AFTER THIS SET   C
C          KODE=0        COMPUTES BISTATIC SCATTERING PATTERN            C
C          KODE=1        COMPUTES BACKSCATTERING PATTERN                 C
C          ZFAC          A COMPLEX FACTOR MULTIPLYING ALL ELEMENT        C
C          WAVE          WAVELENGTH                                      C
C          FIRST         INITIAL SCATTERING AND INCIDENCE ANGLE          C
C          LAST          FINAL ANGLE                                     C
C          INK           ANGULAR INCREMENT                               C
C                                                                         C
C  CARD 3  FORMAT (I2,5X,7F10.5) N,Z,XA,YA,XB,YB,ANG                      C
C          N             NUMBER OF SAMPLING POINTS ON THIS SEGMENT       C
C          Z             NORMALIZED IMPEDANCE OF THE SEGMENT             C
C          XA,YA,XB,YB   SEGMENT ENDPOINTS                               C
C          ANG           ANGLE SUBTENDED BY THE SEGMENT                  C
C                              ZERO IN COL 2 SHUTS OFF                    C
C                              READING OF SEGMENTS                        C
C                                                                         C
C  CARD 4  FORMAT (I2,I3,F10.5)   MORE,KODE,ZFAC,FIRST,LAST,INK           C
C                             THIS CARD IS USED ONLY IF,                  C
C                             ON CARD 2, MORE=1                           C
C*************************************************************************C
C                                                                         C
C   IO SPECIFICATIONS:                                                    C
C     5:INPUT DATA: 6:OUTPUT(PRINTER): 7:OUTPUT(GRAPHICS)                 C
C                                                                         C
C*************************************************************************C
      COMPLEX*8 A(100,101),PHI(100),PINK(100),ZS(10)
      COMPLEX*8 DEL,SUM,ZFAC
      REAL*4 LAST,INK
      REAL*4 X(200),Y(200),XN(200),YN(200),S(200),DSO(10),ASUM(361),RSUM(361)
      INTEGER*4 ID(18),LUMP(200),IPOL(2),LV(100),MM(100)
      DATA MH/100/
      COMMON /PIES/ PI,TPI, PIT, PIPI, Y7,RED,DIG
      DATA IPOL /'EEEE', 'HHHH'/
      DATA IPP/2/
C.....READ INPUT DATA AND GENERATE BODY PROFILE
    5 READ (5,100) ID
      READ (5,200) MORE,KODE,ZFAC,WAVE,FIRST,LAST,INK
      WRITE(7,100) ID
      WRITE(7,101) WAVE
      WRITE(7,199) FIRST,LAST,INK,IPP
  101 FORMAT(' LAMBDA=',F5.2,' MICRONS')
  199 FORMAT(1X,3F10.5,I3)
      IWHICH=1
      IF(REAL(ZFAC).EQ.0.AND.AIMAG(ZFAC).EQ.0.)
     &ZFAC=(1.E-20,1.E-20)
      WRITE (6,150) ID
      WRITE (6,300)
      CALL GEOM(LUMP,X,Y,XN,YN,S,DSO,ZS,M)
      MT=M/2
      LL=LUMP(M)
```

```
   20   IF (KODE.NE.0) GO TO 25
        NINC=1
        NBIT=1+IFIX((LAST-FIRST)/INK)
        GO TO 30
   25   NBIT=0
        NINC=1+IFIX((LAST-FIRST)/INK)
    30  WRITE (6,150) ID
        WRITE (6,400) IPOL(IPP),LL,MT,NINC,NBIT,WAVE,ZFAC
        WRITE (6,425) FIRST
    38  DO 35 I=1,LL
        ZS(I)=ZS(I)*ZFAC
   35   DSO(I)=DSO(I)/WAVE
        XK=TPI/WAVE
C.....CONSTRUCT MATRIX ELEMENTS
        IF(IWHICH.EQ.2) GO TO 37
        CALL MTX(M,MH,XK,X,Y,XN,YN,DSO,LUMP,ZS,A)
C.....COMPUTE INCIDENT FIELD AND INVERT MATRIX
    37  TETA=RED*FIRST
        CT=COS(TETA)
        ST=SIN(TETA)
        DO 60 I=2,M,2
        HOLD=-XK*(CT*X(I)+ST*Y(I))
        DEL=CMPLX(COS(HOLD),SIN(HOLD))
    60  PINK(I/2)=DEL*(XN(I)*CT+YN(I)*ST)
        CALL FLIP(A,MT,MH,LV,MM,PINK,PHI,IWHICH)
C.....PRINT OUT CURRENTS AND ELEMENT PROPERTIES FOR FIRST ANGLE
        WRITE (6,500)
        IT=0
        DO 65 I=2,M,2
        IT=IT+1
        AMP=CABS(PHI(IT))
        PHASE=DIG*ATAN2(AIMAG(PHI(IT)),REAL(PHI(IT)))
        ISEG=LUMP(I)
   65   WRITE (6,250) IT,ISEG,X(I),Y(I),S(I),DSO(ISEG),ZS(ISEG),AMP,PHASE
C.....DOPE OUT THE APPROPRIATE FIELD FACTORS
        THE=FIRST-INK
        K=0
        IF (KODE.EQ.1) GO TO 70
        WRITE (6,800) FIRST
        GO TO 75
   70   WRITE (6,600)
   75   THE=THE+INK
        IF (THE.GT.LAST) GO TO 105
        IF (THE.EQ.FIRST) GO TO 85
C.....IN THE FOLLOWING LOOP, PINK IS NOT NECESSARILY THE INCIDENT FIELD
        TETA=RED*THE
        CT=COS(TETA)
        ST=SIN(TETA)
        DO 80 J=2,M,2
        HOLD=-XK*(CT*X(J)+ST*Y(J))
        DEL=CMPLX(COS(HOLD),SIN(HOLD))
```

```
   80 PINK(J/2)=DEL*(XN(J)*CT+YN(J)*ST)
      IF (KODE.EQ.0) GO TO 85
      CALL FLIP(A,MT,MH,LV,MM,PINK,PHI,2)
   85 SUM=CMPLX(0.0,0.0)
C.....ADD UP THE CURRENTS
      DO 95 J=2,M,2
      JT=J/2
   95 SUM=SUM+PHI(JT)*PINK(JT)*DSQ(LUMP(J))
      SUMR=REAL(SUM)
      SUMI=AIMAG(SUM)
      SUMSQ=SUMR*SUMR+SUMI*SUMI
      SCAT=10.*ALOG10(SUMSQ)+1.9612
      K=K+1
      ASUM(K)=SUMSQ
      RSUM(K)=REAL(SUM)
      PHASE=DIG*ATAN2(SUMI,SUMR)
      WRITE(6,901) THE,SCAT,PHASE
      WRITE(7,900) THE,SCAT,PHASE
      GO TO 75
  105 DIFF=LAST-FIRST
      IF(DIFF .NE. 180.0 .AND. DIFF .NE. 360.0) GO TO 205
      IODD=MOD(K,2)
      IF(DIFF .EQ. 360.0 .AND. IODD .NE. 1) GO TO 205
      IF(DIFF .EQ. 180.0) FAC=2.0
      IF(DIFF .EQ. 360.0) FAC=1.0
C*** SIMPSON INTEGRATION OF CROSSECTIONS
      KLAST=K
      IF(IODD .EQ. 0) KLAST=KLAST-3
      SIGT=ASUM(1)+ASUM(KLAST)
      SIG=0.0
      DO 203 I=2,KLAST,2
  203 SIG=SIG+ASUM(I)
      SIGT=SIGT+4.0*SIG
      SIG=0.0
      KLAST=K-2
      DO 210 I=3,KLAST,2
  210 SIG=SIG+ASUM(I)
      SIGT=SIGT+2.0*SIG
      SIGT=SIGT*INK/3.0
      IF(IODD .EQ. 0) SIGT=SIGT+3./8.*INK*
     &(ASUM(K-3)+ASUM(K)+3.*(ASUM(K-2)+ASUM(K-1)))
      SIGT=SIGT*FAC*RED/4.
C*** END SIMPSON INTEGRATION
      KF=K
      IF(FAC .EQ. 1) KF=(K+1)/2
      SIGF=-RSUM(KF)
      SIGA=-SIGT+SIGF
      IF(KODE) 220,220,240
  220 SIGTDB=10.0*ALOG10(SIGT)
      IF(SIGA .LE. 0.0) GO TO 225
      SIGADB=10.0*ALOG10(SIGA)
      GO TO 230
```

```
225 WRITE(6,825) SIGT,SIGA,SIGF
    WRITE(7,825) SIGT,SIGA,SIGF
    GO TO 205
230 SIGTDB=10.0*ALOG10(SIGT)
    WRITE(6,850) SIGT,SIGTDB,SIGA,SIGADB
    WRITE(7,851) SIGT,SIGTDB,SIGA,SIGADB
    GO TO 205
240 SIGTDB=10.0*ALOG10(SIGT)
    WRITE(6,875) SIGT,SIGTDB
825 FORMAT(///,5X,40H*FOUL*   NEGATIVE ABSORPTION CROSSECTION,//,
   &15X,5HSIGT=,F8.5,5X,5HSIGA=,F8.5,5X,5HSIGF=,F8.5)
850 FORMAT(///,15X,5HSIGT=,F8.5,F8.2,3H DB,5X,5HSIGA=,F8.5,F8.2,
   &3H DB)
851 FORMAT(///,15X,'SIGMA(T)/LAMBDA=',F8.5,F8.2,' DB',5X,
   &'SIGMA(A)/LAMBDA=',F8.5,F8.2,' DB')
875 FORMAT(///,15X,7HSIGAVE=,F8.5,F8.2,3H DB)
205 IF (MORE.EQ.0) GO TO 5
    DO 103 I=1,LL
    ZS(I)=ZS(I)/ZFAC
103 DSQ(I)=DSQ(I)*WAVE
    DEL=ZFAC
    PWAVE=WAVE
    READ (5,200) MORE,KODE,ZFAC,WAVE,FIRST,LAST,INK
    WRITE(7,100) ID
    WRITE(7,101) WAVE
    WRITE(7,199) FIRST,LAST,INK,IPP
    IWHICH=1
    IF(REAL(ZFAC).EQ.0.AND.AIMAG(ZFAC).EQ.0.)
   &ZFAC=(1.E-20,1.E-20)
    IF(REAL(ZFAC).EQ.REAL(DEL).AND.AIMAG(ZFAC).EQ.AIMAG(DEL)
   &.AND.WAVE.EQ.PWAVE) IWHICH=2
    GO TO 20
100  FORMAT (18A4)
150  FORMAT (1H1,18A4)
200  FORMAT (I2,I3,6F10.5)
250  FORMAT (2I5,7F10.5,F10.3)
300  FORMAT (10HOSEG   NUM,11X,24HENDPOINTS OF THE SEGMENT,19X,
   &18HSEGMENT PARAMETERS/11H NUM  CELLS,6X,2HXA,8X,2HYA,8X,2HXB,8X,
   &2HYB,6X,24HANGLE   RADIUS    LENGTH,4X,14HRE-Z       IM-Z/)
400  FORMAT (//31X,14HKEY PARAMETERS//
   &16X,21HINCIDENT POLARIZATION,22X,1A1/
   &16X,23HNUMBER OF SEGMENTS USED,I21/
   &16X,33HTOTAL NUMBER OF CELLS ON THE BODY,I11/
   &16X,35HNUMBER OF INCIDENT FIELD DIRECTIONS,I9/
   &16X,29HNUMBER OF BISTATIC DIRECTIONS,I15/
   &16X,10HWAVELENGTH,F34.5/
   &16X,16HIMPEDANCE FATOR,F16.5,' ,',F10.5)
425  FORMAT (////,36X,18HSURFACE FIELD DATA/,27X,
   &29HFOR INCIDENT FIELD DIRECTION=,F7.2)
500  FORMAT (11H0   I   SEG,4X,4HX(I),6X,4HY(I),6X,4HS(I),5X,6HDSQ(I),
   &4X,6HRS(I) ,4X,6HXS(I) ,4X,6HMOD(J),4X,6HARG(J)/)
```

```
 600  FORMAT (1H1,27X,28HBACKSCATTERING CROSS SECTION//23X,
     &36HTHETA     SIGMA/LAMBDA,DB    PHASE,DEG)
 800  FORMAT (1H1,23X,33HBISTATIC SCATTERING CROSS SECTION/23X,
     &29HFOR INCIDENT FIELD DIRECTION=,F7.2//23X,
     &36HTHETA     SIGMA/LAMBDA,DB    PHASE,DEG)
 900  FORMAT (15X,F13.2,F14.2,F16.1)
 901  FORMAT (15X,F13.2,F14.2,F15.1)
      END
      SUBROUTINE MTX(M,MH,XK,X,Y,XN,YN,DSO,LUMP,ZS,A)
C     RICH VERSION, H-POLARIZATION
      REAL*4 X(1),Y(1),XN(1),YN(1),DSO(1)
      INTEGER*4 LUMP(1)
      COMPLEX*8 A(MH,1),ZS(1),HZ,H1A,H1B,DUM,H1BL,HZA,HZB,HZBL
      COMMON /PIES/ PI,TPI, PIT, PIPI, YZ,RED,DIG
      IH=0
      IL=0
      DO 10 I=2,M,2
      IH=IH+1
      XI=X(I)
      YI=Y(I)
      XNI=XN(I)
      YNI=YN(I)
      JH=0
      DO 25 J=2,M,2
      JH=JH+1
      ISEG=LUMP(J)
      DS=DSO(ISEG)
      IF(IH.EQ.JH)GO TO 50
      JA=J-1
      JB=J+1
      IF(J.EQ.M) JB=1
      XJA=X(JA)
      YJA=Y(JA)
      XJB=X(JB)
      YJB=Y(JB)
      XNJA=XN(JA)
      YNJA=YN(JA)
      XNJB=XN(JB)
      YNJB=YN(JB)
      RX=XI-X(J)
      RY=YI-Y(J)
      R=SQRT(RX*RX+RY*RY)
      SDSP=XNI*XN(J)+YNI*YN(J)
      RK=R*XK
      CALL HANKZ1(RK,0,HZ,DUM)
      HZ=HZ*SDSP
      RX=XI-XJB
      RY=YI-YJB
      R=SQRT(RX*RX+RY*RY)
      SDR=(RX*YNI-RY*XNI)/R
      SDSP=XNI*XNJB+YNI*YNJB
      RBK=R*XK
```

```
      CALL HANKZ1(RBK,2,HZB,H1B)
      H1B=H1B*SDR
      HZB=SDSP*HZB
      IF(XJA.EQ.XJBL.AND.YJA.EQ.YJBL.AND.I.EQ.IL) GO TO 15
      RX=XI-XJA
      RY=YI-YJA
      R=SQRT(RX*RX+RY*RY)
      SDR=(RX*YNI-RY*XNI)/R
      SDSP=XNI*XNJA+YNI*YNJA
      RAK=R*XK
      CALL HANKZ1(RAK,2,HZA,H1A)
      H1A=H1A*SDR
      HZA=SDSP*HZA
      GO TO 20
   15 H1A=H1BL
      HZA=HZBL
   20 A(IH,JH)=PIT*DS/6.*(HZA+4.*HZ+HZB)-0.25*(H1B-H1A)
      XJBL=XJB
      YJBL=YJB
      H1BL=H1B
      HZBL=HZB
      GO TO 25
   50 A(IH,JH)=ZS(ISEG)+
     &CMPLX(PIT*DS/2.,1./DS/PIPI+DS*(ALOG(DS)+0.02879837)/2.)
   25 IL=I
   10 CONTINUE
      RETURN
      END
      SUBROUTINE GEOM(LUMP,X,Y,XN,YN,S,DSO,ZS,M)
C    THIS VERSION READS AND GENETATES SEGMENTS IN COUNTER-CLOCKWISE DIRECTION.
C    THE SURFACE MUST BE CLOSED.
C    POINTS ARE GENERETED AT  THE START AND MIDPOINTS OF EACH CELL;
C    THE START POINT OF THE FIRST CELL EVENTUALLY COINCIDES
C    WITH THE END POINT OF THE LAST CELL.
      COMPLEX*8 ZS(1),Z
      REAL*4 X(1),Y(1),XN(1),YN(1),S(1),DSO(1)
      INTEGER*4 LUMP(1)
      COMMON /PIES/ PI,TPI, PIT, PIPI, YZ,RED,DIG
      I=0
      L=0
C.....READ INPUT PARAMETERS AND PREPARE TO GENERATE SAMPLING POINTS
   10 READ (5,200) N,Z,XA,YA,XB,YB,ANG
      IF(N.LT.1) GO TO 120
      LIM=2*N
      TX=XA-XB
      TY=YA-YB
      D=SQRT(TX*TX+TY*TY)
      L=L+1
      ZS(L)=Z
      IF (ANG.EQ.0.0) GO TO 20
      T=0.5*RED*ANG
```

```
      TRX=TX+TY*COTAN(T)
      TRY=TY-TX*COTAN(T)
      RAD=0.5*D/SIN(T)
      ARC=2.0*RAD*T
      ALF=T/N
      DSO(L)=2.0*RAD*ALF
      GO TO 30
   20 RAD=999.999
      ARC=D
      DSO(L)=D/N
C.....START GENERATING
   30 DSS=0.
      DS=DSO(L)/2.
      DO 50 JJ=1,LIM
      I=I+1
      J=JJ-1
      S(I)=DSS
      DSS=DSS+DS
      LUMP(I)=L
      IF (ANG.EQ.0.0) GO TO 40
      ARG=J*ALF
      SINQ=SIN(ARG)
      COSQ=COS(ARG)
      X(I)=XA-0.5*(TRX*(1.0-COSQ)-TRY*SINQ)
      Y(I)=YA+0.5*(TRX*SINQ+TRY*(1.0-COSQ))
      XN(I)=+0.5*(TRX*COSQ+TRY*SINQ)/RAD
      YN(I)= 0.5*(TRX*SINQ-TRY*COSQ)/RAD
      GO TO 50
   40 X(I)=XA-0.5*J*TX/N
      Y(I)=YA-0.5*J*TY/N
      XN(I)=-TY/D
      YN(I)= TX/D
   50 CONTINUE
  100 WRITE(6,300)L,N,XA,YA,XB,YB,ANG,RAD,ARC,Z
      GO TO 10
  120 M=I
      LL=L
  200 FORMAT(I2,3X,7F10.5)
  300 FORMAT(I3,I6,4X,4F10.5,F7.2,4F10.5)
      RETURN
      END
      SUBROUTINE HANKZ1(R,N,HZERO,HONE)
C.....HANKEL FUNCTIONS ARE OF FIRST KIND--J+IY

C.....    N=0 RETURNS HZERO
C.....    N=1 RETURNS HONE
C.....    N=2 RETURNS HZERO AND HONE
C.....SUBROUTINE REQUIRES R>0
C.....SUBROUTINE ADAM MUST BE SUPPLIED BY USER
```

```
      DIMENSION A(7),B(7),C(7),D(7),E(7),F(7),G(7),H(7)
      COMPLEX HZERO,HONE
      DATA A,B,C,D,E,F,G,H/1.0,-2.2499997,1.2656208,-0.3163866,
     &0.0444479,-0.0039444,0.00021,0.36746691,0.60559366,-0.74350384,
     &0.25300117,-0.04261214,0.00427916,-0.00024846,0.5,-0.56249985,
     &0.21093573,-0.03954289,0.00443319,-0.00031761,-0.00001109,
     &-0.6366198,0.2212091,2.1682709,-1.3164827,0.3123951,-0.0400976,
     &0.0027873,0.79788456,-0.00000077,-0.0055274,-0.00009512,
     &0.00137237,-0.00072805,0.00014476,-0.78539816,-0.04166397,
     &-0.00003954,0.00262573,-0.00054125,-0.00029333,0.00013558,
     &0.79788456,0.00000156,0.01659667,0.00017105,-0.00249511,
     &0.00113653,-0.00020033,-2.35619449,0.12499612,0.0000565,
     &-0.00637879,0.00074348,0.00079824,-0.00029166/
      IF (R.LE.0.0) GO TO 50
      IF (N.LT.0.OR.N.GT.2) GO TO 50
      IF (R.GT.3.0) GO TO 20
      X=R*R/9.0
      IF (N.EQ.1) GO TO 10
      CALL ADAM(A,X,BJ)
      CALL ADAM(B,X,Y)
      BY=0.6366198*ALOG(0.5*R)*BJ+Y
      HZERO=CMPLX(BJ,BY)
      IF (N.EQ.0) RETURN
10    CALL ADAM(C,X,Y)
      BJ=R*Y
      CALL ADAM(D,X,Y)
      BY=0.6366198*ALOG(0.5*R)*BJ+Y/R
      HONE=CMPLX(BJ,BY)
      RETURN
20    X=3.0/R
      IF (N.EQ.1) GO TO 30
      CALL ADAM(E,X,Y)
      FOOL=Y/SQRT(R)
      CALL ADAM(F,X,Y)
      T=R+Y
      BJ=FOOL*COS(T)
      BY=FOOL*SIN(T)
      HZERO=CMPLX(BJ,BY)
      IF (N.EQ.0) RETURN
30    CALL ADAM(G,X,Y)
      FOOL=Y/SQRT(R)
      CALL ADAM(H,X,Y)
      T=R+Y
      BJ=FOOL*COS(T)
      BY=FOOL*SIN(T)
      HONE=CMPLX(BJ,BY)
      RETURN
50    WRITE(6,90) N,R
90    FORMAT(32HOSICK DATA IN HANKZ1  *QUIT*  N=,I2,2X,2HR=,F11.3)
      CALL SYSTEM
      END
      SUBROUTINE ADAM(C,X,Y)
      DIMENSION C(7)
      Y=X*C(7)
      DO 10 I=1,5
```

```
10   Y=X*(C(7-I)+Y)
     Y=Y+C(1)
     RETURN
     END
     SUBROUTINE FLIP(A,N,MI,L,M,X,Y,IAT)
     COMPLEX A(MI,1),X(1),Y(1),D,BIGA,HOLD
     DIMENSION L(1),M(1)
     IF (IAT.GT.1) GO TO 150
     D=CMPLX(1.0,0.0)
     DO 80 K=1,N
     L(K)=K
     M(K)=K
     BIGA=A(K,K)
     DO 20 J=K,N
     DO 20 I=K,N
10   IF (CABS(BIGA).GE.CABS(A(I,J))) GO TO 20
     BIGA=A(I,J)
     L(K)=I
     M(K)=J
20   CONTINUE
     J=L(K)
     IF (J.LE.K) GO TO 35
     DO 30 I=1,N
     HOLD=-A(K,I)
     A(K,I)=A(J,I)
30   A(J,I)=HOLD
35   I=M(K)
     IF (I.LE.K) GO TO 45
     DO 40 J=1,N
     HOLD=-A(J,K)
     A(J,K)=A(J,I)
40   A(J,I)=HOLD
45   IF (CABS(BIGA).NE.0.0) GO TO 50
     D=CMPLX(0.0,0.0)
     RETURN
50   DO 55 I=1,N
     IF (I.EQ.K) GO TO 55
     A(I,K)=-A(I,K)/BIGA
55   CONTINUE
     DO 65 I=1,N
     DO 65 J=1,N
     IF (I.EQ.K.OR.J.EQ.K) GO TO 65
     A(I,J)=A(I,K)*A(K,J)+A(I,J)
65   CONTINUE
     DO 75 J=1,N
     IF (J.EQ.K) GO TO 75
     A(K,J)=A(K,J)/BIGA
75   CONTINUE
     D=D*BIGA
80   A(K,K)=1.0/BIGA
     K=N
```

```
100   K=K-1
      IF (K.LE.0) GO TO 150
      I=L(K)
      IF (I.LE.K) GO TO 120
      DO 110 J=1,N
      HOLD=A(J,K)
      A(J,K)=-A(J,I)
110   A(J,I)=HOLD
120   J=M(K)
      IF (J.LE.K) GO TO 100
      DO 130 I=1,N
      HOLD=A(K,I)
      A(K,I)=-A(J,I)
130   A(J,I)=HOLD
      GO TO 100
150   DO 200 I=1,N
      Y(I)=CMPLX(0.0,0.0)
      DO 200 J=1,N
200   Y(I)=A(I,J)*X(J)+Y(I)
      RETURN
      END
      BLOCK DATA
      COMMON/PIES/PI,TPI,PIT,PIPI,YZ,RED,DIG
      DATA PI,TPI,PIT,PIPI,YZ,RED,DIG/3.1415927,6.2831853,
     &1.5707963,9.8696044,0.0026525824,0.01745329,57.29578/
      END
```